Electrochemical capacitive properties of nickel oxide and nickel tetra-aminophthalocyanine based electrodes

by

Katlego Makgopa

Submitted in fulfilment of the requirements for the degree of

Master of Science

Department of Chemistry

In the Faculty of Natural and Agricultural

Science

University of Pretoria

January 2012

Supervisor: Prof. K.I. Ozoemena

DEDICATION

This thesis is dedicated to my wife Mpho Kgabo Makgopa, friends and family for their unlimited support.

DECLARATION

I declare that the dissertation, which I hereby submit for the degree Magister Scientae in the faculty of Natural and Agricultural Sciences at the University of Pretoria, is my own work and has not previously been submitted by me for a degree at this, or any other tertiary institution.

_____

Katlego Makgopa

s28383762

ACKNOWLEDGEMENTS

Firstly, I would like to express my sincere gratitude to the Almighty Father God in Heaven and my Lord Jesus Christ for the strength and perseverance throughout my M.Sc programme. I would also like to be grateful to my supervisor Prof. K. I. Ozoemena for his uncompromising guidance. Thank you for everything that you have helped me with, you are truly my inspiration and it has been a privilege to work in conjunction with one of the leading academics in South Africa who has greatly influenced my interest to continue research in the electrochemistry field.

Much appreciation to the Chemistry Department, University of Pretoria and the National Research Foundation (NRF) for the prestigious nanoflagship bursary, I am grateful. To my family and all my cousins (especially Lesley Papiki, Granny, Mamokete, Salphy and Nthabiseng), my mother Sinah Mohube, my sister Vinoliah and my brothers Eddie and Thabo, thank you for the moral support and encouragement; to all the members of our research group Joel, Bose and Charl, we really had a wonderful time, despite all inconveniences. I am forever grateful to my dear friends, Selby Shubane, Khulekane Dlamini, and Dumisane Hlongwane; for all the best times we had together and the support you gave through this period of my life. You are the best guys. Finally, to everyone, who have in one way or another impacted positively to this M.Sc studies, I am grateful and thank you so much.

ABSTRACT

This study reports on an electrochemical capacitive properties of nickel tetraaminophthalocyanine (NiTAPc), nickel tetraaminophthalocyanine incorporated with Nickel oxide (NiTAPc-NiO) and nickel oxide incorporated with multi-walled carbon nanotubes (NiO-MWCNT), using three different techniques known as successive ionic layer adsorption reaction (SILAR), electrodeposition and dip-dry. This study also reports on the effect of undoped polymer of poly-pyrrole on NiTAPc. The physical properties of the synthesised materials were investigated using SEM and EDX and the electrochemical properties were investigated using cyclic voltammetry (CV), charge-discharge (CD) and electrochemical impedance spectroscopy (EIS). The supercapacitive properties of NiTAPc film on nickel foam showed a maximum specific capacitance of 416.0 Fg^{-1}, a maximum power density of $15.50x10^{3}$ WKg^{-1} and a maximum specific energy of 66.0 $WhKg^{-1}$. The NiO-MWCNT film on nickel foam gave a maximum specific capacitance of 1034.0 Fg^{-1}, a maximum power density of $10.41x10^{3}$ WKg^{-1} and a maximum specific energy of 132.0 $WhKg^{-1}$. The NiTAPc-NiO_E film on nickel foam was found to possess a maximum specific capacitance of 1117.0 Fg^{-1}, a maximum power density of $20.48x10^{3}$ WKg^{-1} and a maximum specific energy of 119.0 $WhKg^{-1}$. The NiTAPc-NiO_{E-S} film on nickel foam gave a maximum specific capacitance of 1279.0 Fg^{-1}, a maximum power density of $26.96x10^{3}$ WKg^{-1} and a maximum specific energy of 114.0 $WhKg^{-1}$. Finally, the NiO mixed with an

oxidant ($NiO_{S\text{-}ox}$) film on nickel foam gave a maximum specific capacitance of 1403.0 Fg^{-1}, power density of $14.44x10^{3}$ WKg^{-1} and a maximum specific energy of 147.0 $WhKg^{-1}$. In addition, the electrodes were found to be very stable even after repetitive cycling. These electrodes have clearly proved that they may be suitable for use as potential supercapacitors. Further research is necessary to fully explore their supercapacitive behaviour in single cell (2-electrode) systems.

TABLE OF CONTENTS

LIST OF ABBREVIATIONS

Ag|AgCl	=	Silver|Silver Chloride Reference Electrode
CA	=	Chronoamperometry
CD	=	Charge-Discharge
C.E	=	Counter Electrode
CME	=	Chemically Modified Electrode
CNT	=	Carbon Nanotube
CPE	=	Constant Phase Angle Element
CV	=	Cyclic Voltammetry
DMF	=	*N*,*N*-Dimethylformamide
EDX	=	Energy-Dispersive X-Ray
EIS	=	Electrochemical Impedance Spectroscopy
IUPAC	=	International Union of Pure and Applied Chemistry
KCl	=	Potassium Chloride
LoD	=	Limit of Detection
MPc	=	Metallophthalocyanine
MTAPc	=	Metallotetraamino-phthalocyanine
MWCNT	=	Multi-Walled Carbon Nanotube
NaCl	=	Sodium Chloride
NF	=	Nickel Foam
Ni	=	Nickel
NiTAPc	=	Nickel(II) Tetraamino-Phthalocyanine
NiTAPc- PPY	=	Nickel(II) Tetraamino-Phthalocyanine -Polypyrrole

Pc	=	Phthalocyanine
PPY	=	Polypyrrole
PTFE	=	Polytetrafluoroethylene
PVDF	=	Polyvinylidene fluoride
R_{ct}	=	Charge Transfer Resistance
R.E	=	Reference Electrode
R_s	=	Solution Resistance
SEM	=	Scanning Electron Microscopy
SILAR	=	Successive Ionic Layer Adsorption Reaction
SWCNT	=	Single-Walled Carbon Nanotube
W.E	=	Working Electrode

LIST OF FIGURES

LIST OF SCHEMES

LIST OF TABLES

Chapter One

Introduction

1. Introduction

1.1 General Overview

Several advances in nanomaterials during the past few years as well as recently, have shown a great help in development of sustainable energy devices that can be extensively applied to a wide variety of applications, to resolve problems that are of analytical grade. Electrochemical methods exhibited a great potential in the society due to the fact that they are fast, simple, cost effective, portable and can be easily used, as compared to their relative analytical methods. Due to high demand in energy, there is a need to design and develop high performance electrochemical energy storage devices that can withstand harsh conditions as well as maintain their performance in order to deliver to the society. Supercapacitors, fuel cells and batteries are the three main electrochemical energy storage and conversion systems**.** Supercapacitors, which are sometimes known as Ultracapacitor or Electrochemical double layer capacitors, are electric components which serve as a source of energy storage, and the energy storage is by means of electrostatic interaction. The capacitance value of this electric component reaches almost thousands of Farads and due to this capacitance value, most of the scientists developed great interests in characterization and refinement of supercapacitors worldwide. Supercapacitors have higher specific power than batteries in power applications and also other advantages are related to higher cycle life,

rapid charging-discharging as well as operation in extended temperature range. Recently, the manufacturing technology of commercial supercapacitors is based on carbon material as well as conductive compounds for their electrodes. The electrode by which a supercapacitor is fabricated has a great impact on its properties. A significant amount of research on carbon material as potential supercapacitor electrode has therefore been undertaken over the past few years. Hybrid capacitors that make use of carbon nanotubes, metal oxides and conducting polymers have been probed for the same applications. Nevertheless, there have been fewer reports so far on the use of metallophthalocyanines as supercapacitor electrode materials.

In this project, focus will be on the carbon nanofibres and activated carbons as well as to examine the properties of nickel, phthalocyanines and conducting polymers. Carbon nanotubes are the strongest and stiffest materials in terms of tensile strength and elastic modulus respectively. Due to their strength and flexibility, they are used in controlling other nano structures. They have been used as composite fibre in polymers to improve the mathematical, thermal and electrical properties of the bulk product. The electrical property of carbon nanotubes creates essential interest in characterization of supercapacitors.

1.1.1 Aim of Study:

i. To characterize redox-active materials such as NiTAPc , NiTAPc complexed with nickel oxide and poly-pyrrole (PPY) , nickel oxide (NiO) and nickel oxide (NiO) integrated with MWCNT using electrochemical techniques such as: cyclic voltammetry (CV), charge-discharge (CD), and electrochemical impedance spectroscopy (EIS).

ii. To employ successive ionic layer adsorption reaction (SILAR), Pulsed laser deposition and Electrodeposition for fabrication of bare nickel foam electrode with nickel oxide (NiO) and its composites, Nickel tetraamine phthalocyanine (NiTAPc) integrated with poly-pyrrole (PPY), and Nickel tetraamine phthalocyanine (NiTAPc) integrated with nickel oxide.

iii. To investigate supercapacitive performance of nickel oxide (NiO) and its composites, Nickel tetraamine phthalocyanine (NiTAPc) integrated with poly-pyrrole (PPY), and Nickel tetraamine phthalocyanine (NiTAPc) integrated with nickel oxide.

This introduction section provides a general overview of electrode modification processes, Supercapacitors, electrochemistry, electrochemical techniques (cyclic voltammetry (CV), charge-discharge (CD), electrochemical impedance spectroscopy (EIS)), metallophthalocyanines, carbon nanotubes, metal oxides, conducting

polymers, microscopic and spectroscopic characterization of supercapacitor materials.

In chapter two, the procedure adopted for the experiment is provided. Chapter three to six discusses the results obtained.

1.2 Electrochemistry: An Overview

1.2.1 Basic Concept

Electrochemistry is best understood as a study of the use of chemical reactions to produce electric power [1]. Is another branch of chemistry that studies chemical reactions which take place in a solution at the interface of an electron conductor (a metal or a semiconductor) and an ionic conductor (the electrolyte), which involves electron transfer between the electrode and the electrolyte or any species in solution [1, 2]. Electrochemistry is interplay between electricity and chemistry, namely the measurements of electrical quantities such as current, potential, and charge, and their relationship to chemical parameters [3]. There are wide ranges of application in industrial quality control, environmental monitoring and biomedical analysis that use these electrical measurements for analytical purpose [4]. These chemical reactions involve the transfer of electrons to and from a molecule or ion (and are often referred to as redox (reduction-oxidation)) reactions.

As compared to many other chemical measurements, which involve homogeneous bulk solution, the fundamental electrochemical reactions are heterogeneous in nature as they take place at interfaces, usually electrode-solution boundaries. The electrode creates a phase boundary that differentiates otherwise identical solute molecules; those at a

distance from the electrode, and those close enough to the surface of the electrode to participate in the process of electron transfer [3-5].

The work described in this dissertation employed three main electroanalytical techniques; namely: cyclic voltammetry (CV), charge-discharge (CD), and electrochemical impedance spectroscopy (EIS). They were employed in the characterization of nickel oxide, nickel tetraamine phthalocyanine and their composites, using nickel foam as a current collector electrode. A closer look at the electrode processes and these three electroanalytical techniques follows.

1.2.1.1 The Electrode-Solution Interface

The illustration on figure 1.1 shows the electrode-solution interface also known as "electric double layer". It is the currently accepted model[6] produced by stern, and is a development from the Helmholtz model which regards the interface as a single capacitor and the Guoy-Chapman model which explains the interface as a Boltzman distribution of ions. As illustrated on figure 1.1 below, the electrical double layer is a complex structure of several distinct parts. The inner layer that is closest to the electrode, where the contact adsorbed ions that are not fully solvated and solvent molecules are found is known as the Inner Helmholtz Plane (IHP). The outer layer, the Outer Helmholtz Plane (OHP) is the imaginary plane passing through the solvated cations [6, 7].

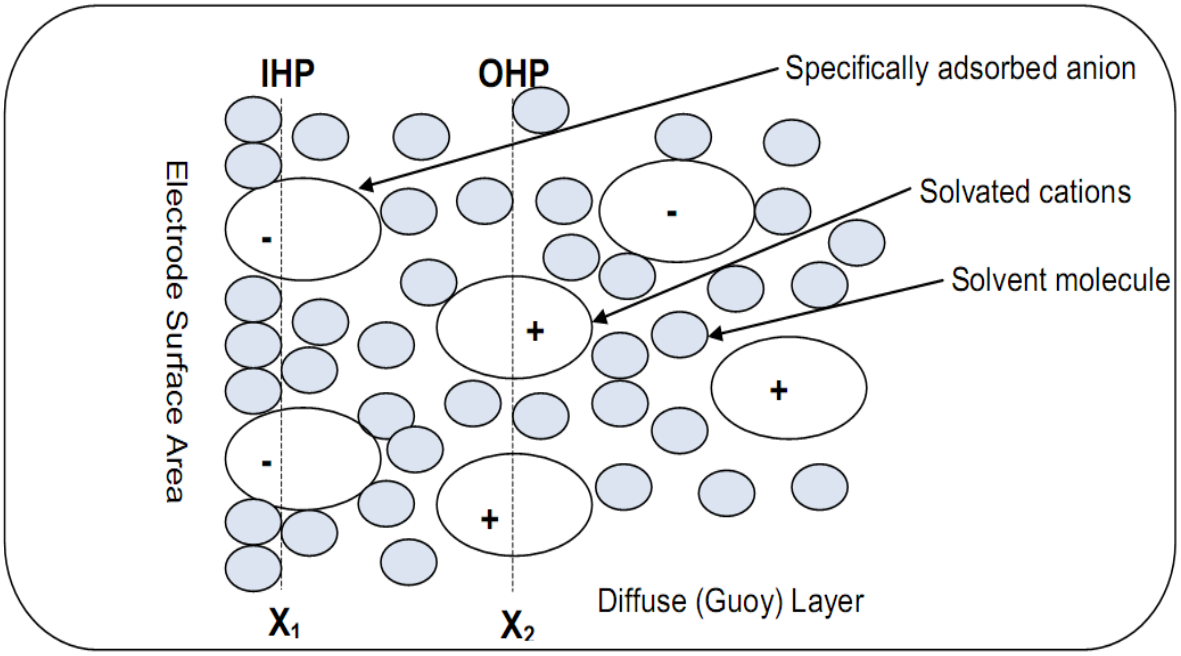

Figure 1.1: Representation of Electrode-electrolyte double layer region [6].

The solvated cations undergo nonspecific adsorption and are pulled towards the electrode surface by long range coulombic forces. These planes cannot be measured exactly, nor do they strictly exist, but the distance from the electrode to the IHP (X_1) will be the radius of the ion and to the OHP (X_2) will be about two water molecules plus the radius of the cation [7-9]. These two layers are strongly held by the electrode and they remain at the surface even if the electrode is removed from the solution. The layer, a three dimensional region of scattered ions, which extends from the OHP to the bulk solution, is referred to as the Gouy layer or "diffuse layer". The ion distribution in the diffuse layer is a consequence of the balance between the disorder caused by the random thermal motion and order due to the electrostatic force of attraction and repulsion from the electrode surface. Beyond the diffuse layer, it becomes

impossible for the ions in the homogeneous bulk to experience or "feel" the presence of the electrode [10, 11]. A closer look of some of the electroanalytical techniques and electrode processes employed in this dissertation are detailed in this section.

1.2.1.2 Classification of Electrochemical Techniques.

The flowchart in figure 1.2 represents the classes and sub-division of the electrochemical techniques.

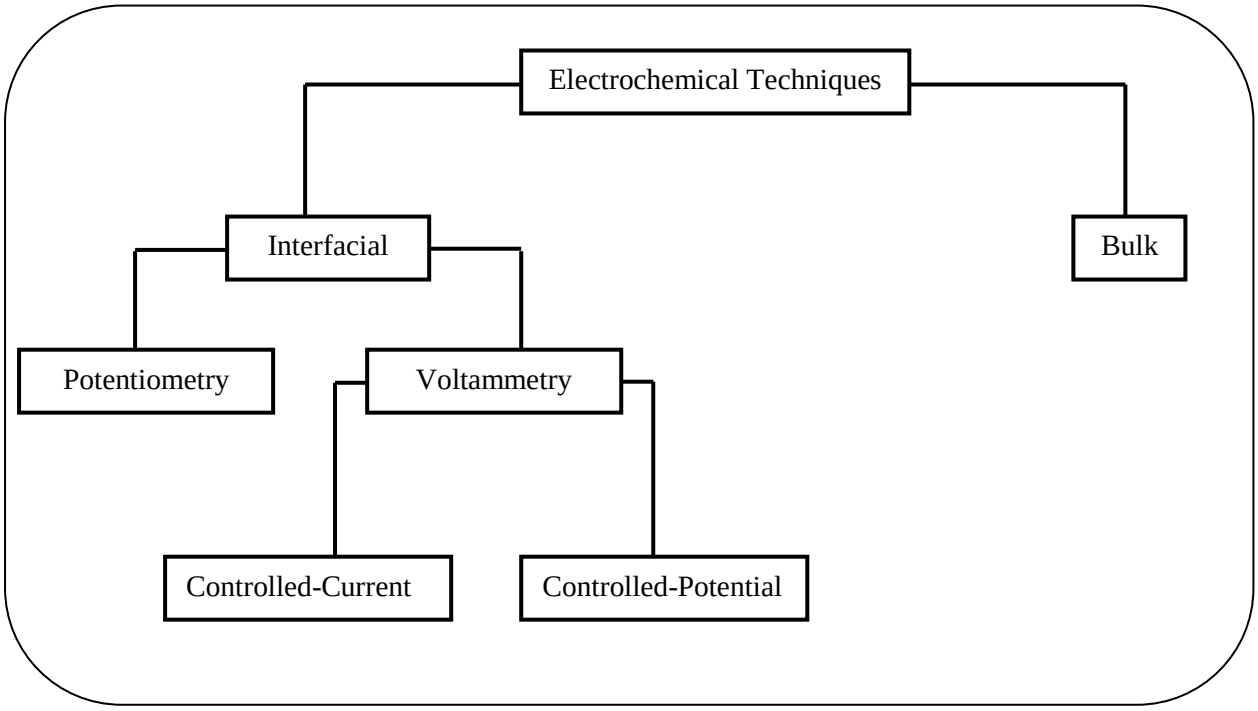

Figure 1.1.2: The flowchart representing the Electrochemical Techniques

There are two classes in which the electrochemical techniques can be divided: bulk and interfacial technique. Bulk techniques are based on the phenomena that occur in the core of the solution and one example is

conductimetry. In contrast, interfacial techniques are based on the phenomena taking place at the electrode-solution interface. Interfacial techniques are further classified into equilibrium and dynamic methods, with potentiometric measurements as one of the examples of equilibrium. The dynamic methods are sub-divided into controlled potential and controlled current methods. The controlled-potential methods are undoubtedly more popular and include a vast array of techniques such as voltammetry, chronoamperometry as well as bulk electrolysis. The controlled-potential techniques involve the measurement of current, while the potential is controlled. The advantages of these techniques include high sensitivity and selectivity towards electroactive species, wider linear range, portable and low cost instrumentation.

1.2.1.3 Faradaic and Non-Faradaic processes.

All current-measuring (voltammetric/amperometric) techniques make use of a three-electrode electrochemical cell (fig.1.3)

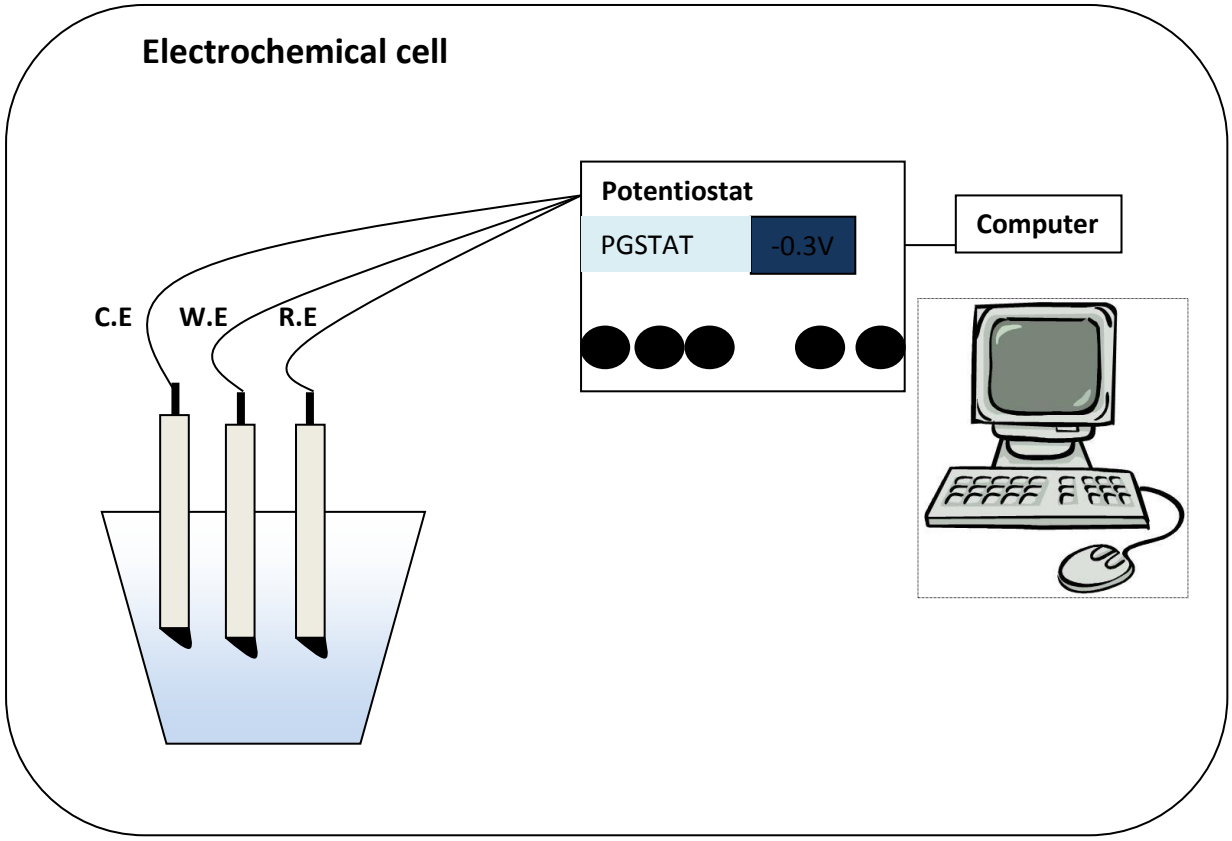

Figure 1.3: A diagrammatic representation of an electrochemical cell of a conventional three-electrode system connected to the potentiostat and computer.

The surface of the working electrode, W.E., serves as the platform where the electrochemical reactions are being studied. R.E. is the reference electrode, in which the measured potential is in reference to it, whiles the counter electrode C.E., completes the electric circuit. The best reference electrode is the one whose potential does not shift from the equilibrium (i.e. non polarisable). In order to minimize the potential shift, reference electrodes with a very large surface are mostly used [12]. Potentiostats based on operation amplifiers are often used in the complete elimination of reference electrode polarization. As shown in figure 1.3, the

potentiostat maintains the potential difference, ΔE, between the reference electrode (R.E) and the working electrode (W.E) and supplies the current, *i*, needed for affecting the charges occurring at the working electrode (W.E).There are many reference electrodes employed in electroanalytical experiments, but the most commonly used is silver/silver chloride (Ag/AgCl, saturated potassium chloride) electrode, though recently there is rapid evolution in the usage of other reference electrodes for example saturated calomel electrode (SCE) [13]. Silver/silver chloride is a piece of silver wire anodized with silver chloride which is immersed in potassium chloride or sodium chloride solution and are encased in a glass tube. The electrode is therefore being protected from the bulk solution by a non-selective salt bridge. The electrode functions as a redox electrode and the reaction is between the silver metal (Ag) and its salt, silver chloride (AgCl, also called silver (I) chloride). The counter electrode, also called the auxiliary electrode, is an electrode used in a three electrode electrochemical cell for voltammetric analysis or other reactions in which an electrical current is expected to flow. Counter electrodes are often fabricated from electrochemically inert materials such as gold, platinum wire, loops, gauze, foil or carbon. The auxiliary electrode is distinct from the reference electrode, which establishes the electrical potential against which other potentials may be measured, and the working electrode, at which the cell reaction takes place [13, 14]. Common working electrodes can consist of inert metals such as gold, silver or platinum, to inert carbon

such as glassy carbon or pyrolytic carbon, and mercury drop and film electrodes [14].

1.2.1.4 Mass Transport processes

For a fixed electrode area (A), the reaction can be controlled by two factors. First is the rate constant and second is the surface concentration of the reactant. If the rate constant is large in such a way that any reactant close to the interface is immediately converted to its products, then the current will be controlled by the amount of fresh reactant reaching the interface from the bulk solution of the electrolyte. Thus movement of reactant in and out of the interface is important in predicting the current which is flowing. In this section, various ways in which material can move within solution to the surface of the electrode are being outlined. There are three forms of mass transport which facilitate the movement of a charged or neutral species in an electrochemical cell to the surface of the electrode, namely: diffusion, convection and migration [11, 14-16].

Diffusion is a process of mass transport whereby analyte species move in a spontaneous manner from the region of higher concentrations to a region of lower concentrations. It occurs in all solutions and arises from local uneven concentrations of the reagents. Entropic forces act to smooth out these uneven distributions of concentrations and are therefore the

main driving force for this process. A concentration difference develops at the electrode surface due to depletion or production of some species. Consequently, there will be a lower reactant concentration at the electrode than in bulk solution as well as a higher concentration of product near the electrode than further out into the solution.

Migration is another process of mass transport that is due to electrostatic effects which arises due to the application of a voltage on the electrodes. This effectively creates a charged interface (the electrodes) and any charged species near that interface will either be attracted or repelled from it by electrostatic forces. In most voltammetric analysis, migration is often undesirable, therefore by adding a large quantity of the supporting electrolyte (relative to the reactants), it is possible to ensure that the electrolysis reaction is not significantly affected by migration [17]. The purpose of introducing a supporting (background) electrolyte into a solution is not however solely to remove migration effect as it also acts as a conductor to aid the passage of current through the solution.

Convection is a mass transport achieved by some form of external energy acting on the solution or on the electrode such as stirring the solution, solution flow or rotation and/or vibration of the electrode.

1.3 Electrochemical Capacitor

1.3.1 Electrochemical Capacitor Concept

Electrochemical capacitors also known as supercapacitors, ultracapacitors or power capacitors are energy devices that have high cycling stability, energy and power density [18, 19]. Supercapacitor and ultracapacitor are the two terms that are widely used for the description of these energy storage devices. Ultracapacitors based on the double electrochemical double layer capacitance (EDLC) are electrical energy storage devices that store and release energy by nanoscopic charge separation at the electrochemical interface between an electrode and an electrolyte [20]. As the energy stored is inversely proportional to the thickness of the double layer, these capacitors have an extremely high energy density compared to conventional dielectric capacitors. They are able to store a large amount of charge which can be delivered at much higher power ratings than rechargeable batteries. Supercapacitors can be used in a wide range of energy capture and storage applications and are used either by themselves as the primary power source or in combinations with batteries or fuel cells [20, 21].

1.3.2 Historical background of electrochemical capacitors

The history of electrochemical capacitors began with the General Electric engineers, when they were experimenting with devices using porous carbon electrodes. They first observed the electric double layer capacitor (EDLC) effect in 1957 [7, 22], and believed that the energy was stored in the carbon pores and the device exhibited "exceptionally high capacitance", although the mechanism was unknown at that time. So the General Electric did not immediately follow up on this work, therefore around 1966, researchers at Standard Oil of Ohio developed the modern version of the devices, after they accidentally re-discovered the effect while working on experimental fuel cell design [23, 24]. Their cell design used two layers of activated charcoal separated by a thin porous insulator, and this basic mechanical design remained the basis of most electric double-layer capacitors. The Standard Oil did not commercialize this invention of their own but instead, they licensed the technology to NEC, whom they finally marketed the results as supercapacitors in 1978, in order to provide backup power for maintaining computer memory. Then market expanded slowly for some time until the mid-1990s where various advances in materials science and refinement of the existing systems led to rapid improvement of the performance and an equally rapid reduction in cost. The first trials of supercapacitors in industrial applications were carried out for the energy supply to robots [25]. In 2005 aerospace systems and Controls Company Diehl Luftfahrt Elektronik GmbH decided to use

supercapacitors to power emergency actuation systems for doors and evacuation slides in airliners, including the new Airbus 380 jumbo jet. In 2005, the cost of the supercapacitor on the market was between US $272 million and $400 million, depending on the source. Since 2007, all solid state micrometer-scale electric double-layer capacitors based on advances superionic conductors had been for low-voltage electronics such as deep-sub-voltage nanoelectronics and related technologies (i.e. the 22 nm technological node of CMOS and beyond) [26, 27]. And currently, Maxwell technologies are one of the major manufactures of supercapacitors in the world.

1.3.3 The Design and Operational principle of Electrochemical capacitors

The first step in designing a supercapacitor is to make a choice between different types of technologies and designs available such as the type of electrolytes. Like conventional parallel plate capacitors, supercapacitors consist of two electrodes separated by a thin insulator called separator, all immersed inside a conductive solution called electrolyte [23]. Separator is made of porous material that allows ions of the electrolyte to pass through so as to cover or immerse both the surface of the two electrodes with the electrolyte solution. Supercapacitors operate on the same principle as conventional capacitors although they make use of the

electrodes that have much higher surface area. Capacitance increases with the increase in the surface area of the electrodes and also with the decrease in the distance between the two electrodes. Supercapacitors improve the conventional capacitors in two ways: firstly. they work on the principle that a double layer is generated when a voltage is applied to electrodes in an electrically conducting solution known as electrolyte. The charge separation occurs in molecular dimension (few nanometres) resulting in extremely large capacitance. And secondly, the activated carbon electrode material used has enormous surface area of the electrode available and this result in small devices of supercapacitors with capacitance of few thousand farads. From a conceptual point of view, the supercapacitor cell may be considered as an assembly of three parts, namely: the active part consisting of the electrodes and the separator, the electrolyte impregnant, and the packaging [25, 26]. The active part is made in most of the case of two electrodes with spacer between the electrodes, the separator, which its function is to provide an electronic insulation between the electrodes, while leaving the ions moving through its porosity to insure the ionic conduction. The active part is impregnated with an electrolyte made of a solvent containing a dissociated salt and is closed in a tight package [28]. The schematic representation showing the mechanism of a supercapacitor made of porous carbon electrode is illustrated by figure 1.4.

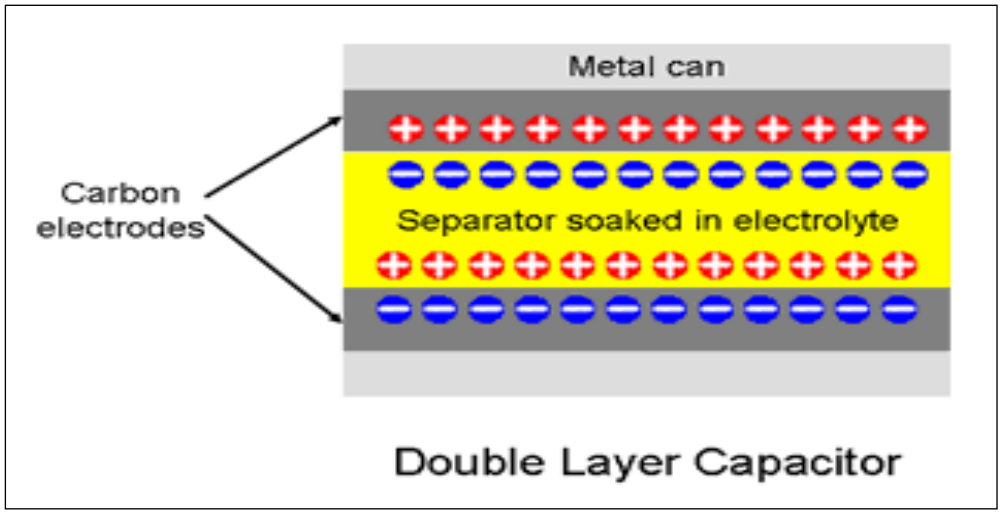

Figure 1.4: Schematic representation of supercapacitor made of porous carbon material [22].

1.3.3.1 The Fundamental Principles Of Electrochemical Capacitors

The first type of supercapacitor is made of a metal sheet with activated carbon electrodes [7, 29, 30]. The microscopic pores in the carbon material are typically few nanometers in size and have a great effect of providing an enormous increased internal surface area. The only possible way of utilizing this additional active surface area, it is by the use of an electrically conductive liquid electrolyte. On each of the electrodes, an electrical double layer of charge is formed between the carbon electrode and the electrolyte ions (figure 1.4). A complete capacitor is obtained at each of electrode which provides the complete device two capacitors connected in series. A supercapacitor based on this principle is called an electrochemical double-layer capacitor (EDLC). Figure 1.5 is an illustration of the principle of electrochemical double-layer capacitor (a) and also a simple circuit illustrating two capacitors connected in series (b).

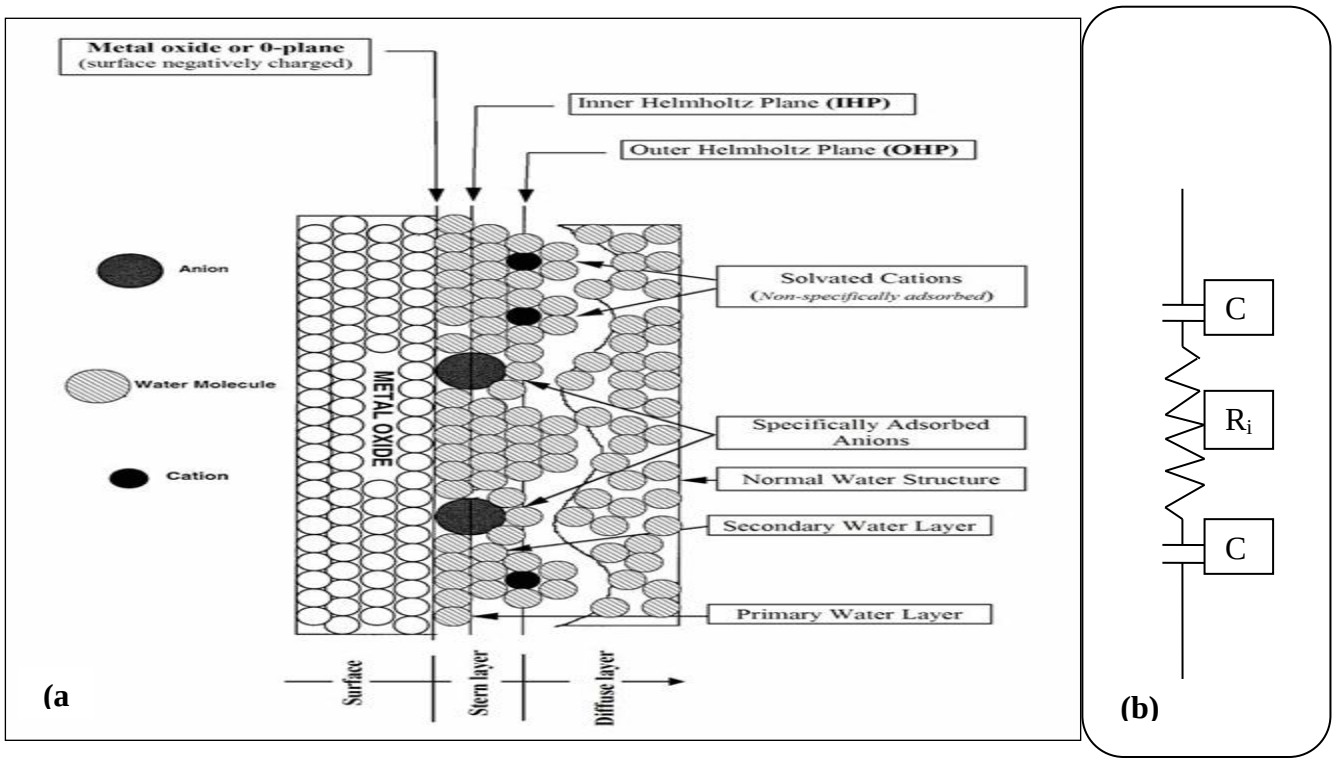

Figure 1.5: A representation of a proposed model of the electrochemical double-layer region at an electrode-electrolyte interface [31] (a) and also a simple circuit illustrating two capacitors connected in series. (b)

A variety of electrolytes can be used in supercapacitors, including water-based (aqueous) solutions such as potassium hydroxide (KOH) or sulphuric acid (H_2SO_4). However, since water tends to dissociates into its components hydrogen and oxygen at the voltages over 1V, these type of supercapacitors can only be used up to 1V. But if a water free organic electrolyte is used, then supercapacitors that can be used up to 2.5V or even higher may be obtained [18, 32]. The structure of the double-layer at the electrode-electrolyte interface can affect the rates of the electrode processes in as much as it can be affected by the structure of the electrode and the electrolyte layer itself. Due to different mechanisms of

charge storage, different classes of supercapacitors have evolved. From figure 1.5 (b), C_1 and C_2 represent the double layer capacitances of the anode and cathode respectively, and R_i is the internal resistance of the electrochemical cell.

When a voltage is applied to a capacitor, opposite charges accumulates on the surface of each electrode [33]. The charges are kept separate by the dielectrics, thus producing an electric field that allows the capacitor to store energy. This is illustrated in figure 1.4, above. Capacitance (C) is defined as the ratio of stored (positive) charge (Q) to the applied voltage (V), see equation 1.4 below.

$$C = \frac{Q}{V} \tag{1.4}$$

For a conventional capacitor, C is directly proportional to the surface area (A) of each electrode and is inversely proportional to the distance (D) between the electrodes.

$$C = \varepsilon_0 \varepsilon_r \frac{A}{D} \tag{1.5}$$

The product of the first two factors on the right hand side of equation 1.5 is a constant of proportionality wherein ε_0 is the dielectric constant (or permittivity) of free space and ε_r is the dielectric constant of the insulating material between the electrodes. In order to achieve high capacitance value for electrochemical capacitors, the area (A) has to be increased and or the distance (D) be decreased. This can be easily done by using the

porous electrodes on the current collector. Capacitance values are determined by various factors and some of these factors will be explained. There are two systems that can be employed in supercacitors [7, 28], namely: two electrode system and a three electrode system. The capacitance of a two electrode system and the three electrode system vary significantly by a factor of four (4). Therefore in many cases, when the capacitance measurement is reported, the type of the electrode system used for the measurement is mostly stated.

The two primary attributes of a capacitor are its energy density and power density. For either of both measures, the density can be calculated as a quantity per unit mass or per unit volume. The energy (E) stored in a capacitor is directly proportional to its capacitance and this relationship is given by equation 1.6

$$E = \frac{1}{2} CV^2 \qquad (1.6)$$

And power (P) in general, is the energy expanded per unit time. To determine power for a capacitor, equation 1.7 can be employed.

$$P_{\max} = \frac{V^2}{4(ESR)} \qquad (1.7)$$

Where ESR (Equivalent Series Resistance) is the resistance contributed by the internal components of the capacitor (i.e. current collectors, electrodes and dielectric materials).

1.3.4 The Importance of Electrochemical Capacitors in Energy Devices

Conventional capacitors have relatively high power densities but relatively low energy densities when compared to the electrochemical batteries and to fuel cells. Energy density and power density are two terms mainly employed in comparing energy content and rate capabilities respectively, and they are expressed in Wh/kg for energy density and W/kg for power density. The relationship between these two intrinsic factors is demonstrated by using a unique plot known as Ragone plot, which give comparison for various energy devices. Figure 1.6 illustrates the performance characteristics of any energy storage and conversion systems in terms of their power and energy densities (Ragone plot).

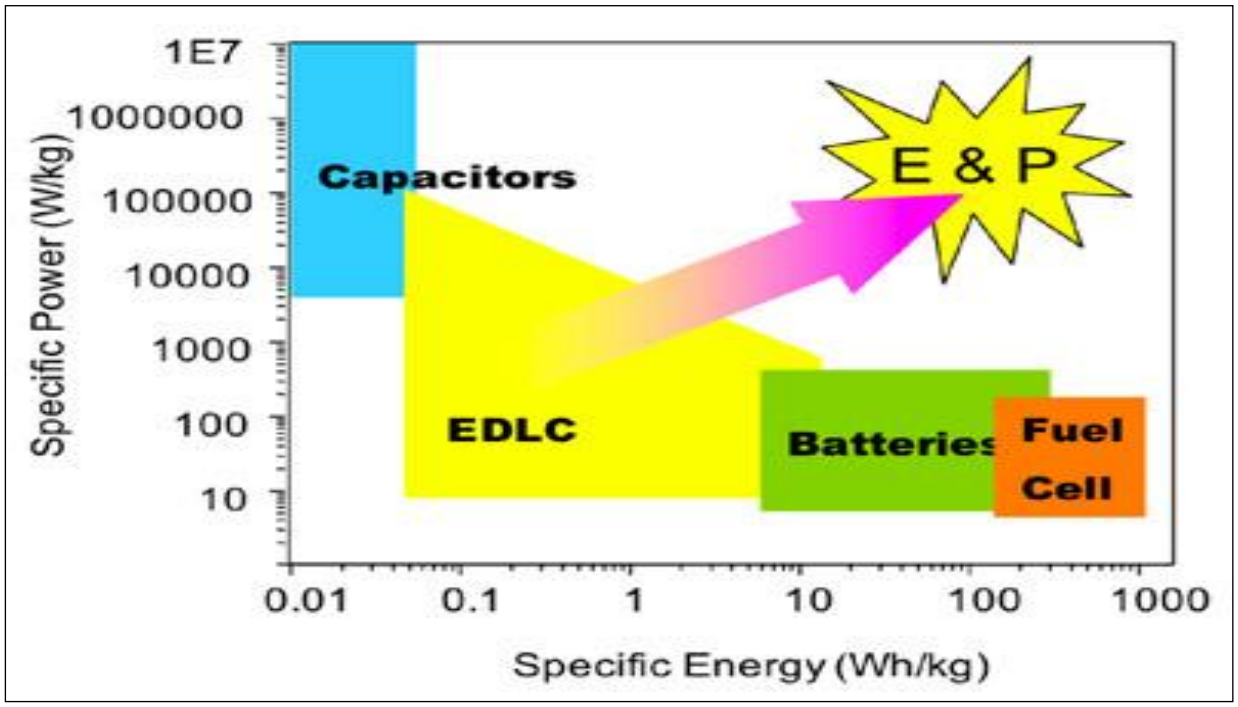

Figure 1.6: A simplified Ragone plot illustrating specific power versus specific energy for various energy devices [28, 34].

From figure 1.6, it can be clearly seen that supercapacitors serve as an intermediate systems that bridge the gap between conventional capacitors (high power) and batteries (high energy). The conventional capacitors exhibit high power density but low energy density when compared with batteries and fuel cells. This indicates the fact that, batteries are able to store more energy than a capacitor, but the delivery time of this energy is longer hence a lower power density. Although a capacitor stores less energy, it can quickly release large amounts of power resulting in a high density. Therefore, the significance of the supercapacitors as the link between conventional capacitors and batteries is clearly highlighted by the Ragone plot. Nevertheless, though supercapacitors provide greater capacitance, they still have limitations in energy density as compared to that of batteries and fuel cells. For this reason, this work focuses only on the improvement of supercapacitors for better capacitance at the electric double-layer as well as the energy density of the device. Supercapacitors, due to their long cycle life and stability, have numerous applications such as in car audio systems, photo and video cameras, solar lanterns, lightweight electronic fuses, starting power of fuel cells, memory protection of computer electronics etc.

1.3.5 Classification of Electrochemical Capacitors

Based upon the current research and development trends, supercapacitors can be divided into three general classes: 1. Electrochemical double-layer capacitors (EDLC), 2. Pseudocapacitors, 3. Hybrid capacitors. These classes and their sub-classes are listed in figure 1.7 below.

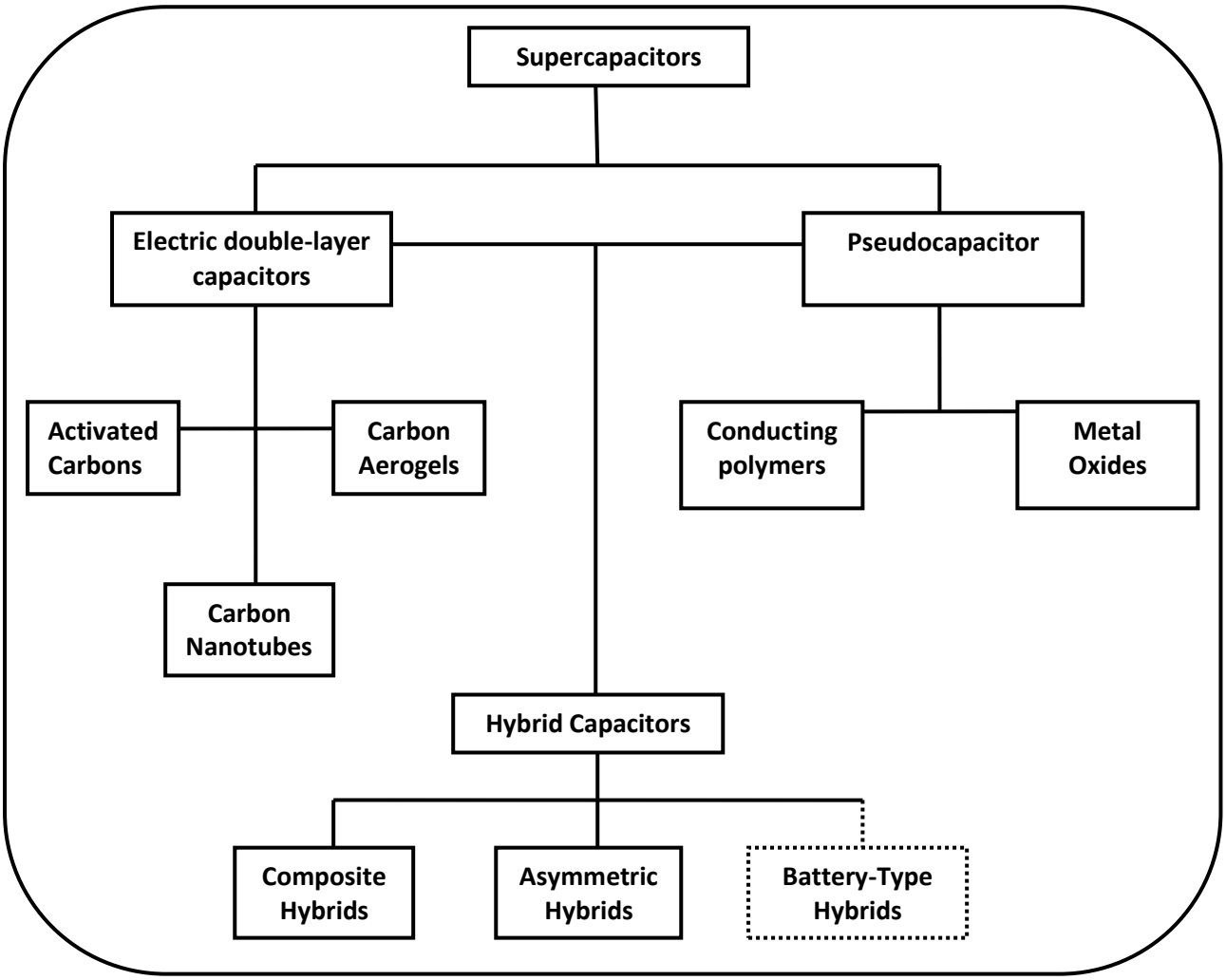

Figure 1.7: Illustration of the taxonomy of supercapacitors [35].

Each class is characterized by its unique mechanism of storing charge. These are respectively, non-Faradaic processes, Faradaic processes and a combination of the two processes. Faradaic processes such as oxidation-reduction reactions involve the transfer of a charge between the electrode and the electrolyte. A non-Faradaic process, in contrast, does not use a chemical mechanism; rather charges are distributed on the surface by physical processes that do not involve the breaking of chemical bonds. This section presents an overview of each of these three classes of supercapacitors and their subclasses distinguished by the electrode material. Electrochemical double-layer capacitors (EDLC) make use of high surface area carbon materials such as activated carbon, carbon aerogels, carbon nanotubes, and carbon nanofibres. Pseudocapacitors employ metal oxide materials such as RuO_2, NiO_2, MnO_2 and conducting polymers such as poly-pyrrole (Ppy), poly-aniline (Pani) and poly (3,4-thylene-dioxythiophene) (PEDOT) as electrode materials [36-39]. Recently, rapid interests in development of supercapacitors that involve the integration of electrochemical double-layer capacitor (EDLC) and pseudocapacitor materials to achieve extremely high performance supercapacitors known as hybrid capacitors is embarked.

1.3.5.1 Electrochemical Double-Layer Capacitors (EDLC)

Much research in electrochemical double-layer capacitors focusing on improved materials that offer high usable surface area has already been developed. Carbon nanotubes, activated carbon, carbon aerogels and other carbon materials, have attracted a great interest from scientists in the industry of supercapacitors. This ground breaking idea of using carbon as a material of choice for the manufacturing of supercapacitor electrode began after the follow up by researchers at Standard Oil of Ohio in 1966 on energy devices, and ever since then, carbon has become one of the most frequently used electrode material in different modifications. The investigation of carbon based electrodes for supercapacitor has largely been influenced by the attractive properties of carbon [40, 41]. Carbon is relatively cheap, and has a surface area of about 2000m^2/g while its porous nature gives carbon based electrodes the ability to store charges in the pores. Pore size in supercapacitor is one of the important factors contributing to the increase in capacitance due to the charge storage. Mesopores are the ideal pores for supercapacitor since the micropores provide a slow rate of electrolyte diffusion while the macropores are too large to retain hydrated ions that are needed for capacitive properties. Frackowiak *et al.* [19] has shown that ionic conductivity relates the mobility of ions inside the pores. The rate of electrochemical accessibility is dictated by the movement of ions inside the pores. Larger pores are easily accessible whereas smaller pores are difficult to access, resulting in the difficulties of ions to move. Frackowiak *et al.* [42] postulated a network of

resistors due to the non-uniformity in resistance throughout the electrode material as a whole. In most applications, the pore structure, especially the pore size, size distribution and pore volume have become the crucial factors determining the applicability of the porous materials [43, 44].

a. Activated Carbons

Activated carbons are very less expensive and posses a larger surface area than other carbon based materials, and due to this, they are most commonly used electrode in electrochemical double-layer capacitors [19]. In the activation process, activated carbons can be modified in such a way that the distribution of pores, pore size and pore volume can be controlled. This material utilizes a complex porous structure composed of different sized micropores, mesopores and macropores to achieve the high surface area. Although capacitance is directly proportional to the surface area, there is some empirical evidence suggesting that, for activated carbons, not all the high surface area contributes to the capacitance of the device. And this is believed to be because of the electrolyte ions that are too large to diffuse into smaller micropores, thus preventing some pores from contributing to charge storage. Shi *et al.* [45] studied the relationship between the surface area, total pore volume, average pore size, pore distribution, capacitance, and showed that there is no linear relationship between the specific capacitance and surface area. Activated carbons achieved by treatment with potassium hydroxide

(KOH) have been reported to display a high oxygen content that influences the electrochemical characteristics [46].

b. Carbon Nanotubes

There is an ongoing interest in the use of carbon nanotubes as a EDLCs electrode material [47]. Electrodes made from this material, commonly are grown as an entangled carbon nanotubes with an open and accessible network of mesopores. As compared to other carbon based electrodes, the mesopores in carbon nanotube electrodes are interconnected, allowing a continuous charge distribution that uses almost all of the available surface area. Therefore, the surface area of carbon nanotube is used more efficiently to achieve capacitance comparable to those in activated carbon based supercapacitors [48].

Carbon nanotubes are highly porous in nature, they are both chemically and thermally stable with high surface area, and due to this extreme characteristics, carbon nanotubes have an edge over other materials being studied as potential supercapacitor electrodes. Ions from the electrolyte have an easy access to the pores of the electrode due to the porous nature of carbon nanotubes. Carbon nanotubes exist in many forms depending on the number of layers they have, and most intensively studied carbon nanotubes are the one having only one layer and are called single-walled carbon nanotube (SWCNT) as well as the one made of many layers called multi-walled carbon nanotube (MWCNT). There are

other types of carbon nanotubes like double-layer carbon nanotube (DLCNT) and triple-layer carbon nanotube (TLCNT) etc. One of the ways to significantly enhancing the capacitance of carbon nanotubes is by first functionalizing them. In order to functionalize carbon nanotubes, harsh conditions are assembled and these involve treatment with nitric acid/ sulphuric acid mixture resulting in defects on the walls of the carbon nanotubes. By functionalizing carbon nanotubes, carboxyl functional groups are added or attached at the surface of the carbon nanotubes and this result in a deviation from the ideal nature of double layer capacitive behavior, hence pseudocapacitance. The use of binders such as PVDF and PTFE have also been reported to enhance the specific capacitance of carbon nanotube based supercapacitors [42].

c. Carbon Aerogels

Carbon aerogels are formed from a continuous network of conductive carbon nanoparticles with interspersed mesoporous. And since they have a favorable characteristic of continuous structure and their ability to bond chemically to the current collector, carbon aerogels do not require the use of an additional adhesive binding agent in their application. The fact that they are binderless electrodes, carbon aerogels have been good candidates for supercapacitor electrodes and have shown to have a lower ESR than activated carbon [49].

1.3.5.2 Pseudocapacitors

Another type of supercapacitor, referred to as a pseudocapacitor, derives its capacitance from the storage of charge in the bulk of a redox material in response to a redox reaction. This fast redox reaction acts like capacitance hence it is called pseudocapacitor. A pseudocapacitor typically stores a greater amount of capacitance per gram than in electrochemical double-layer capacitor (EDLC), as the bulk of the material (not just the surface layer) reacts [9, 46, 50]. An example of a pseudocapacitive material is a conducting polymer (CP), the conductivity of which was first reported in 1963 by Weiss and co-workers [51] in Australia and first utilized in supercapacitors in the mid-1990s. There are other examples such as metal oxides, RuO_2 as well as other oxides from diversity of transition metals [36, 43, 52, 53]. Conway described pseudocapacitance as arising from the surface area in faradaic processes and in such instances, charge, Q, passed during the oxidation and reduction process is continuously and reversibly dependant on the electrode potential [7, 28].

The charging and discharging of pseudocapacitor takes place through the Faradaic processes that involve electron transfer across the electrode-electrolyte interface. Cyclic life of the capacitor is reduced due to the redox processes that take place in the electroactive electrode material. There are two electrode materials that are used to store charge in pseudocapacitors: Metal Oxides and Conducting polymers.

a. Metal Oxides Based Electrochemical Capacitors

Metal oxides have also been explored as possible electrode materials, due to their high conductivity. Most intensively investigated metal oxide is ruthenium oxide (RuO_2) and this was triggered by the fact that, the capacitance of ruthenium oxide is achieved through the insertion and removal, or intercalation, of protons into its amorphous structure. Hu and Chen reported that the specific capacitance of RuO_2 [54] was even as high as 1500 Fg^{-1} in RuO_2/AC composite electrode. However, the cost of ruthenium metal has retarded the commercial acceptance of RuO_2 as electrode materials in electrochemical capacitors. And this limitation has encouraged more researchers to find cheaper materials with similar capacitive behavior to RuO_2 [38, 53, 55, 56].

The capacitance of metal oxides can be enhanced by coupling them with high surface area carbon materials to make nanocomposites which combine double-layer capacitance and pseudocapacitance. It is also reported by Zheng *et al.* [57] in their work that multi-walled carbon nanotubes significantly improved the electrochemical capacitive behaviour of nickel oxide (NiO). Lately, it has been demonstrated that metal hydroxides can achieve higher capacitance as compared to the native metal oxides [58, 59].

b. Conducting Polymer Based Electrochemical Capacitors

Many attempts have been devoted to the use of electronically conducting polymers (ECPs) as electrode materials in electrochemical capacitors. The great interest in such polymers is stimulated by the demand of active materials with high specific capacitance, for maximum specific energy and specific power of the device. Polymeric materials, especially, polyaniline (PANI), polypyrrole (PPy) and polythiopheres have been considered as the most promising materials for supercapacitor application due to their excellent capacity for energy storage, easy synthesis, high conductivities, high energy density and power density, "rapid" charge-discharge processes and good thermal as well as chemical stability as compared to carbon based electrode materials. However, the long-term stability during cycling is a crucial demand for an industrial application of electronically conducting polymers [60, 61].

The drawback to these materials is the swelling and shrinkage that lead to degradation of the electrode during cycling. It occurs because the doping of polymers requires the insertion and removal of ions, which cause a volume change. Thus the mechanical stress in the polymer film relates directly with the cycle-life of polymer based capacitors . These problem has been overcome to some extent by the use of composites structures for example, a combination of electronically conducting polymers and insulating polymers with good mechanical properties such as poly-N(vinyl

alcohol) and polystyrene, though this lowers the conductivity of the composite materials as compared to the pristine conducting polymers. There are two polymer configurations, where one is negatively charged (n-doped) and the other is positively charged (p-doped). Arbizzani *et al.* [60] reported the limited use of negatively doped polymers compared to the positively doped polymers. A combination of n-doped and p-doped configurations, as negative and positive electrodes respectively has been reported to be more promising [36, 62].

1.3.5.3 Hybrid Capacitors

Hybrid capacitors in recent years have been extensively studied as power sources of many electronic devices. The difference from the most known symmetric supercapacitors is that, hybrid capacitors use different active materials for the positive and the negative electrodes. Hybrid capacitors attempt to exploit the relative advantages and alleviate the relative disadvantages of electrochemical double-layer capacitors and pseudocapacitors for better performance characteristics [25, 63, 64]. Hybrid capacitors utilize both faradaic and non-Faradaic processes to store charge, and they have achieved energy and power densities greater than that of double-layer capacitors without the sacrifices in cycling stability and affordability that has limited the success of pseudocapacitors. There are different types of hybrid capacitors that have been intensively investigated: composites hybrid, asymmetric and battery-type.

a. Composite hybrid

Composites electrode put together carbon based materials with other conducting polymer or metal oxide materials for supercacitors electrodes [65, 66]. And they integrate both physical and chemical charge storage mechanism together in a single electrode. The carbon based materials are responsible to facilitate a capacitive double-layer of charge and also provide high surface area backbone that increases the contact between deposited pseudocapacitive materials and electrolyte while the pseudocapacitive materials are able to further increase the capacitance of the composite electrode through Faradaic reactions. Composite electrodes constructed from carbon nanotubes and polypyrrole have exhibited to be successful combination. The capacitance of this composites is higher than those of its components, carbon nanotubes and polypyrrole, due to a three-dimensional distribution of charge [38, 67]. And this has shown to limit the mechanical stress caused by the insertion and removal of ions in the deposited polypyrrole.

b. Asymmetric

This type of hybrid capacitor uses both Faradaic and non-Faradaic processes to achieve high power and energy densities than pseudocapacitors and electrochemical double-layer capacitors [68-70]. In asymmetric supercapacitors, the two electrodes are each made up of different materials, and in particular, the coupling of an activated carbon

as a negative electrode with a conducting polymer as a positive electrode has received a great deal of attention. Arbizzani *et al.* [71] reported the use of p-doped poly (3-methylthiophene) as a positive electrode and activated carbon as a negative electrode.

c. Battery Type

Just as the asymmetric hybrids, battery type hybrids combine two different electrodes. Battery type hybrids are distinctive in blending a supercapacitor electrode with a battery electrode. This special configuration reflects the demand for higher energy supercapacitors and higher power batteries, combining the energy characteristics of batteries with the power, cycle life and recharging time of supercapacitors. The most common materials for the battery electrode are metal hydroxides. Not much research has been done on this type of supercapacitor despite the fact that it has been forecasted to bridge the gap between the batteries and supercapacitors [28, 72].

1.4 Carbon Nanotubes

Interesting properties of nanotubes have caused many researchers and companies to consider using them in several fields. The hollow tubular nanostructure of carbon nanotubes have been rediscovered in 1991 by Sumio Iijima, who was an electron microscopist of NEC in Tsukuba, Japan [73]. The discovery of carbon nanotubes remains unclear as some researchers believe that this material existed ever since 1952 by Marc Monthioux and Vladimir Kuznetsov [74]. The well known types of carbon nanotubes is in their singly-walled and multi-walled known as a single-walled carbon nanotube (SWCNT) and multi-walled carbon nanotube (MWCNT) respectively, though there are other types such as double-walled carbon nanotube (DWCNT), Torus, nanobud etc, that have not been intensively applied in many specializations [37, 75-77]. Carbon nanotubes attained many applications from since they were discovered. Medical researchers use this smart material to deliver drugs directly to the diseased cells due to the fact that they are able to penetrate easily the membranes such as cell walls [76]. Multi-walled carbon nanotubes are made up of concentric cylinders of graphite that resembles the graphite sheet with an adjacent layer separation of 0.34 nm and diameter of 1 nm [78-80]. Single-walled carbon nanotubes are relatively similar to the ideal fullerenes. The connectivity between these two interesting forms of carbon lies in their functionality, with carbon nanotubes acting as a nanowires and carbon fullerenes as quantum dots. Applied quantum chemistry, specifically orbital hybridization, best describes the chemical

bonding in nanotubes. They are composed of sp^2 bonds that are similar to those of graphite and this provides the unique strength of carbon nanotubes. Smalley and co-workers in their work gave a detailed synthesis of bundles of aligned single-walled carbon nanotubes (SWCNTs) with a yield of more than 70% [81].

1.4.1 Structure of Carbon Nanotubes

Carbon nanotubes are long tubes that are normally described as being entangled at the surface of its support. The tubular structure of carbon nanotubes makes them unique among different forms of carbon, and they can thus be exploited as an alternative material for catalysis. Figure 1.8 gives an illustration of a typical SEM image of normal carbon nanotubes.

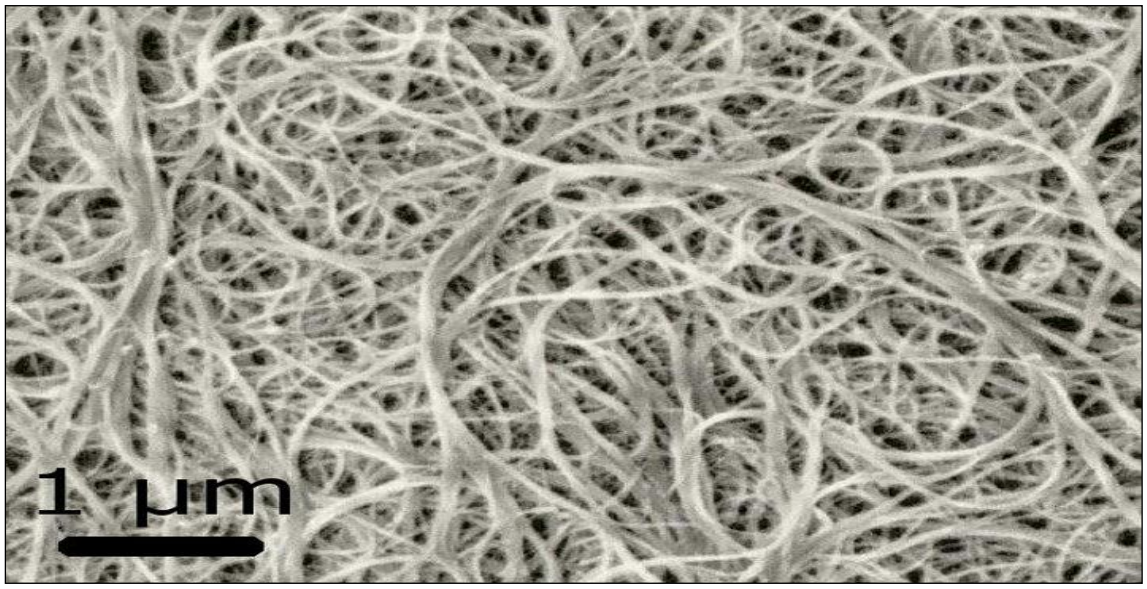

Figure 1.8: SEM image of typical entangled carbon nanotubes [81].

Carbon nanotubes are made up of sp^2 bond, with each atom joined to three adjacent atoms as in graphite [82]. The tube can be understood as a rolled-up grapheme sheets. There are several ways in which carbon

nanotubes can be synthesized, namely, Laser ablation, chemical vapor deposition (CVD), and arch-discharge [83, 84]. There are three distinct ways that the sheet of graphene can be folded up to form carbon nanotubes, and figure 1.9 gives the illustration of the three types a carbon nanotubes that can exist.

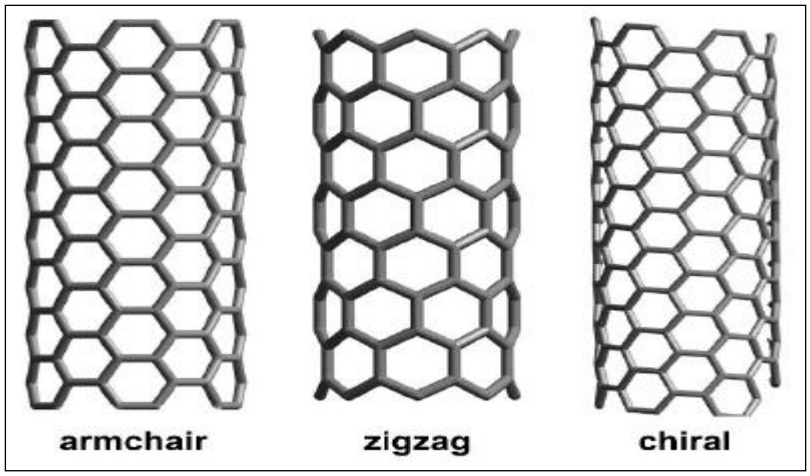

Figure 1.9: An illustration of three forms a carbon nanotube can exist [85].

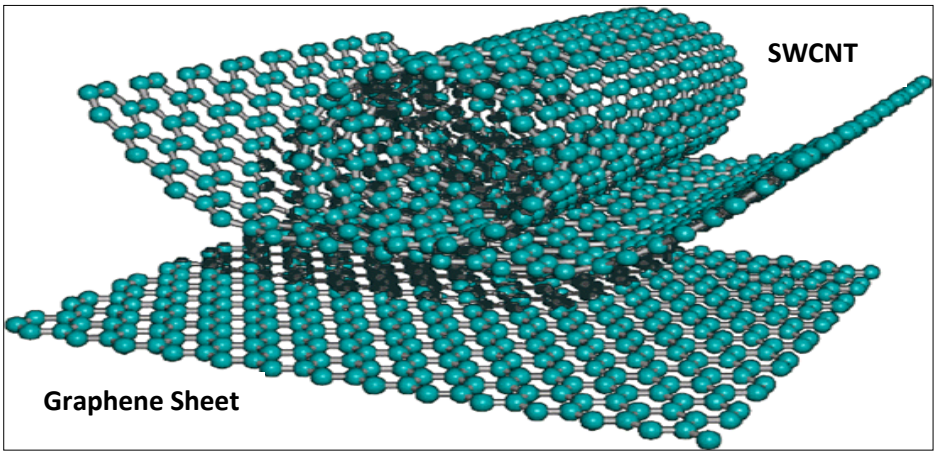

Figure 1.10: Representation of a 2D graphene sheet illustrating the formation of SWCNT from graphene sheet [82].

1.4.2 Properties of Carbon Nanotubes

The properties of single-walled and multi-walled carbon nanotubes are in general the same, although single-walled carbon nanotubes exhibit superior mechanical strength, thermal and electrical conductivity over multi-walled carbon nanotubes [57, 86, 87]. The physical properties of single-walled carbon nanotubes have made them an extremely attractive material for the manufacturing of nano devices while they also have shown to be stronger than steel as estimates for the Young's modulus approaches 1Tpa [76, 77, 88]. Their electrical conductance is comparable to copper with anticipate current densities of upto 10^{13} A/cm^2 and a resistivity as low as 0.34×10^{-4} Ω.cm at room temperature. They also show high thermal conductivity of (3000-6000 W.m/K). Multi-walled carbon nanotubes range from double-walled carbon nanotubes into many walled nanotubes to carbon nanofibers. They are thicker and longer than single-walled carbon nanotubes. The electronic properties of carbon nanotubes structures are based on their chirality or twist in the structure of the tube. Wong *et al.* [87] matched the theoretically predicted properties of carbon nanotubes with experimental data using the atomic force spectroscopy (AFM). And knowledge opened the way for researchers to link the materials with various possible applications. The most prominent properties of carbon nanotubes that make them ideal for supercapacitor electrodes are their surface area. Peigney and co-workers [75] reported the specific surface area of individual carbon nanotubes and bundle of carbon nanotubes as a function of tube diameter (the number of walls and the

number carbon nanotubes in a bundle). One of the great deal of carbon nanotubes is their ability to be dispersed in solvents. Dispersion of carbon nanotubes in water form a stable suspension where precipitation occurs. Therefore, functionalization of carbon nanotubes opens a way for research into their use as composites with other materials. Harsh conditions of acid treatment are the most employed way of functionalizing carbon nanotubes into their carboxylic or sulfonated derivatives depending on the application. Recently, many researchers prefer to use microwave to functionalise carbon nanotubes due to the fact that is not time consuming. Wang *et al.* [89] reported water dispersed carbon nanotubes using microwave synthesis.

1.4.3 Applications of Carbon Nanotubes

The flexibility and strength of carbon nanotubes expose them to various applications such as nanotechnology engineering. Carbon nanotubes are being considered for energy production . Supercapacitors, fuel cells and lithium-ion batteries [73, 88, 90, 91] make use of carbon nanotubes due to fact that they have small dimensions, a smooth surface topology and perfect surface specificity since only the basal graphite planes are exposed in their structure. The rate of electron transfer at carbon electrodes ultimately determines the efficiency of fuel cells and this depends on various factors such as the structure and morphology of carbon nanotubes material used in the electrodes. Due to this fast electron transfer, carbon nanotubes are also widely used in electrochemical

sensing. Carbon nanotubes have found themselves applied as negative electrode in lithium-ion batteries which plays a role in the formation of a double layer. Chidembo *et al.* [35] recently reported the use of multi-walled carbon nanotubes with metallophthalocyanines with high specific capacitance of 981F/g. Much literature is available on the use of carbon nanotube composites for detection of dopamine [14, 92, 93].

1.5 Metallophthalocyanines

Phthalocyanines (Pcs) are 18п-electron aromatic macrocycles that have a characteristic blue green colour that makes them materials of choice for making dyes. Phthalocyanine have adopted its name from Greek where Phthal originated from Naphtha which is a Greek word meaning rock oil, while cyanine means blue. They consist of 16 carbon and 8 nitrogen atoms with more than 70 different metals and non metals that can be incorporated in them [94, 95]. Phthalocyanines are special class of compounds that have similar structure as tetraazoporphyrin with additional four fused benzo rings [96-105]. They have been accidently discovered in the 1900s at the Grangemouth plant for Scottish Dyes Ltd [10, 106-109]. These classes of molecule have high extinction coefficient which are of order of 10^5 M^{-1} cm^{-1} and are both thermally and chemically stable. Metallophthalocyanines attracted enormous attention world-wide because of their interesting properties like chemical inertness, very colouring properties, catalytic activity, semi-conductivity as well as photoconductivity etc.

The ability of incorporating ring substituent in the peripheral and non-peripheral position with its properties like solubility that can be varied by changing the central metal ions, axial ligand have resulted this class of compound into wide range of applications [106]. The metal ion in the central cavity of the phthalocyanine moiety provides the ability to study redox chemistry on this compound. Reduction and oxidation reactions of this

molecules occurs either at the central metal atom, in the phthalocyanine ring itself or on both. Synthesis of phthalocyanines can be achieved using different routes depending on the desired type of phthalocyanine; metal free, symmetrical and asymmetrical metallophthalocyanines. Various precursors such as phthalonitrile [110], phthalic acid, phthalic acid anhydride, phthalimide [96], diiminoisoindoline and o-cyanobenzamide [111] have been developed for this synthesis of metallophthalocyanines complexes. The structure of metallophthalocyanine (Ni^{2+} as a central metal) is illustrated on figure 1.11.

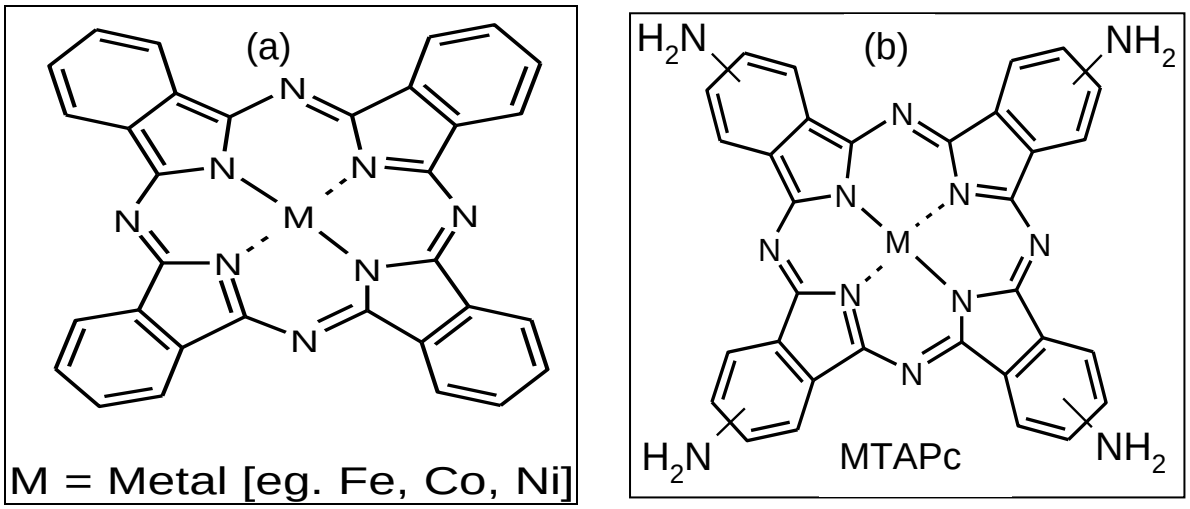

Figure 1.11: Molecular structure of (a) Metallophthalocyanine and (b) Metallo-tetraaminophthalocyanine (MTAPc) complex.

1.5.1 Application of Phthalocyanines

Over the years, phthalocyanines complexes have attracted many applications in area such as catalysis, sensors and photodynamic therapy [112-116]. Due to their properties such as not being soluble in aqueous solvents but soluble in some organic solvents, phthalocyanines have recently applied in ink jet printing, electrophotography, electrochemical sensors and energy storage such as supercapacitors [15]. Extensive research work has been carried out to improve the electrical conductivity of phthalocyanines via doping mechanism and polymerization methods. And this modification opens even more extra application for this tremendous class of complexes. Phthalocyanines complexes have drastically established themselves as excellent electrocatalysts for several organic and inorganic analytes [117-121] and have been intensively reviewed by Ozoemena and Nyokong [14, 107, 108].

1.6 Microscopic and Spectroscopic Techniques for Electrochemical Capacitors Materials

1.6.1 Scanning Electron Microscopy (SEM)

A scanning electron microscopy (SEM) is a type of electron microscope that make images of a sample by scanning the sample with a high energy beam of electrons in a raster scan manner [122, 123]. The electrons interact with the atoms of the sample, producing signals that contain significant information about the sample's surface topography, electrical conductivity with other properties such as the sample's composition. The discovery of SEM began in 1935, when an image of silicon steel was obtained by Max Knoll, illustrating electron channeling contrast. And in 1937, further development was performed by Manfred von Ardenne [124], on the physical principles of the scanning electron microscopy (SEM) and beam specimen interactions. The SEM was further developed by Professor Sir Charles Oatley and his postgraduate students, who first marketed it in 1965 as the "Stereoscan". Scanning electron microscopy is particularly important in the field of nanotechnology and supercapacitor studies where nanomaterials are frequently used.

Scanning electron microscopy (SEM) instrument allows observation of nanomaterials on a very small scale ranging from nanometers to micrometers. On its operation, SEM has an electron gun at the top of its column that generates a beam of electrons which are attracted through

anode, condensed with condenser lens and focused with objective lens as a fine point onto the sample. These electrons are then collected by a secondary detector or a backscatter detector. Then the secondary detector produces a clear and focused topographical image of the sample while the backscatter reflects an elemental composition of the sample and is used for energy dispersive X-ray analysis. Scanning electron microscopy (SEM) provides useful detailed information on supercapacitor electrodes such as the porous structure of the electrodes and the alignment of the nanometerials that are essential for the storage of charge in the electrical double layer [122, 123, 125-127].

1.6.2 Transmission Electron Microscopy (TEM)

One of the widely used microscopic techniques whereby a beam of electrons is transmitted through an ultra-thin specimen, interacting with the specimen as it passes through is known as transmission electron microscopy (TEM) [13, 128]. An image in transmission electron microscopy (TEM) is formed from the interaction of the electrons that are transmitted through the specimen, and then the image is then magnified and focused onto the imaging devices with photographic film or to be detected by a sensor. The types of imaging device and sensor that detect the focused image are fluorescent screen and CCD camera respectively [129-131]. The

first transmission electron microscopy (TEM) was built by Max Knoll and Ernest Ruska in 1931. They developed the first TEM with resolving power that was greater than that of light in 1933 and then it was commercialized at around 1939. Transmission electron microscopy (TEM) is designed in a way to reveal the internal details of interests such as the morphology (shape, size and arrangement of the particle), the crystallographic information (the atom arrangement) as well as the compositional information (the elemental composition) of the sample analyzed. TEM forms a major analysis method in a range of scientific fields, in both physical and biological sciences[132-135]. TEM find application in cancer research, virology, material science as well as pollution, nanotechnology and semiconductor research. Transmission electron microscopy (TEM) when operated at smaller magnifications, it gives image contrast which resulted due to absorption of electrons in the material.

1.7 Electrode Fabrication Techniques

1.7.1 Ways for Modification on the Surface of the Electrode

•Successive Ionic Layer Adsorption and Reaction (SILAR). In this technique, growth is performed (layer-by-layer) by sequentially dipping the substrate into stable precursor solutions [136]. Each reaction involves rinsing in between to remove the unabsorbed ions from the surface of the electrode. For a traditional SILAR technique, one SILAR cycle is made up of four steps: the substrate is (i) immersed in a reaction solution containing the aqueous cation precursor, (ii) rinsed with water, (iii) then be immersed in the anion solution, (iv) and finally be rinsed more with water. The interest of this method lies within the fact that is extremely simple, fast, and cheap, and suitable for large area of deposition of any configuration [137-139].

SILAR also allows the easiness to control the thickness of the film by monitoring and counting the deposition cycles. This technique has been widely employed in various studies especially in supercapacitors and in surface chemistry. Intense studies have been conducted on this method so as to refine as well as to gain knowledge on its effect towards thin film deposition [140, 141].

•**Electrochemical Deposition.** Is a process by which a film of solid metal is deposited from a solution of ions onto an electrically conducting electrode surface. The electrode substrate is immersed in an electrolyte solution containing one or more dissolved salts or other ions that permit the flow of electricity and subjected to electrochemical treatment. Used in electroplating; by coating a conductive metal with a thin layer of material [44, 57, 142-145].

•**Pulsed Laser Deposition.** Is a technique where a high power pulsed laser beam is focused inside a vacuum chamber to strike a target of the material that is to be deposited. The material is vaporized from the target, inside a plasma plume, which deposits it as a thin film on a substrate (e.g silicon wafer facing the target) [146-149].

•**Dip Coating.** In this technique, the substrate is immersed in a solution for a period of time and be allowed to form film on the surface of the electrode by adsorption, and be allowed to dry. Normally the coating is being done at the constant speed. The thin layer deposits itself on the substrate while the substrate is pulled up. Excess liquid is then drained from the surface of the substrate while the solvent evaporate [150].

•**Covalent Bonding.** This type of modification involves the linking agents which are being utilized to covalently attach one of several monomolecular layers of the chemical modifier to the surface of the electrode [151, 152].

1.8 Nickel Foam Electrode

Nickel foam is a low density material that is very permeable and also contains various applications. Nickel foam is made up of the transition metal known as nickel. Nickel is a silvery white, conductor of heat and electricity [153]. This transitional metal is the 28th element on the periodic table. The outstanding characteristic of nickel foam is that, it is a very high porous material with its void spaces comprising almost 75-95% of the volume and its typical porosity is illustrated in Figure 1.12

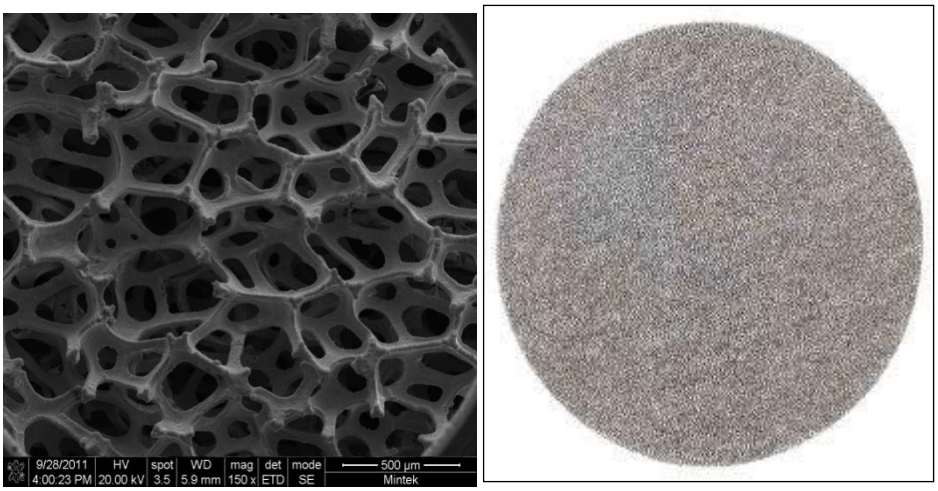

(a) (b)

Figure 1.12: Representation of the (a) SEM image and (b) disc form of the nickel foam electrode.

Many scientists who engage themselves in electroanalysis are continuously seeking new electrocatalytic surfaces so as to achieve modified electrode surfaces that serve as electrocatalytic platforms.

Various experiments have been reported using metal oxide especially nickel oxide modified nickel foam electrodes [19, 50]. Metallic foams have obtained variety of applications in various fields such as heat exchangers, energy adsorption, lightweight optics as well as a substrate for catalysts that require a large surface area. Due to the unique open cell structure, low pressure drop, intrinsic strength and resistance to thermal shock, nickel foam has been used in energy processes as a substrate for various materials ranging from nano to micro in structures [31, 137, 154-157]. Therefore, because of these unique properties, nickel foam has been employed in this study as a current collector substrate.

1.9 Electrochemical Characterization of Electrochemical capacitor Electrodes

1.9.1 Cyclic voltammetry (CV)

Cyclic voltammetry also known as CV is a type of potentiodynamic electrochemical technique whereby measurement of the current response of an electrode to a linearly increasing and decreasing potential cycle is performed [1, 8, 16]. During a cyclic voltammetry experiment, the potential of an electrode is scanned linearly from an initial potential to a final potential and then back to the initial potential. The potential at which the peak current occurs is known as the peak potential (E_p) where the redox species has been depleted at the electrode surface and the current is diffusion limited. The magnitude of the Faradaic current (I_{pa} - anodic peak current) or (I_{pc} - cathodic peak current), gives an indication of the rate at which electrons are being transferred between the redox species and the electrode [158-160].

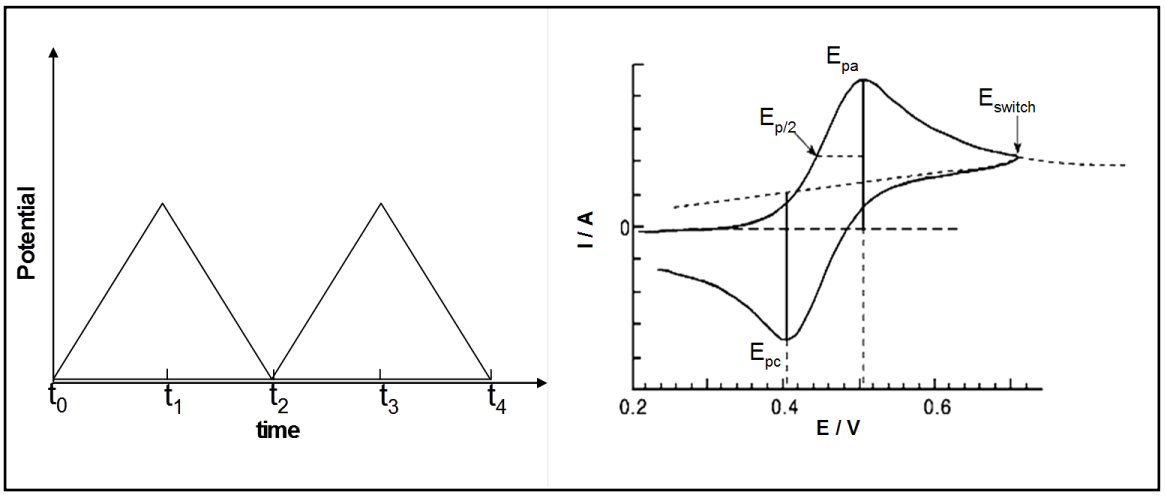

Figure 1.13: Representation of the potential-time waveform and a typical cyclic voltammogram of a reversible redox process in supercapacitors [18].

In this technique, the electrode potential ramps in a linear form against time and this ramping is known as the measurements scan rate (V/s). Cyclic voltammetry is used to reveal the reactivity of new materials and as well as providing information on the potential at which oxidation or reduction processes occur, the oxidation state of the redox species, the total number of electrons involved in the process, how fast is the electron transfer, as well as other possible chemical processes associated with the electron transfer etc. Cyclic voltammetric processes could be reversible, quasi-reversible and irreversible.

1.9.1.1 Reversibility

A reversible process is one in which the electron transfer process is rapid, and the electroactive species that is being oxidised (or reduced) in the forward scan is in equilibrium with the electroactive species that is being reduced (or oxidised) in the reverse scan (equation 1.1). Reversibility is a direct and straight forward means of probing the stability of an electroactive species. An unstable species reacts as it is formed and hence produces no current wave in the reverse scan whereas a stable species remains in the vicinity of the electrodes surface and produces a current wave of opposite polarity to the forward scan. Larger differences or asymmetric reduction and oxidation peaks are an indication of irreversible reactions. Irreversibility is a result of slow exchange between the redox species and the working electrode [161-166]. The appearance of the reversible behavior of individual species depend on the relative value of electron transfer rate (k_s) and mass transport, since there is no ideal equilibrium existing between the surface and bulk concentrations, because reactants are transported continuously to the surface of the electrode by diffusion (see equation 1.2 above). The peak current is given by the Randles-Sevcik equation at 25°C [16, 167, 168]:

$$i_p = \left(2.69 \times 10^5\right) n^{3/2} AC\left(D\nu\right)^{1/2} \qquad (1.9)$$

where, i_p = peak current (A)

n = number of electrons transferred

A = electrode area (cm^2)

C = concentration ($mol\ cm^{-3}$)

D = diffusion coefficient ($cm^2\ s^{-1}$)

v= scan rate (Vs^{-1})

The peak current, i_p for irreversible process is given by equation 1.10.

$$i_p = \left(2.99\times10^5\right)n\left[(1-\alpha)n\right]^{1/2}Ac\left(D\nu\right)^{1/2} \qquad (1.10)$$

Where α is the rate of electron transfer, and other symbols are defined above in equation 1.9.

1.9.1.2 Irreversibility

The process of irreversibility in electrochemistry is brought about when the charge-transfer step is very slow, i.e., the standard rate constant (k_s) as well with the exchange current density (j_o) become very small compared to scan rate [27, 169-171]. For an irreversible process, only forward oxidation (reduction) peak is observed but at times with a weak reverse reduction (oxidation) peak as a result of slow electron exchange or slow chemical reactions at the electrode surface. In this case the anodic and cathodic reactions are never simultaneously significant. For one to observe any current, the charge-transfer reaction has to be strongly activated either in cathodic or in anodic direction by applying

overpotential. These processes are characterized by a shift of the peak potential with the scan rate. In case of a totally irreversible system, ΔE_p is calculated from equation 1.11

$$\Delta E = E^o - \frac{RT}{\alpha n_a F}\left[0.78 - \ln\frac{k^o}{D^{1/2}} + \ln\left(\frac{\alpha n_a F}{RT}\nu\right)^{1/2}\right] \qquad (1.11)$$

Where α is the electron transfer coefficient of the rate determining step and n_α is the number of electrons involved in the charge transfer step and k^o is the standard electrode reaction rate constant in cms^{-1}. At 25°C, the peak potential and the half-peak potential differ by 0.048 Vαn. Hence, the voltammogram becomes more drawn-out with the decrease in αn. In an irreversible process, only forward oxidation or reverse reduction peak is observed. It is common to observe a weak reverse peak at increased scan rates during forward oxidation at times, because of slow electron exchange . The Nernst equation is not applicable in the case of irreversible process. This is due to the fact that the rate of electron transfer is insufficient to maintain surface equilibrium and thus the oxidized and reduced species are not at equilibrium. The peak current, I_p for an irreversible process can be calculated from equation (1.12):

$$I_p = \left(2.99x10^5\right)n\left[(1-\alpha)n\right]^{1/2} AcD^{1/2}\nu^{1/2} \qquad (1.12)$$

Where α denotes the electron transfer coefficient and n the number electrons transferred in the rate determining step.

1.9.1.3 Quasi-reversibility

Contrasting the reversible process in which the current is purely mass-transport controlled, currents resulting from quasi-reversible process are controlled by a mixture of mass transport and charge transfer kinetics [12, 159, 172]. Since mass transport plays a major role in controlling the concentration of the redox couple, the expressions for reversible processes also apply for quasi-reversible processes.

The process occurs when the relative rate of electron transfer with respect to that of mass transport is not enough to maintain Nernst equilibrium at the surface of the electrode. For quasi-reversible process, the current peak i_p increases with $\upsilon^{1/2}$ but not in a linear relationship and $\Delta E > 0.059/n$ V [167, 170]. When cyclic voltammetry is applied to immobilised redox systems, distinct peak shape and peak currents may be observed. The peak current now becomes directly proportional to the scan rate.

$$I_p = \frac{n^2 F^2 \Gamma A \nu}{4RT} \qquad (1.13)$$

Where the peak current I_p is directly proportional to v, the scan rate, and Γ the surface concentration for the immobilised redox system. A plot of log I_p vs. log v allows diffusion controlled processes and processes involving surface immobilised redox systems to be distinguished. For diffusion controlled process, the slope of the plot is 0.5 and for a surface

confined (adsorption) process the slope of the plot is 1. The slight differences in three cyclic voltammetric processes are summarized in Table 1.1.

Table 1.1: The diagnostic criteria for reversible, irreversible and quasi-reversible cyclic voltammetric process

Parameter	**Cyclic Voltammetry Process**		
	Reversible	*Irreversible*	*Quasi-reversible*
E_p	Independent of ν	Shifts cathodically by $30/\alpha n$ mV for a 10-fold increase in V	Shifts with ν
$E_{pc} - E_{pa}$	~ 59/n mV at 25°C and independent of ν	_	May approach 60/n mV at low ν but increases as ν increases
$i_p / \nu^{1/2}$	Constant	Constant	Virtually independent of ν
i_{pa} / i_{pc}	Equals 1 and independent of ν	No current on the reverse side	Equals 1 only for α = 0.5

1.9.2 Galvanostatic Charge-Discharge (CD)

The Galvanostatic charge /discharge (CD) technique is one of the widely used techniques for determination of a specific capacitance of the supercapacitor electrodes [34, 40]. The concept of Galvanostatic charge/discharge is very similar to that of potentiodynamic electrochemical measurements known as cyclic voltammetry. An excitation signal is applied to the system and causes the potential to scan from the starting potential to the final potential and back again resulting in the first scan. In this technique, current can be manipulated so as to give different current densities that can be utilized to calculate specific capacitance of the electrode material being analyzed.

A typical constant charge/discharge profile of an ideal supercapacitor illustrated on figure 1.14 below is characterized by linear charging and discharge profiles. Furthermore, a mirror image of the charging curve and the discharging curve indicates a typical supercapacitor [173, 174]. A supercapacitor that is characterized by pseudocapacitance exhibits non-linear charge and discharge profiles.

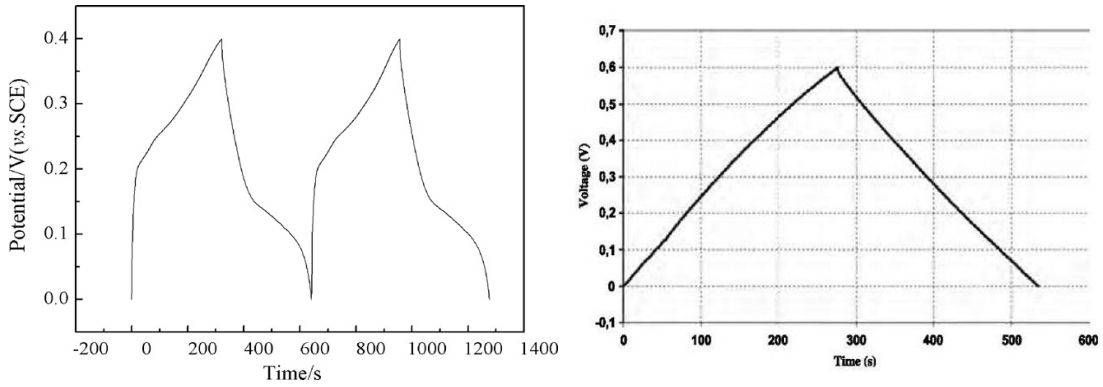

Figure 1.14: Typical constant charge/discharge profile of cobalt nanowire based supercapacitor.

Galvanostatic charge/discharge experiments are generally helpful in the determination of the specific capacitance, specific energy as well as specific power and are widely used by many researchers [173-175]. Obtaining the calculated values of these specific energy and specific power using equation 1.15 and 1.16 enables one to plot Ragone plots which results from plotting specific power against specific energy.

$$SC(F/g) = \frac{[i(A) \times \Delta t(s)]}{[\Delta E(V) \times m(g)]} \quad (1.14)$$

$$SE(Whkg^{-1}) = \frac{[i(A) \times t(s) \times \Delta E(V)]}{m(kg)} \quad (1.15)$$

$$SP(Wkg^{-1}) = \frac{[i(A) \times \Delta E(V)]}{m(kg)} \quad (1.16)$$

Where *i* is the discharge current in ampere,

Δt is the discharge time in seconds,

ΔE, the potential difference in volts and

m, the mass of the electroactive material in grams.

(For specific energy and specific power the mass m is in kg).

1.9.3 Electrochemical Impedance Spectroscopy (EIS)

Electrochemical impedance spectroscopy (EIS) is a powerful technique for the characterization of electrochemical systems. The reliability of EIS comes from the fact that, with its single experimental procedure encompassing a sufficiently broad range of frequencies, the influence of the governing physical and chemical phenomena may be isolated and be differentiated at a given applied potential. EIS has found numerous applications with a tremendous increase in popularity in recent years. It is used mostly in the characterization of batteries, fuel cells, coatings, corrosion phenomena, interfacial electrochemistry, sensor, liquid-liquid interfaces and recently in supercapacitor materials. Electrochemical impedance spectroscopy studies the variation of total impedance of an electrochemical cell with frequency of a small-amplitude AC perturbation. EIS also provides a wealth of information when it comes to the study of interfacial and pseudocapacitance of the electrode structure [176, 177].

1.9.3.1 Principles of Electrochemical Impedance Spectroscopy

The fundamental approach of impedance measurements is to apply a small amplitude sinusoidal excitation signal to the system under investigation and record the response (current or voltage or any signal of

interest). Ohm's law gives a simple relation between dc-potential (E) and dc-current (I)

$$R = \frac{E}{I} \tag{1.17}$$

where R, is a resistor. Ohms law is only limited to one circuit element which is an ideal resistor. Other elements come into existence when performing experiments and these elements have to be considered as well. And due to this factor, equation 1.17 changes into equation 1.18 when an ac-signal is applied to a cell.

$$Z(\omega) = \frac{\Delta E(\omega)}{\Delta I(\omega)} \tag{1.18}$$

where Z (ω) is the complex impedance. ΔE (ω) is the change in potential and ΔI (ω), the change in current. In the following figure 1.15, a non-linear current or potential curve against time for a theoretical electrochemical system is illustrated. The impedance is typically measured by applying an AC potential to an electrochemical cell and measuring the current through the cell. Application of a sinusoidal potential excitation to the electrode interface results the cell's response to be pseudo-linear. The current response leads or lags the voltage by a phase angle of θ.

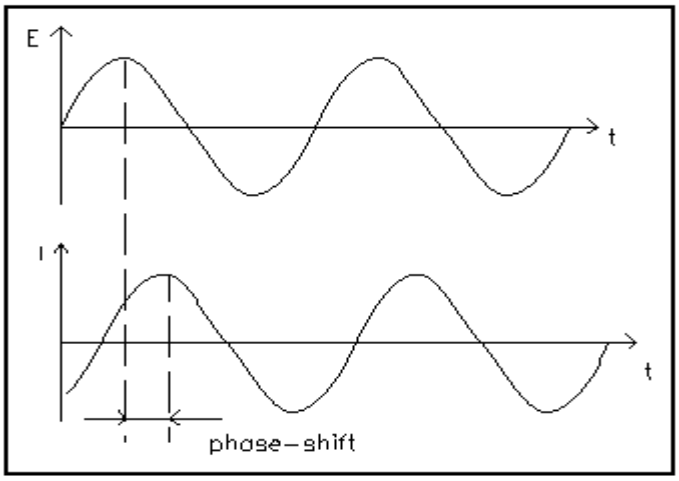

Figure 1.15: Sinusoidal current and potential against time curve for a theoretical electrochemical system

The capacitance of the electrode is determined using equation 1.19. The impedance of a capacitor is a function of frequency and has only an imaginary part. A capacitor's impedance decrease as the frequency is increased.

$$Z = \frac{1}{j\omega C} \qquad (1.19)$$

The total impedance is given by the following equation that incorporates both the real and imaginary components of the impedance. The angular frequency ω is expressed as $2\pi f$.

$$Z(\omega) = Z'(\omega) + j.Z''(\omega) \qquad (1.20)$$

Z is the total impedance, Z', the imaginary impedance and Z″ the real impedance. Z represent a vector quantity that is plotted in the plane with

either polar or rectangular coordinates as shown below in figure 1.16 with $\theta = \tan^{-1}(Z''/Z')$. The phase difference, θ, between the voltage and the current is equal to zero for a pure resistor and 90° for a pure capacitor.

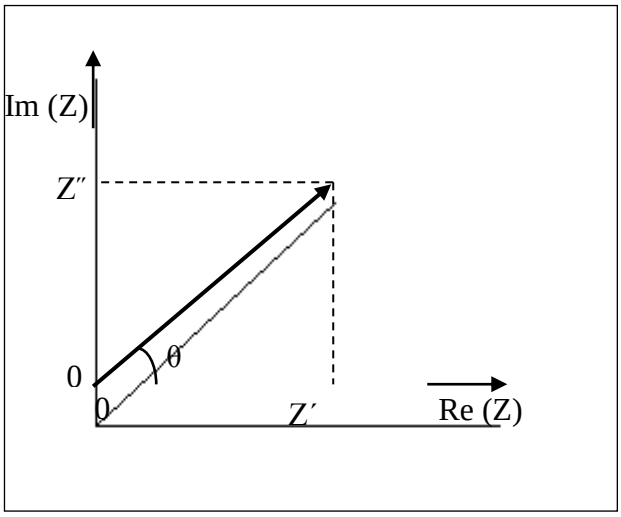

Figure 1.16: Plot of Z″ versus Z' representing Z with rectangular or polar coordinates.

1.9.3.2 Data representation of EIS

In Electrochemical impedance spectroscopy, electrical equivalent circuits are utilized for the analysis of the data resulted from the impedance, and also data within the circuit, simple electric elements such as resistance (R) and capacitance (C) are connected to model the electrochemical processes [176, 177]. The resistance obtained in the equivalent circuit represents the electrical conductivity of the electrolyte and the constant phase element (CPE) caused by the charge which is in excess at the electrode-electrolyte interface. Randles equivalent circuit represented in Figure 1.17 is the most widely used circuit to fit electrochemical data. The

Randles equivalent circuit shows the solution or electrolyte resistance, R_S connected in series to the parallel combination of charge transfer resistance, R_{CT} and the CPE. In other systems the reaction rate might be controlled by transport phenomenon and this effect needs to be taken into consideration, the measured impedance can be explained by the component that depends on the conditions of the transport or diffusion of electroactive species [178]. This component is called the Warburg impedance (Z_W) and is connected in series to the charge transfer resistance.

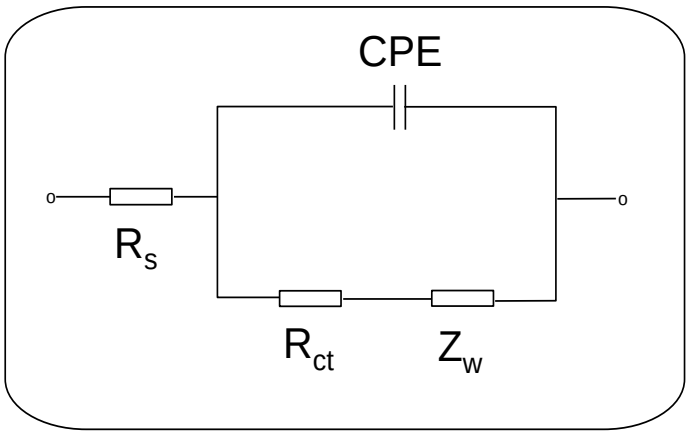

Figure 1.17: Randles circuit representing and electrochemical system.

In electrochemical impedance measurements, the relationship between the impedance and frequency is very useful and can be displayed in various ways for example Nyquist plot illustrated on figure 1.18a or Bode plot illustrated by figure 1.18b [178-181]. Nyquist plot is parametric plot of a transfer function in automatic and signal processing (displays Z_{Im} *vs.* Z_{Re} for different values of ω) whereas Bode plot is a graph of the transfer

function of a linear, time-invariant system versus frequency (is a plot of log \Z\ and θ against log ω). Bode plots are very useful and give more explicit information regarding frequency. Both these representations will be dealt with in more detail in chapter 3-6. EIS data is commonly analyzed by fitting it to an equivalent electrical circuit model. Most of the circuit elements in the model are common electrical elements such as resistors, capacitors, and inductors. A summary of all the circuit elements is given in the table 1.

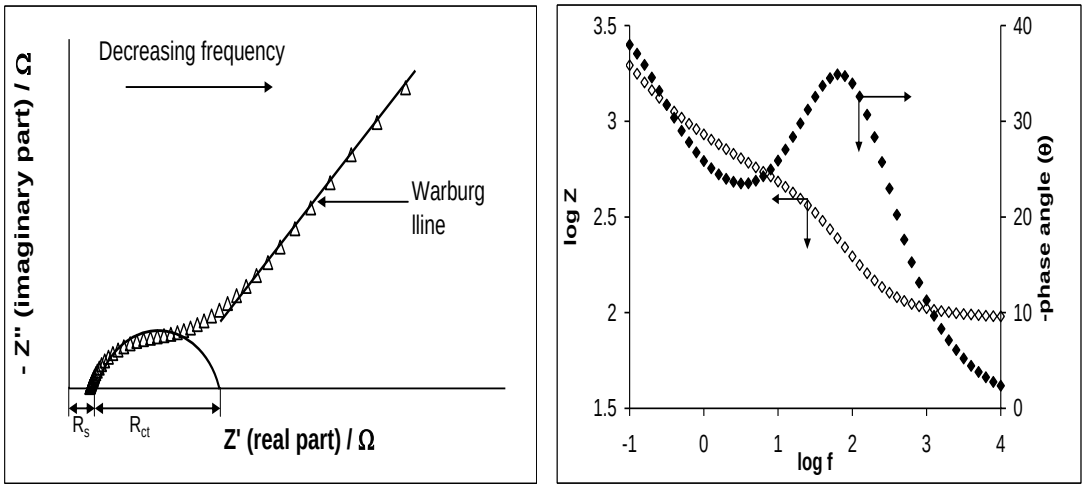

(a) (b)

Figure 1.18: Nyquist (a) and the corresponding Bode plot (b) for the Randles equivalent circuit.

Table 1.2. A summary of some of the circuit elements used in the description of equivalent circuits.

Element	**Symbol**
Charge transfer Resistance	R_{CT}
Solution Resistance	R_S
Capacitance	C
Inductance	L
Constant Phase Element	Q
Warburg Diffusion	W

Despising the sensitivity, non destructive as well as being accurate, EIS, like any other technique, has its advantages and limitations. This technique it is not always understood and this might be due to the fact that, existing reviews on EIS are often very difficult to understand by non-specialist. However this technique is not a stand alone technique but needs to be complimented by other techniques such as cyclic voltammetry and charge discharge [179, 181]. EIS is used in situ and has a fast rate of generating results. The interpretation of EIS data can also prove to be complex. In conclusion, the three electrochemical techniques discussed above when coupled together; provide useful information for analysis and study on supercapacitor electrodes.

REFERENCES:

1. A. J. Bard and L. R. Faulkner, *Electrochemical Methods: Fundamentals and Applications*, John Willey & Sons, New York, 1996.
2. H. Bach and F. Baucke, *Electrochemistry of glasses and glass melts: including glass electrodes*, Springer Verlag, 2001.
3. J. M. Campina, A. Martins and F. Silva, *The Journal of Physical Chemistry C*, 2007, 111, 5351-5362.
4. H. S. White, J. D. Peterson, Q. Cui and K. J. Stevenson, *The Journal of Physical Chemistry B*, 1998, 102, 2930-2934.
5. W. Schmickler, *Interfacial Electrochemistry*, Oxford University Press, Inc, New York, 1996.
6. I. Burgess, B. Seivewright and R. B. Lennox, *Langmuir*, 2006, 22, 4420-4428.
7. B. E. Conway, V. Birss and J. Wojtowicz, *Journal of power sources*, 1997, 66, 1-14.
8. A. J. Bard, G. Inzelt, F. Scholz and C. Ebooks, *Electrochemical dictionary*, Springer Heildelberg, Berlin, 2008.
9. A. E. Kaifer and M. GÃ³mez-Kaifer, *Supramolecular electrochemistry*, Wiley Online Library, New York, 1999.
10. M. P. Siswana, K. I. Ozoemena and T. Nyokong, *Electrochimica Acta*, 2006, 52, 114-122.
11. J. Pillay and K. I. Ozoemena, *Electrochimica Acta*, 2007, 52, 3630-3640.

12. E. R. Brown and R. F. Large, *Physical Methods of Chemistry. Electrochemical Methods* Wiley-Interscience, New York, 1971.
13. J. O. M. Bockris and S. U. M. Khan, *Surface electrochemistry: a molecular level approach*, Plenum Pub Corp, New York, 1993.
14. K. I. Ozoemena, J. Pillay and T. Nyokong, *Electrochemistry Communications*, 2006, 8, 1391-1396.
15. B. O. Agboola and K. I. Ozoemena, *Journal of power sources*, 2010, 195, 3841-3848.
16. J. E. B. Randles, *Trans. Faraday Soc.*, 1948, 44, 327-338.
17. A. J. Bard and L. R. Faulkner, *Electrochemical Methods: Fundamentals and Applications*, John Wiley & Sons, Hoboken, NJ, 2001.
18. B. E. Conway, *Electrochemical supercapacitors: scientific fundamentals and technological applications*, Springer, 1999.
19. E. Frackowiak and F. Beguin, *Carbon*, 2001, 39, 937-950.
20. L. Li, H. Song, Q. Zhang, J. Yao and X. Chen, *Journal of power sources*, 2009, 187, 268-274.
21. J. W. Lang, L. B. Kong, W. J. Wu, Y. C. Luo and L. Kang, *Chemical Communications*, 2008, 4213-4215.
22. F. S. Garcia, A. A. Ferreira and J. A. Pomilio, IEEE, 2009, pp. 826-832.
23. J. Garthwaite, Earth2Tech. GigaOM Network, 2008.
24. N. L. Wu, S. L. Kuo and M. H. Lee, *Journal of power sources*, 2002, 104, 62-65.

25. J. R. Miller and A. F. Burke, *Interface-Electrochemical Society*, 2008, 17, 53-57.

26. T. Ohzuku and R. J. Brodd, *Journal of power sources*, 2007, 174, 449-456.

27. K. B. Oldham and J. C. Myland, *Fundamentals of electrochemical science*, Academic Press, San Diego, 1994.

28. B. E. Conway and W. G. Pell, *Journal of Solid State Electrochemistry*, 2003, 7, 637-644.

29. E. Frackowiak, S. Gautier, H. Gaucher, S. Bonnamy and F. Beguin, *Carbon*, 1999, 37, 61-69.

30. R. Kotz and M. Carlen, *Electrochimica Acta*, 2000, 45, 2483-2498.

31. Y. Chen, X. Zhang, P. Yu and Y. Ma, *Journal of power sources*, 2010, 195, 3031-3035.

32. W. C. Chen and T. C. Wen, *Journal of power sources*, 2003, 117, 273-282.

33. C. D. Lokhande, S. S. Kulkarni, R. S. Mane, O. S. Joo and S. H. Han, *Ceramics International*, 2011.

34. E. Frackowiak and F. Beguin, *In Recent Advances in Supercapacitors, (Ed.: V. Gupta)*, Transworld Research Network, Kerala, India, 2006.

35. A. T. Chidembo, K. I. Ozoemena, B. O. Agboola, V. Gupta, G. G. Wildgoose and R. G. Compton, *Energy Environ. Sci.*, 2009, 3, 228-236.

36. A. I. Inamdar, Y. S. Kim, S. M. Pawar, J. H. Kim, H. Im and H. Kim, *Journal of power sources*, 2011, 196, 2393-2397.

37. R. W. Pekala, J. C. Farmer, C. T. Alviso, T. D. Tran, S. T. Mayer, J. M. Miller and B. Dunn, *Journal of Non-Crystalline Solids*, 1998, 225, 74-80.

38. Y. Wang and Y. Xia, *Electrochimica Acta*, 2006, 51, 3223-3227.

39. J. P. Zheng, P. J. Cygan and T. R. Jow, *Journal of the Electrochemical Society*, 1995, 142, 2699.

40. E. Frackowiak and F. Beguin, *Carbon*, 2002, 40, 1775-1787.

41. S. Iijima, C. Brabec, A. Maiti and J. Bernholc, *Journal of Chemical Physics*, 1996, 104, 2089-2092.

42. E. Frackowiak, K. Jurewicz, S. Delpeux and F. Beguin, *Journal of power sources*, 2001, 97, 822-825.

43. J. Y. Lee, K. Liang, K. H. An and Y. H. Lee, *Synthetic metals*, 2005, 150, 153-157.

44. S. Shen, J. Shi, P. Guo and L. Guo, *International Journal of Nanotechnology*, 2011, 8, 523-591.

45. H. Shi, *Electrochimica Acta*, 1996, 41, 1633-1639.

46. X. Jiang and T. Wang, *Applied surface science*, 2006, 252, 8029-8035.

47. A. T. Chidembo and K. I. Ozoemena, *Electroanalysis*, 2010, 22, 2529-2535.

48. Y. Zhang, H. Li, L. Pan, T. Lu and Z. Sun, *Journal of Electroanalytical Chemistry*, 2009, 634, 68-71.

49. H. D. Abruna, Y. Kiya and J. C. Henderson, *Physics Today*, 2008, 61, 43-47.

50. V. Gupta and N. Miura, *Materials Letters*, 2006, 60, 1466-1469.

51. G. A. Snook, P. Kao and A. S. Best, *Journal of power sources*, 2011, 196, 1-12.

52. J. Jiang and A. Kucernak, *Electrochimica Acta*, 2002, 47, 2381-2386.

53. C. C. Hu and C. C. Wang, *Electrochemistry Communications*, 2002, 4, 554-559.

54. C. C. Hu, W. C. Chen and K. H. Chang, *Journal of the Electrochemical Society*, 2004, 151, A281.

55. R. R. Bi, X. L. Wu, F. F. Cao, L. Y. Jiang, Y. G. Guo and L. J. Wan, *The Journal of Physical Chemistry C*, 2010, 114, 2448-2451.

56. C. Peng, S. Zhang, D. Jewell and G. Z. Chen, *Progress in Natural Science*, 2008, 18, 777-788.

57. Y. Zheng, M. Zhang and P. Gao, *Materials research bulletin*, 2007, 42, 1740-1747.

58. A. Malak, K. Fic, G. Lota, C. Vix-Guterl and E. Frackowiak, *Journal of Solid State Electrochemistry*, 2010, 14, 811-816.

59. R. B. Rakhi, D. Cha, W. Chen and H. N. Alshareef, *The Journal of Physical Chemistry C*, 2011.

60. C. Arbizzani, M. Mastragostino and L. Meneghello, *Electrochimica Acta*, 1996, 41, 21-26.

61. K. Jurewicz, S. Delpeux, V. Bertagna, F. Beguin and E. Frackowiak, *Chemical physics letters*, 2001, 347, 36-40.

62. V. Khomenko, E. Frackowiak and F. Beguin, *Electrochimica Acta*, 2005, 50, 2499-2506.

63. S. W. Lee, B. M. Gallant, H. R. Byon, P. T. Hammond and Y. Shao-Horn, *Energy Environ. Sci.*, 2011.

64. P. Simon and Y. Gogotsi, *Nature Materials*, 2008, 7, 845-854.

65. M. Adachi, M. Sakamoto, J. Jiu, Y. Ogata and S. Isoda, *The Journal of Physical Chemistry B*, 2006, 110, 13872-13880.

66. M. A. Anderson and K. C. Leonard, Google Patents, 2007.

67. T. Y. Chang, X. Wang, D. A. Evans, S. L. Robinson and J. P. Zheng, *Journal of power sources*, 2002, 110, 138-143.

68. V. Ganesh, S. Pitchumani and V. Lakshminarayanan, *Journal of power sources*, 2006, 158, 1523-1532.

69. V. Khomenko, E. Raymundo-Pinero, E. Frackowiak and F. Beguin, *Applied Physics A: Materials Science & Processing*, 2006, 82, 567-573.

70. Y. Xue, Y. Chen, M. L. Zhang and Y. D. Yan, *Materials Letters*, 2008, 62, 3884-3886.

71. C. Arbizzani, M. Biso, D. Cericola, M. Lazzari, F. Soavi and M. Mastragostino, *Journal of power sources*, 2008, 185, 1575-1579.

72. E. S. David and P. Su-Moon, *Journal of the Electrochemical Society*, 1988, 135, 2491-2496.

73. S. Iijima and T. Ichihashi, *Nature* 1993.

74. M. Monthioux and V. L. Kuznetsov, *Carbon*, 2006, 44, 1621-1623.

75. A. Peigney, C. Laurent, E. Flahaut, R. R. Bacsa and A. Rousset, *Carbon*, 2001, 39, 507-514.

76. J. P. Salvetat, G. A. D. Briggs, J. M. Bonard, R. R. Bacsa, A. J. Kulik, T. Stockli, N. A. Burnham and L. ForrÃ³, *Physical Review Letters*, 1999, 82, 944-947.

77. J. P. Salvetat, A. J. Kulik, J. M. Bonard, G. A. D. Briggs, T. Stockli, K. Metenier, S. Bonnamy, F. Beguin, N. A. Burnham and L. ForrÃ³, *Advanced Materials*, 1999, 11, 161-165.

78. S. Iijima, M. Yudasaka, R. Yamada, S. Bandow, K. Suenaga, F. Kokai and K. Takahashi, *Chemical physics letters*, 1999, 309, 165-170.

79. C. L. Kane and E. J. Mele, *Physical Review Letters*, 1997, 78, 1932-1935.

80. P. Nikolaev, M. J. Bronikowski, R. K. Bradley, F. Rohmund, D. T. Colbert, K. A. Smith and R. E. Smalley, *Chemical physics letters*, 1999, 313, 91-97.

81. R. E. Smalley, Y. Li, V. C. Moore, B. K. Price, R. Colorado Jr, H. K. Schmidt, R. H. Hauge, A. R. Barron and M. James, *Journal of the American Chemical Society*, 2006, 128, 15824-15829.

82. M. S. Dresselhaus, G. Dresselhaus and R. Saito, *Carbon*, 1995, 33, 883-891.

83. K. Guo, *Synthesis and applications of Carbon Nanotubes in Nano-Electro-Mechanical System*, ProQuest, 2008.

84. G. Zhou, G. Xie and X. Bao, *International Journal of Smart and Nano Materials*, 2010, 1, 136-171.

85. S. B. Legoas, V. R. Coluci, S. F. Braga, P. Z. Coura, S. O. Dantas and D. S. Galvao, *Nanotechnology*, 2004, 15, S184.

86. S. Niyogi, M. A. Hamon, H. Hu, B. Zhao, P. Bhowmik, R. Sen, M. E. Itkis and R. C. Haddon, *Accounts of chemical research*, 2002, 35, 1105-1113.

87. E. W. Wong, P. E. Sheehan and C. M. Lieber, *Science*, 1997, 277, 1971.

88. A. Thess, R. Lee, P. Nikolaev, H. Dai, P. Petit, J. Robert, C. Xu, Y. H. Lee, S. G. Kim and A. G. Rinzler, *Science*, 1996, 273, 483.

89. Y. Wang, Z. Iqbal and S. Mitra, *Journal of the American Chemical Society*, 2006, 128, 95-99.

90. S. T. Hussain, M. Mazhar, S. Gul and M. A. Khan, Google Patents, 2008.

91. Y. P. Sun, K. Fu, Y. Lin and W. Huang, *Accounts of chemical research*, 2002, 35, 1096-1104.

92. A. S. Adekunle, B. O. Agboola, J. Pillay and K. I. Ozoemena, *Sensors and Actuators B: Chemical*, 2010, 148, 93-102.

93. B. O. Agboola, J. Pillay, K. Makgopa and K. I. Ozoemena, *Journal of the Electrochemical Society*, 2010, 157, F159.

94. J. Alzeer, P. J. C. Roth and N. W. Luedtke, *Chemical Communications*, 2009, 1970-1971.

95. P. A. Gregory, A. G. Bert, E. L. Paterson, S. C. Barry, A. Tsykin, G. Farshid, M. A. Vadas, Y. Khew-Goodall and G. J. Goodall, *Nature cell biology*, 2008, 10, 593-601.

96. M. Hanack and M. Lang, *Advanced Materials*, 1994, 6, 819-833.

97. G. Kalyuzhny, A. Vaskevich, G. Ashkenasy, A. Shanzer and I. Rubinstein, *The Journal of Physical Chemistry B*, 2000, 104, 8238-8244.

98. M. L. Kaplan, A. J. Lovinger, W. D. Reents Jr and P. H. Schmidt, *Molecular Crystals and Liquid Crystals*, 1984, 112, 345-358.

99. R. P. Linstead, J. A. Elvidge and M. Whalley, *A course in modern techniques of organic chemistry*, Butterworths, 1955.

100. Z. Liu, K. Suenaga, P. J. F. Harris and S. Iijima, *Physical Review Letters*, 2009, 102, 15501.

101. N. B. McKeown, *Phthalocyanine materials: synthesis, structure, and function*, Cambridge Univ Pr, 1998.

102. J. Padilla and W. E. Hatfield, *Inorganica chimica acta*, 1991, 185, 131-136.

103. C. Rimington, S. F. Mason and O. Kennard, *Spectrochimica Acta*, 1958, 12, 65-77.

104. J. M. Robertson, R. P. Linstead and C. E. Dent, *Nature*, 1935, 135, 506-507.

105. J. M. Robertson and A. R. Ubbelohde, *Proceedings of the Royal Society of London. Series A. Mathematical and Physical Sciences*, 1939, 170, 222.

106. B. Agboola, K. I. Ozoemena and T. Nyokong, *Electrochimica Acta*, 2006, 51, 4379-4387.

107. K. Ozoemena, N. Kuznetsova and T. Nyokong, *Journal of Photochemistry and Photobiology A: Chemistry*, 2001, 139, 217-224.

108. K. I. Ozoemena and T. Nyokong, *Talanta*, 2005, 67, 162-168.

109. J. H. Zagal, S. Griveau, K. I. Ozoemena, T. Nyokong and F. Bedioui, *Journal of Nanoscience and Nanotechnology*, 2009, 9, 2201-2214.

110. Z. Jin, K. Nolan, C. R. McArthur, A. B. P. Lever and C. C. Leznoff, *Journal of organometallic chemistry*, 1994, 468, 205-212.

111. C. M. Allen, W. M. Sharman and J. E. Van Lier, *Journal of Porphyrins and Phthalocyanines*, 2001, 5, 161-169.

112. K. Hegetschweiler, M. Worle, M. D. Meienberger, R. Nesper, H. W. Schmalle and R. D. Hancock, *Inorganica chimica acta*, 1996, 250, 35-47.

113. J. E. Kuder, H. N. Yoon and R. N. DeMartino, *Journal of applied polymer science*, 1992, 45, 583-590.

114. K. R. Rajesh and C. S. Menon, *Materials Letters*, 2001, 51, 266-269.

115. J. Simon and P. Bassoul, *In Phthalocyanine: Properties and Applications, lever A.P.B; Leznoff, C.C., Ed.*, VCH Publishers, New York, 1993.

116. D. Worle and D. Meissner, *Advanced Materials*, 1991, 3, 129-138.

117. E. Ben-Hur and I. Rosenthal, *International Journal of Radiation Biology*, 1985, 47, 145-147.

118. M. R. Hoffmann, S. T. Martin, W. Choi and D. W. Bahnemann, *Chemical reviews*, 1995, 95, 69-96.
119. Y. Lu and R. G. Reddy, *Electrochimica Acta*, 2007, 52, 2562-2569.
120. L. N. Menard and S. H. Bergens, *Journal of power sources*, 2009, 194, 298-302.
121. M. Thamae and T. Nyokong, *Journal of Electroanalytical Chemistry*, 1999, 470, 126-135.
122. R. T. Kachoosangi, C. E. Banks and R. G. Compton, *Electroanalysis*, 2006, 18, 741-747.
123. C. M. Welch, C. E. Banks, A. O. Simm and R. G. Compton, *Analytical and bioanalytical chemistry*, 2005, 382, 12-21.
124. M. von Ardenne, *The Beginnings of Electron Microscopy (PW Hawkes ed) Adv Electronics Electron Phys Suppl*, 1985, 16, 1-21.
125. P. E. Alvarez, S. B. Ribotta, M. E. Folquer, C. A. Gervasi and J. R. Vilche, *Corrosion science*, 2002, 44, 49-65.
126. C. A. Gervasi, P. E. Alvarez, M. V. Fiori Bimbi and M. E. Folquer, *Journal of Electroanalytical Chemistry*, 2007, 601, 194-204.
127. J. M. Goddard and J. H. Hotchkiss, *Progress in polymer science*, 2007, 32, 698-725.
128. J. J. Bozzola, *Electron microscopy*, Wiley Online Library, 1992.
129. A. P. Day, *Journal of Microscopy*, 2008, 230, 472-486.
130. X. Tan, H. He and J. K. Shang, *Journal of materials research*, 2005, 20, 1641-1653.

131. D. B. Williams and C. B. Carter, *Transmission Electron Microscopy*, 2009, 3-22.
132. J. M. Aguilera and P. J. Lillford, *Food engineering*, 2000, 23-38.
133. T. L. Hayes, *Journal of Microscopy*, 1974, 100, 133-142.
134. J. D. Swalen, D. L. Allara, J. D. Andrade, E. A. Chandross, S. Garoff, J. Israelachvili, T. J. McCarthy, R. Murray and R. F. Pease, *Langmuir*, 1987, 3, 932-950.
135. A. H. Zewail, *Annu. Rev. Phys. Chem.*, 2006, 57, 65-103.
136. K. E. Tettey, M. I. Dafinone and D. Lee, *Materials Express*, 2011, 1, 89-104.
137. Y. Gao, S. Chen, D. Cao, G. Wang and J. Yin, *Journal of power sources*, 2010, 195, 1757-1760.
138. O. Lupan, S. Shishiyanu, L. Chow and T. Shishiyanu, *Thin solid films*, 2008, 516, 3338-3345.
139. S. C. Shei, S. J. Chang and P. Y. Lee, *Journal of the Electrochemical Society*, 2011, 158, H208.
140. V. N. Popov, *Materials Science and Engineering: R: Reports*, 2004, 43, 61-102.
141. J. Yang, Z. Jin, Y. Chai, H. Du, T. Liu and T. Wang, *Thin solid films*, 2009, 517, 6617-6622.
142. J. J. Gooding, D. B. Hibbert and W. Yang, *Sensors*, 2001, 1, 75-90.
143. T. F. Hsieh, C. C. Chuang, W. J. Chen, J. H. Huang, W. T. Chen and C. M. Shu, *Carbon*, 2011.

144. L. Netzer and J. Sagiv, *Journal of the American Chemical Society*, 1983, 105, 674-676.

145. B. F. Watkins, J. R. Behling, E. Kariv and L. L. Miller, *Journal of the American Chemical Society*, 1975, 97, 3549-3550.

146. Z. Chen and Y. Zhou, *Surface and Coatings Technology*, 2006, 201, 2419-2430.

147. C. Deng, M. Li, Q. Xie, M. Liu, Y. Tan, X. Xu and S. Yao, *Analytica chimica acta*, 2006, 557, 85-94.

148. G. M. Fuge, T. Holmes and M. N. R. Ashfold, *Chemical physics letters*, 2009, 479, 125-127.

149. R. C. Scott, K. D. Leedy, B. Bayraktaroglu, D. C. Look and Y. H. Zhang, *Applied Physics Letters*, 2010, 97, 072113.

150. F. Ye, C. Cui, A. Kirkeminde, D. Dong, M. M. Collinson and D. A. Higgins, *Chemistry of Materials*, 2010, 22, 2970-2977.

151. X. Cui, V. A. Lee, Y. Raphael, J. A. Wiler, J. F. Hetke, D. J. Anderson and D. C. Martin, *Journal of biomedical materials research*, 2001, 56, 261-272.

152. D. Wei, H. Wang, P. Hiralal, P. Andrew, T. RyhÃ¤nen, Y. Hayashi and G. A. J. Amaratunga, *Nanotechnology*, 2010, 21, 435702.

153. H. B. Dai, Y. Liang, P. Wang and H. M. Cheng, *Journal of power sources*, 2008, 177, 17-23.

154. X. H. Huang, J. P. Tu, Z. Y. Zeng, J. Y. Xiang and X. B. Zhao, *Journal of the Electrochemical Society*, 2008, 155, A438.

155. S. Langlois and F. Coeuret, *Journal of applied electrochemistry*, 1989, 19, 43-50.

156. J. Li, Q. M. Yang and I. Zhitomirsky, *Journal of power sources*, 2008, 185, 1569-1574.

157. P. Zhao, H. Zhang, H. Zhou and B. Yi, *Electrochimica Acta*, 2005, 51, 1091-1098.

158. P. A. Christenson and A. Hamnet, *Techniques and Mechanisms in Electrochemistry* Blackie Academic and Professional, London, 1994.

159. R. G. Compton and C. E. Banks, *Understanding Voltammetry*, World Scientific Publishing Co. Pte. Ltd, London, 2007.

160. D. B. Hibbert, *Introduction to Electrochemistry*, Macmillan, London, 1993.

161. F. Marken, A. Neudeck and A. M. Bond, ed. F. Scholz, Electroanalytical Methods, Springer, Berlin, 2000.

162. F. Marken, A. Neudeck, A. M. Bond and F. Scholz, *Electroanalytical Methods, Springer, Berlin, Heidelberg, New York*, 2002, 51.

163. R. S. Nicholson, *Analytical Chemistry*, 1965, 37, 1351-1355.

164. R. S. Nicholson and I. Shain, *Analytical Chemistry*, 1964, 36, 706-723.

165. M. A. Romski and R. A. Sevcik, *Breaking the speech barrier: Language development through augmented means*, Brookes Publishing Company, Maple Press Distribution Center, I-83 Industrial Park, 1996.

166. T. Takahashi and E. Niki, *Talanta*, 1958, 1, 245-248.

167. D. K. Gosser, *Cyclic voltammetry: simulation and analysis of reaction mechanisms*, Wiley-VCH, New York, 1993.

168. A. Sevcik, *Coll. Czech. Chem. Comm.*, 1958, 13, 349.

169. J. A. Harrison and Z. A. Khan, *Journal of Electroanalytical Chemistry and Interfacial Electrochemistry*, 1970, 28, 131-138.

170. H. A. Laitinen and I. M. Kolthoff, *The Journal of Physical Chemistry*, 1941, 45, 1079-1093.

171. H. A. Laitinen and I. M. Kolthoff, *The Journal of Physical Chemistry*, 1941, 45, 1061-1079.

172. M. T. Carter, M. Rodriguez and A. J. Bard, *Journal of the American Chemical Society*, 1989, 111, 8901-8911.

173. F. Lufrano and P. Staiti, *Electrochimica Acta*, 2004, 49, 2683-2689.

174. T. Shinomiya, V. Gupta and N. Miura, *Electrochimica Acta*, 2006, 51, 4412-4419.

175. X. Lin and Y. Xu, *Electrochimica Acta*, 2008, 53, 4990-4997.

176. D. D. Macdonald, *Electrochimica Acta*, 1990, 35, 1509-1525.

177. J. R. Macdonald and W. B. Johnson, *Impedance Spectroscopy*, John Wiley and Sons Inc., New York, 2005.

178. A. K. Manohar, O. Bretschger, K. H. Nealson and F. Mansfeld, *Bioelectrochemistry*, 2008, 72, 149-154.

179. P. L. Bonora, F. Deflorian and L. Fedrizzi, *Electrochimica Acta*, 1996, 41, 1073-1082.

180. J. B. Jorcin, M. E. Orazem, N. PÃbÃ¨re and B. Tribollet, *Electrochimica Acta*, 2006, 51, 1473-1479.

181. J. Segalini, B. Daffos, P. L. Taberna, Y. Gogotsi and P. Simon, *Electrochimica Acta*, 2010, 55, 7489-7494.

CHAPTER TWO

Experimental

2.1 MATERIALS AND REAGENTS

All chemical reagents and materials used in the preparation are listed in table 2.1 below.

Table 2.1: The list of chemical reagents and materials used.

Reagents and materials	**Specifications**	**Supplier**
Multi-Walled Carbon NanoTubes (MWCNT)	Bundles, ≥ 94% Diameter-10-20nm Length-5-20 μm	NanoLab
Nickel Nitrate ($Ni(NO_3)_2$)	99.5% pure	AnalaR, (BDH chemical Ltd)
Hydrogen Peroxide (H_2O_2)	30% by weight H_2O_2	Merck
Nitric Acid (HNO_3)	65% extra pure	Merck
Sulfuric Acid (H_2SO_4)	95-97%	Sigma-Aldrich
Acetone $(CH_3)_2CO$)	98%	Merck
Hydrochloric Acid (HCl)	32%	Merck

Ammonia solution (NH_3)	25%	AnalaR, (BDH chemical Ltd)
Potassium persulphate ($K_2S_2O_8$)	99%	Merck
Hexadecyltrimethyl Ammonium Bromide (CTAB)	99%	Aldrich
Dimethylformamide (DMF) ($(CH_3)_2NC(O)H$)		SAARCHEM (PTY) Ltd SA.
Potassium chloride (KCl)		Merck
Whatman Filter Paper		Aldrich
pH paper	pH 0-14	Merck
Acetonitrile (CH_3CN)		Aldrich
Cerric Ammonium Nitrate ($(NH_4)_2Ce(NO_3)_6$)		Aldrich
Pyrrole (C_4H_5N)		Aldrich

2.2 FUNCTIONALIZATION OF THE MULTI-WALLED CARBON NANOTUBES

2.2.1 PURIFICATION AND OXIDATION OF MULTI-WALLED CARBON NANOTUBES

Multi-walled carbon nanotubes were obtained from Nanolab with the purity of greater than 94%, diameter of 10-20 nanometer and the length of 5-20 micron, were converted to short and uncapped nanotubes bearing acidic functional groups (mainly into carboxylated) by following the established multi-step acid treatment procedures [1-6], simply referred to in this work as MWCNT. 1 g of pristine MWCNTs was refluxed for the period of 48 hours in 140 ml of 2.6 M Nitric acid (HNO_3). Sediments of carbon nanotube were separated from the reaction and washed with distilled water. The clean sediments were then sonicated in a mixture of concentrated H_2SO_4/HNO_3 (3:1 ratio, 95-97% and 65% purity, respectively) for a period of 24 hours. The sediments were then washed with distilled water followed by stirring at 70 Degree Celsius for half an hour in a mixture of H_2SO_4/H_2O_2 (4:1, 95-97% and 30% purity, respectively). Then the sediments were washed again with de-ionised water and finally, the purified paste-like MWCNTs were then oven dried at 50 Degree Celsius for a period of 48 hours.

Nickel (II) tetra-aminophthalocyanine was synthesised and characterised using the well adapted procedure introduced by Achar and Jayasree [1].

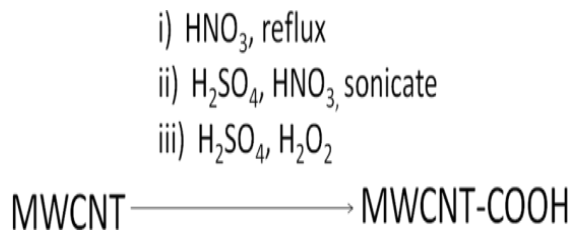

Scheme 2.1: Schematic representation of conversion of pristine Multi-Walled Carbon Nanotube to the carboxylated Multi-Walled Carbon Nanotube.

2.3 EQUIPMENT

All electrochemical experiments were carried out using an Autolab Potentiostat PGSTAT 302 (Eco Chemie, Utrecht, Netherlands) driven by the General Purpose Electrochemical Systems data processing software (GPES, software version 4.9). Electrochemical impedance spectroscopy (EIS) measurements were performed with Autolab Frequency Response Analyser (FRA) software between 100 kHz and 0.1 Hz using a 5 mV rms sinusoidal modulation. Bare or modified nickel foam was used as the working electrode. Ag|AgCl wire and glassy carbon were used as pseudo-reference and counter electrodes, respectively. A bench top pH / ISE ORION meter, model 420A, was used for pH measurements. All solutions were de-aerated by bubbling pure nitrogen (Afrox) prior to each electrochemical experiment. All experiments were performed at 25±1°C. Transmission electron microscopy (TEM) was performed with Multi-purpose TEM (Philips 301). Field emission scanning electron microscopy (FESEM) images were obtained on JSM-5800 LV (JEOL, Tokyo, Japan) while Energy dispersive X-ray (EDX) images were obtained on JSM 5800 LV, Noran Vantage (USA) 6, Analytical Systems with 130eV detector (JEOL) at the Microscopy and Microanalysis Laboratory, University of Pretoria and FESEM images obtained at the AuTEK Nanotechnology laboratory of MinTEK were carried out with FEI Nova NanoSEM 200 (Japan).

2.4 SYNTHESIS OF NiTAPc-PolyPyrrole

In the preparation of NiTAPc-PPY, a volume of 20 mL acetonitrile was used as a solvent to make a solution of NiTAPc (0.051g was added). The solution was then sonicated for 30 minutes to obtain dispersion of the solute. After a given time, 0.2 mL of pyrrole monomer was added to form a polypyrrole that is embedded on NiTAPc. The NiTAPc-pyrrole solution was sonicated for 30 minutes while stirring. Then the oxidant, Cerium (IV) ammonium nitrate ($(NH_4)_2Ce(NO_3)_6$) (abbreviated CAN) was introduced to initiate polymerization of pyrrole to form polypyrrole with NiTAPc. The polymerisation reaction took place for 3 hours and the product was washed with water intensively followed by washing with acetone. The black slurry of NiTAPc-PPY was then dried at 80 ^{o}C for 12 hours.

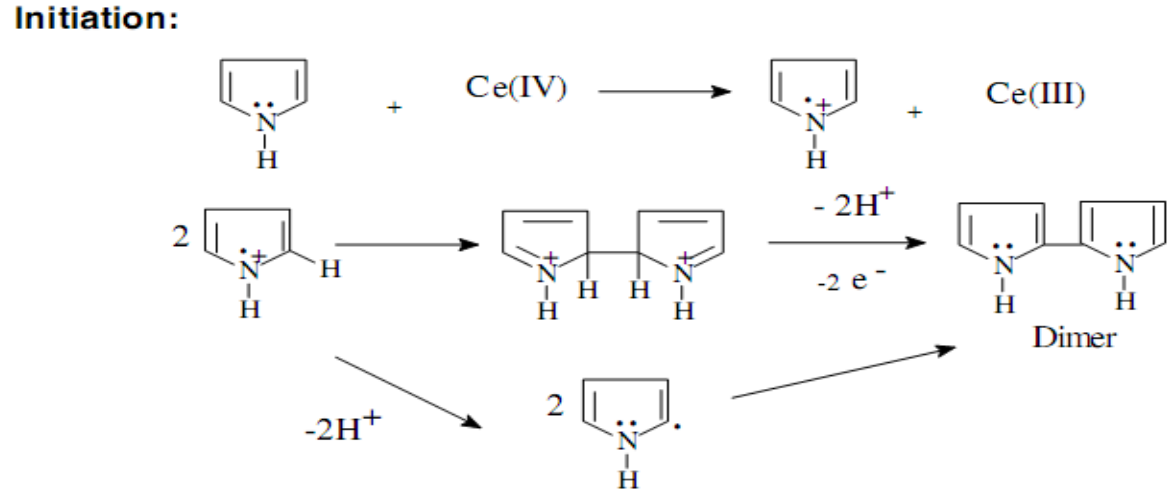

Scheme 2.2: Schematic representation of chemical polymerisation of polypyrrole from its pyrrole monomer using CAN as as oxidant [7].

Scheme 2.3: Schematic representation of NiTAPc-PPy from its precursors

2.5 Electrode Modification and Pre-treatment

Nickel foam used in this experiment was first pre-treated by sonicating it in 1M HCl solution for 10 minutes, then washed with acetone and deionised water, followed by rinsing with 2 M KOH before electrochemical testing [8]. There are three techniques used specifically in this experiment to immobilise electrocatalyst materials onto the surface of the nickel foam.

2.5.1 Preparation Of NF/NiO-MWCNT Based Supercapacitor Electrode

The cationic Ni $(NH_3)_6]^{2+}$ complex was obtained from the mixture of 0.1M $Ni(NO_3)_2$ with aqueous ammonia (NH_3) solution which was used as a cation precursor for SILAR preparation, with hot deionised water as a anion precursor for the formation of NF/NiO supercapacitor electrode. In this technique, growth is performed (layer-by-layer) by sequentially dipping the nickel foam into stable precursor of Ni $(NH_3)_6]^{2+}$ solutions followed by dipping into hot water. Each reaction involves rinsing in between to remove the loosely adsorbed ions from the surface of the electrode. For a traditional SILAR technique, one SILAR cycle is made up of four steps: the substrate is (i) immersed in a reaction solution containing the aqueous cation precursor, (ii) rinsed with water, (iii) then be immersed in the anion solution, (iv) and finally be rinsed more with water (see diagram on scheme 2.4 next page). Addition of MWCNT to the

NiO was archived by incorporating the step (v) in the described process where step (v) contained the MWCNT dispersed in deionised water.

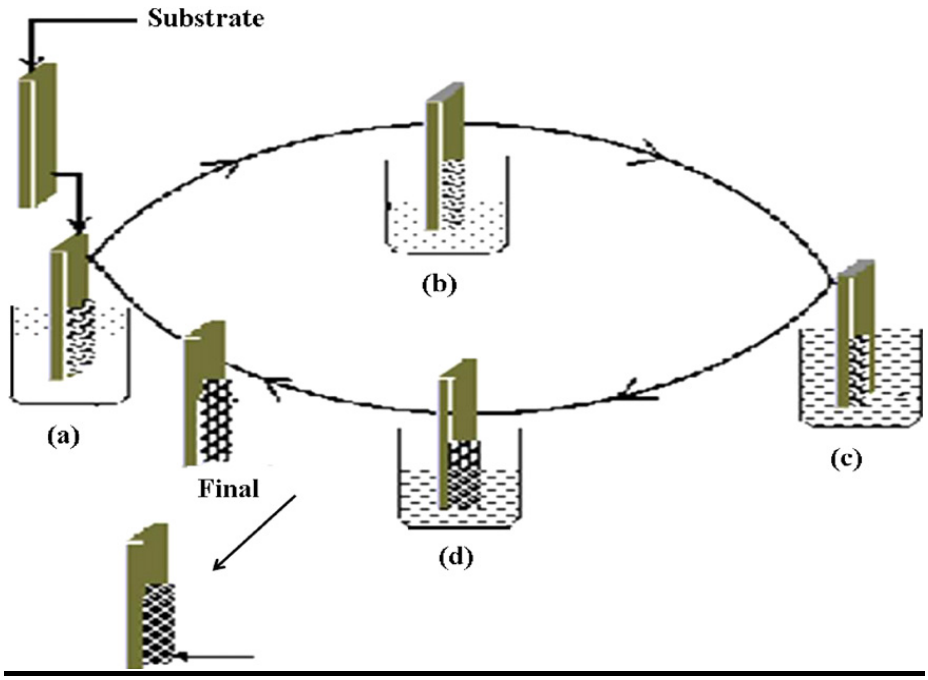

Scheme 2.4: Schematic representation of SILAR method (a: cationic precursor, b and d: rinsing bath, c: anionic precursor) [9].

The following electrodes were synthesised using the above method:

1. **NF/NiO**
2. **NF/NiO with oxidant (using potassium persulphate ($K_2S_2O_8$) as an oxidant)**

2.5.2 Preparation Of NF/NiTAPc-NiO_{E-S} And NF/NiTAPc-NiO_E Based Supercapacitor Electrode

One milli-gram (mg) of NiTAPc was dissolved in 1mL DMF to make a solution of NiTAPc. The electrode substrate was immersed in an electrolyte solution containing one or more dissolved salts or other ions that permit the flow of electricity and subjected to electrochemical treatment. Then the NiTAPc material was modified onto the surface of the bare nickel foam (NF) by the means of electrochemical deposition technique using chronoamperometry with the voltage of 1V and the time set to 1200s and Ag/AgCl used as a reference electrode. NiO was then immobilised on NF/NiTAPc thin film substrate using the SILAR technique as described above. For the synthesis of NiTAPc-NiO_E, both NiTAPc and NiO materials were modified onto the surface of the bare nickel foam (NF) by the means of electrochemical deposition technique as described in this section.

2.5.3 Preparation Of NF/NiTAPc-PPY Based Supercapacitor Electrode

NiTAPc-PPY powder material was modified onto the surface of the bare nickel foam (NF) by the means of pulsed laser deposition technique where a high power pulsed laser beam is focused inside a vacuum chamber to strike a NiTAPc-PPY powder material that is to be deposited. Then the NiTAPc-PPY powder material is vaporized from the target (in a plasma

plume) which deposited it as a thin film on nickel foam. This deposition took place in ultra high vacuum condition.

2.5.4 Preparation Of NF/MWCNT And NF/NiTAPc Based Supercapacitor Electrodes.

Both NF/NiTAPc and NF/MWCNT were immobilised onto the surface of the bare nickel foam (NF) by the means of dip-dry deposition technique. For NF/NiTAPc, only 1mg of NiTAPc was dissolved in 1mL DMF to make a solution of NiTAPc. Then followed by dipping the bare nickel foam substrate into the solution of NiTAPc and be left for overnight then the modified electrode was then washed with deionised water and dried. For NF/MWCNT, the mass of about 8.2 mg of acid functionalised multi-walled carbon nanotubes (MWCNT) were dissolved in 15mL deionised water to form a well dispersed solution of MWCNT. A freshly prepared bare nickel foam was then dipped in the MWCNT solution and be left for overnight. The MWCNT adsorbed onto the nickel foam was then washed with deionised water and dried.

REFERENCES

1. M. P. Siswana, K. I. Ozoemena and T. Nyokong, *Electrochimica Acta*, 2006, **52**, 114-122.
2. H. Murakami and N. Nakashima, *Journal of Nanoscience and Nanotechnology*, 2006, **6**, 16-27.
3. K. I. Ozoemena, J. Pillay and T. Nyokong, *Electrochemistry Communications*, 2006, **8**, 1391-1396.
4. S. K. Pillai, S. S. Ray and M. Moodley, *Journal of Nanoscience and Nanotechnology*, 2007, **7**, 3011-3047.
5. T. Saito, K. Matsushige and K. Tanaka, *Physica B: Condensed Matter*, 2002, **323**, 280-283.
6. J. Zhang, H. Zou, Q. Qing, Y. Yang, Q. Li, Z. Liu, X. Guo and Z. Du, *The Journal of Physical Chemistry B*, 2003, **107**, 3712-3718.
7. N. Kızılcan, N. K. O¨ z, B. Ustamehmetog˘lu and A. Akar, *European Polymer Journal*, 2006, **42**, 2361–2368.
8. W. Xing, S. Qiao, X. Wu, X. Gao, J. Zhou, S. Zhou and S.-B. Hartono, *Journal of Power Sources* 2011, **196**, 4123–4127.
9. C. D. Lokhande, A. M. More and J. L. Gunjakar, *Journal of Alloys and Compounds*, 2009, **486**, 570-580.

CHAPTER THREE

Supercapacitive Behaviour of NiTAPc-PPY Nanocomposites

3.1 SPECTROSCOPIC AND MICROSCOPIC CHARACTERIZATION

This chapter describes the supercapacitance of nickel (II) tetra-aminophthalocyanine integrated with polypyrrole (herein abbreviated as NiTAPc-PPY).

3.1.1 Scanning Electron Microscopy Images

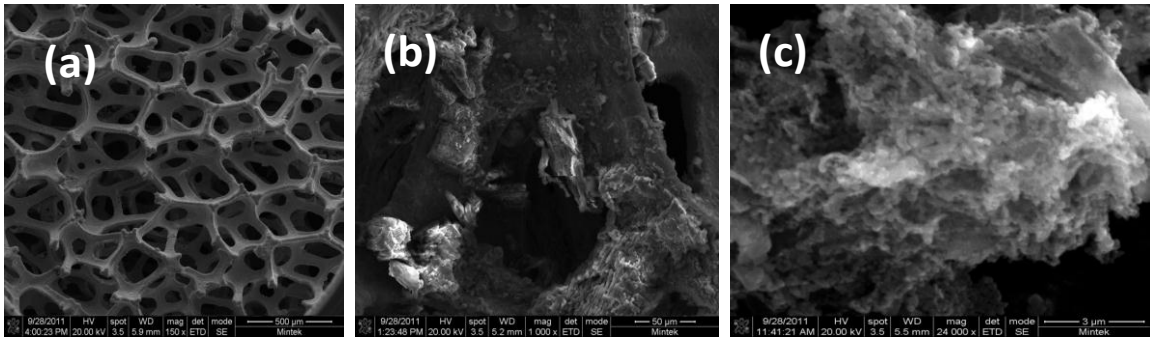

Figure 3.1: Typical SEM images of (a) bare NF (b) NF/NiTAPc, and (c) powder NiTAPc-PPy

Figure 3.1 represents typical SEM images of bare nickel foam (NF), NF/NiTAPc as well as NF/NiTAPc-PPy. The NF image is typical of pure, acid-cleaned nickel foam [1, 2]. The FESEM image of NiTAPc and NiTAPc-PPy are different from that of pure NF indicating the presence as well as the immobilization of these materials onto the nickel foam. The NiTAPc-PPY forms a cluster-like morphology, possibly indicating the π-π interaction

between these two species as would be expected of metal phthalocyanines and aromatic compounds.

3.1.2 Energy-Dispersive X-ray Spectroscopy Analysis

Figure 3.2 represents profiles of the EDX analysis for bare NF, NF/NiTAPc and NiTAPc-PPy. The oxygen impurity is attributed to the atmospheric environment where the EDX was performed. As expected, both NF (a) and NF/NiTAPc (b) gave nickel peaks only. The cerium species found in the NiTAPc-PPy spectrum is due to the cerium-based oxidant used in the chemical synthesis (as described in the Experimental section).

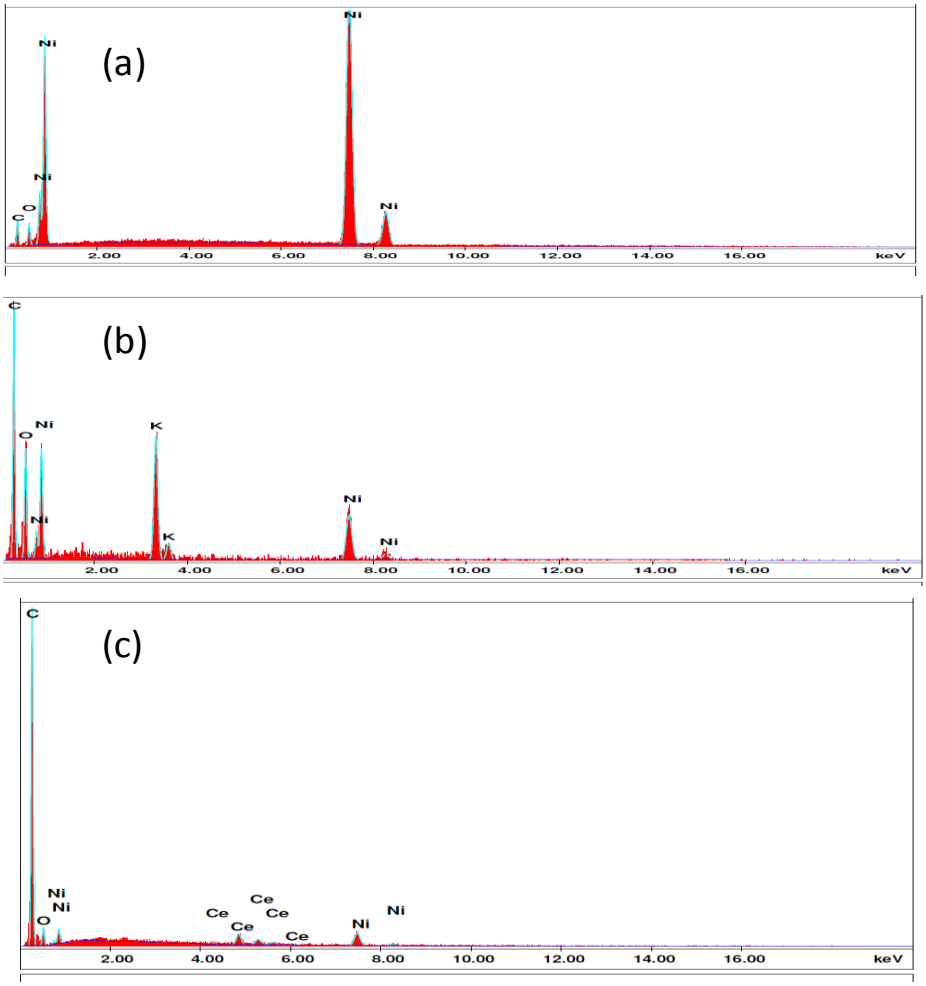

Figure 3.2: Typical EDX images of (a) bare nickel foam (b) NiTAPc on nickel foam (c) NiTAPc-PPy.

3.2 Supercapacitive behavior of NiTAPc-PPy nanocomposites using nickel foam as current collector

3.2.1 Cyclic Voltammetry

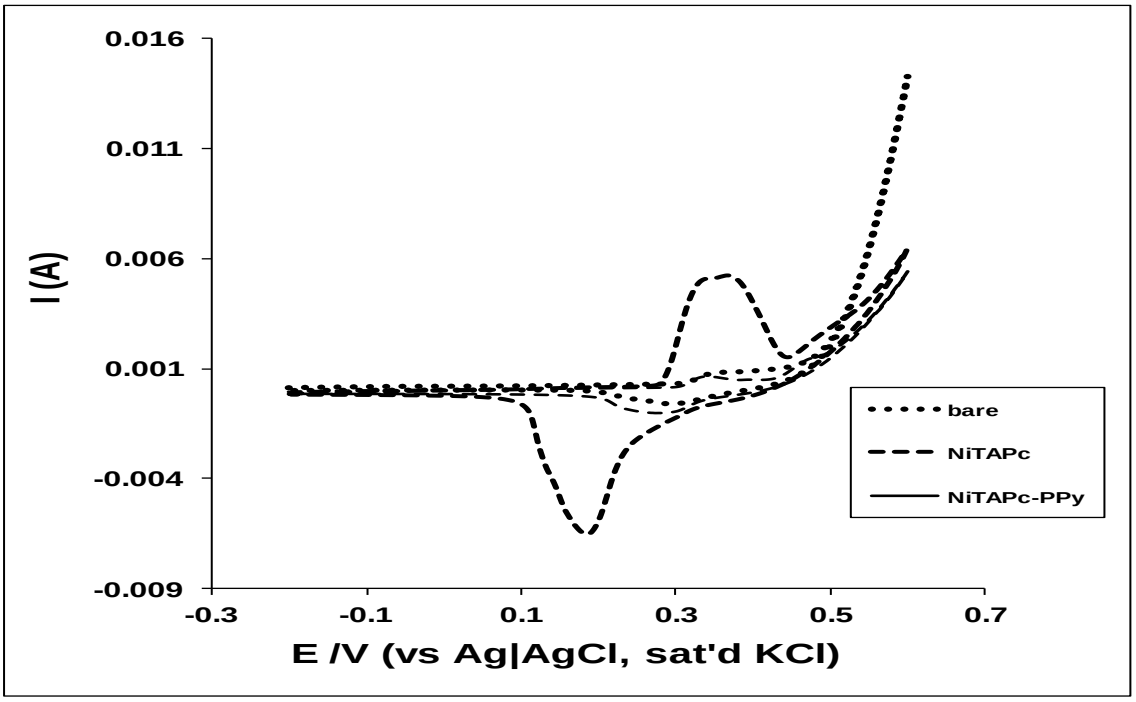

Figure 3.3: Comparative cyclic voltammograms of (a) bare NF (b) NF/NiTAPc (c) NF/NiTAPc-PPy. Electrolyte = 2M KOH

First, the electrochemical capacitive properties of NF/NiTAPc and NF/NiTAPc-PPY were evaluated using cyclic voltammetry. Figure 3.3 compares the cyclic voltammetric evolutions of the bare NF as well as the

NF/NiTAPc and NF/NiTAPc-PPy. NF/NiTAPc gave the highest current response (and hence the higher capacitance) compared to the NF/NiTAPc-PPy and bare NF. The high current value of NF/NiTAPc is expected considering that NiTAPc has recently been reported to exhibit supercapacitive behaviour [3, 4]. Surprisingly, however, there is no detectable difference between the NF/NiTAPc-PPY and nickel foam, which clearly indicates that the PPY suppresses the capacitance of NiTAPc. The reason as I later found out from literature is because the PPy used in this work was not doped and hence less conductive [5].

Considering the high performance of the NF/NiTAPc, this electrode was subjected to scan rate studies with the scan rate varying from 10 to 100 mVs^{-1}. Figure 3.4 shows scan rate studies of the NiTAPc immobilized on nickel foam. Plot of peak current versus scan rate (inset) is linear, indicating diffusion-controlled process.

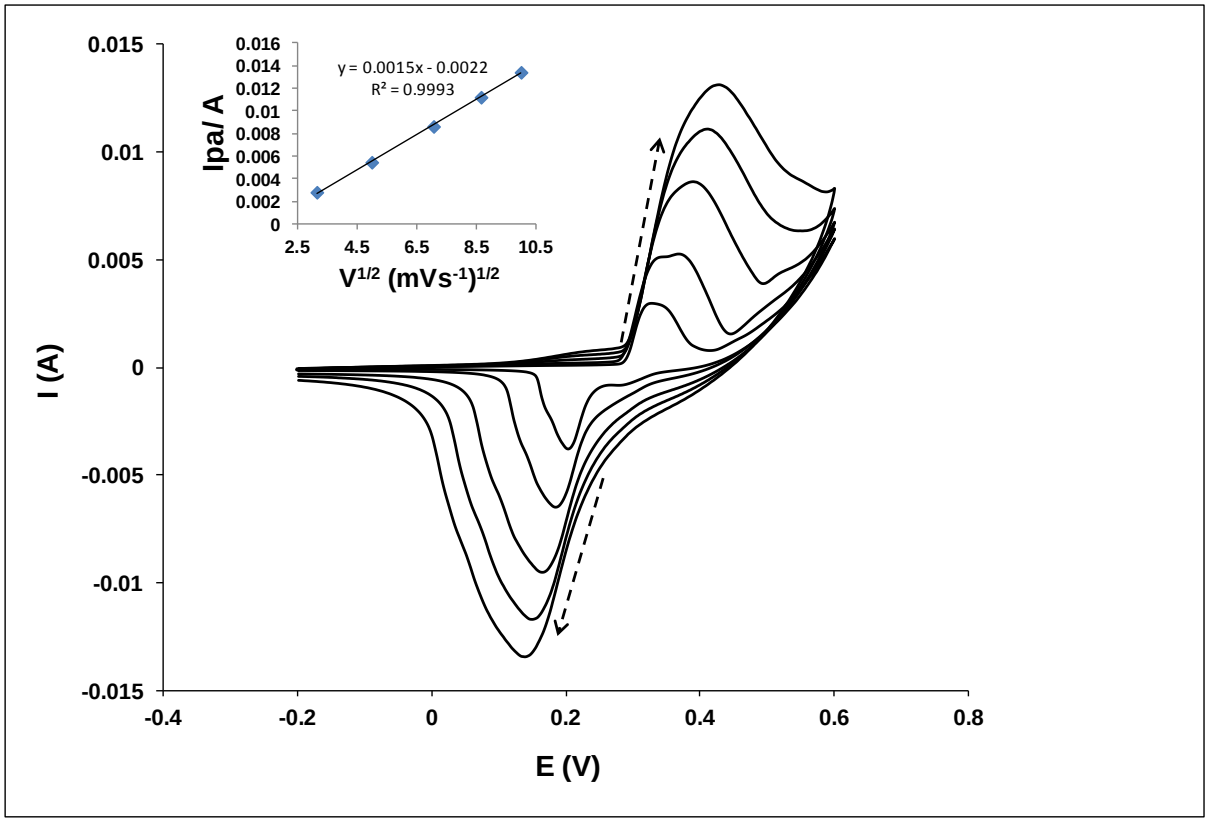

Figure 3.4: Scan rate studies of NF/NiTAPc in 2M KOH. Scan rate increases from inner to outer as indicated by the arrows.

3.2.2 Charge-Discharge

Galvanostatic discharge represents the most accurate and reliable strategy for probing the supercapacitance of materials. Figure 3.5 shows the comparative galvanostatic charge-discharge curves obtained for the three electrodes. The specific capacitance (SC) was evaluated from the discharge curve using equation 3.1:

$$\text{SC (Fg-1)} = \frac{I \times \Delta t}{\Delta E \times m} \qquad (3.1)$$

where Δt is the discharge time in seconds, ΔE is the potential difference in volt, I is the applied current in ampere, m (g) the area of the active material.

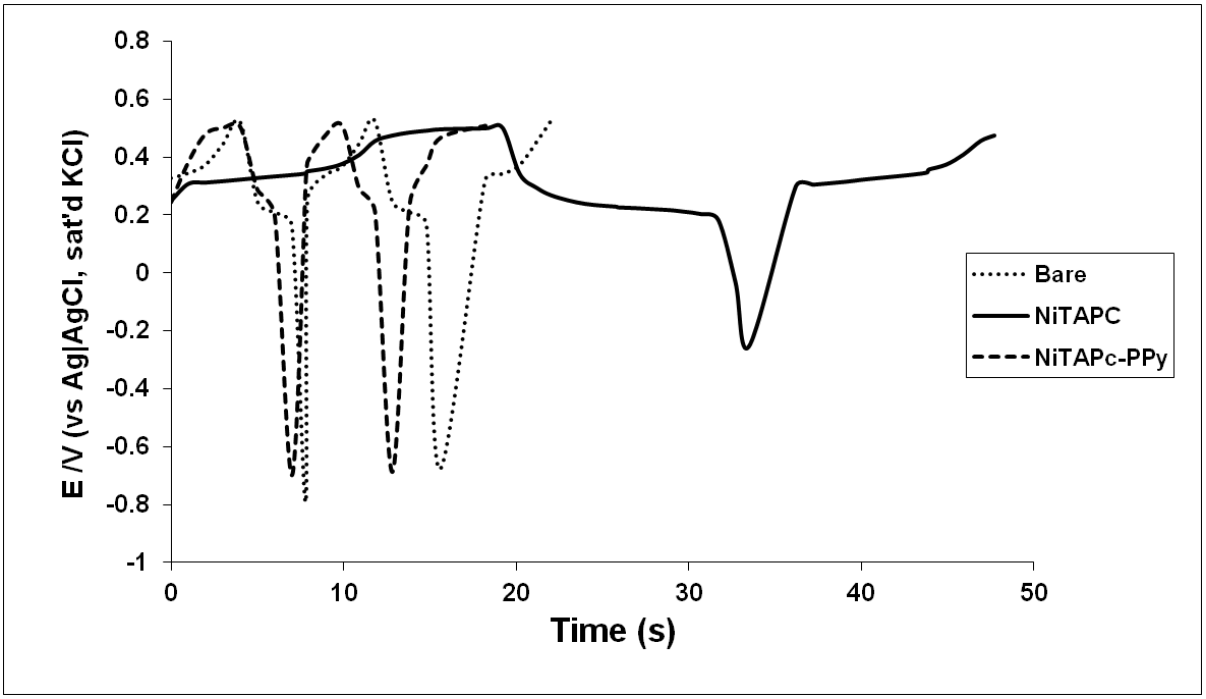

Figure 3.5: Comparative charge-discharge voltammograms of bare NF, NF/NiTAPc and NF/NiTAPc-PPy in 2M KOH.

As summarised in Table 3.1, the specific capacitance follows the same trend as the CV data: NF/NiTAPc (416 Fg^{-1}) >> NF/NiTAPc-PPy (15 Fg^{-1}).

Table 3.1: Supercapacitive parameters of Nickel foam electrode modified with NiTAPc and NiTAPc-PPY

Electrode (On Nickel Foam)	**Supercapacitive parameters**					
	SC (Fg^{-1})	**SP (WKg^{-1})**	**SE ($WhKg^{-1}$)**	**n(%)**	**Applied current density (Ag^{-1})**	**f_o (Hz)**
NF/NiTAPc	415.66	15469.45	65.75	112.89	20.50	28.12
NF/NiTAPc-PPY	15.05	2312.60	5.59	111.97	2.00	17.58

The energy deliverable efficiency (η / %) was obtained from equation 3.2.

$$\eta\ (\%) = \frac{t_d}{t_c} \times 100 \qquad (3.2)$$

where t_d and t_c are discharge time and charging time, respectively [6]. The energy deliverable efficiency for NF/NiTAPc is 112.9%.

The long-term cyclability of NF/NiTAPc as potential supercapacitor materials was investigated. A typical repetitive charge-discharge cycling for 1000 cycles, lasting about 2 days, is shown in Figure 3.6. It is clear from this figure that NF/NiTAPc is capable of undergoing continuous charge and discharge cycles with little or no significant loss in capacitance. This observation also suggests that NF/NiTAPc material does not show significant structural changes during the course of charge-discharge processes.

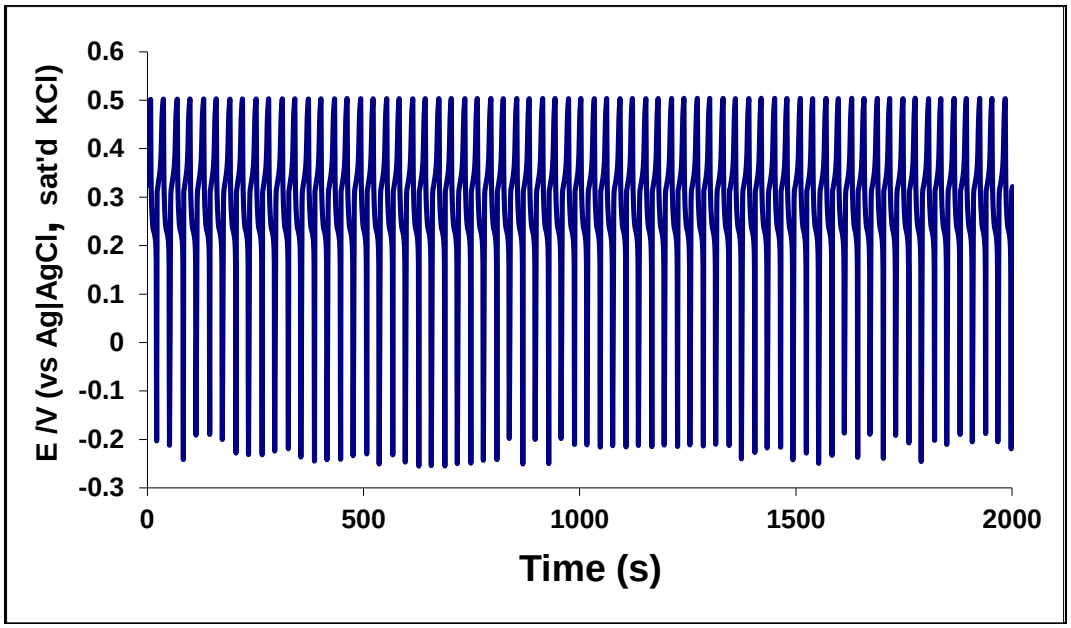

Figure 3.6: Long-term charge-discharge cycling of the NF/NiTAPc in 2M KOH. Current density = 20.5 Ag^{-1}

3.2.3 Electrochemical Impedance Spectroscopy

EIS experiments were performed to obtain further insights into the supercapacitance of the studied materials. EIS data were fitted with this equivalent circuit, ($R_s(Q[R_{ct}C])$. As seen in Table 3.1, the "knee" or "onset" frequency (f_o) (i.e., a measure of the power capability of a supercapacitor) decreases as NF/NiTAPc (28.12 Hz) > NF/NiTAPc-PPy (17.58 Hz). The response time of the NF/NiTAPc is about 36 ms, suggesting that most of the stored energy of NF/NiTAPc as a capacitor material may be accessed at frequencies as high as 28.12 Hz. This is very interesting considering that most commercially available supercapacitors, including those specifically designed for higher power applications, operate at frequencies less than 1 Hz [3, 7].

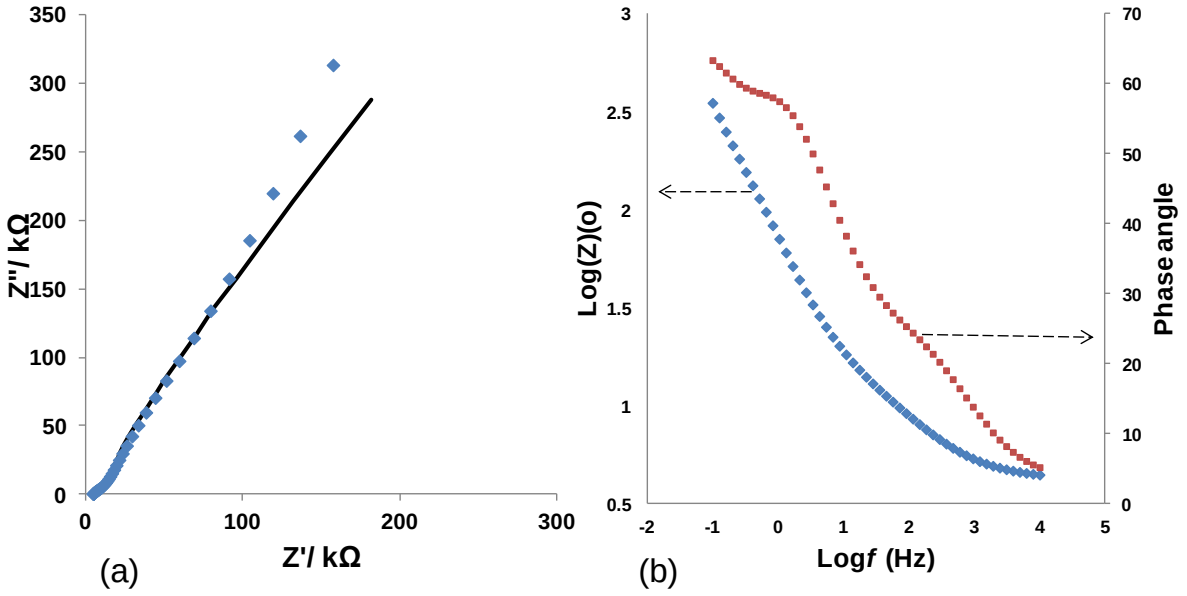

Figure 3.7: Typical Nyquist plot (a) and Bode plot (b) of the NF/NiTAPc. Fixed potential = 0.2V

Table 3.2: Summary of EIS parameters of the NF/NiTAPc electrode obtained from fitted impedance spectral using the modified Randles equivalent circuit model [8].

EIS Parameter			
R_s/Ω	**Q**	**R_{ct}/Ω**	**C/mF**
4.26±0.06	(0.71±0.04)x10^{-4}	33.90 ±1.87	0.63±0.03

CONCLUSIONS

In this chapter, the behaviour of NiTAPc has been interrogated. It is clearly evident, that a thin film of nickel (II) tetra-aminophthalocyanine (NiTAPc) was successfully synthesized and immobilized on nickel foam. Cyclic voltammetry, galvanostatic charge-discharge cycling and impedimetric techniques confirmed that the NiTAPc based electrode exhibit excellent supercapacitance. The capacitive behaviour of NiTAPc based electrode is affected by the introduction of a non conductive material such as PPY as seen from cyclic voltammetry and galvanostatic charge-discharge curves which may be attributed to the negative synergism between the non-doped PPY and NiTAPc. Galvanostatic method shows that NiTAPc is capable of undergoing continuous charge-discharge process for more than a 1000 cycles without any significant deterioration in the stability. High value of specific energy may suggest that, NiTAPc based electrode may be a potential material for battery.

REFERENCES

1. G. Wang, J. Huang, S. Chen, S. Gao and D. Cao, *Journal of Power Sources*, 2011, **196** 5756–5760.
2. W. Xing, S. Qiao, X. Wu, X. Gao, J. Zhou, S. Zhou and S.-B. Hartono, *Journal of Power Sources* 2011, **196**, 4123–4127.
3. A. T. Chidembo and K. I. Ozoemena, *Electroanalysis*, 2010, **22**, 2529-2535.
4. A. T. Chidembo, K. I. Ozoemena, B. O. Agboola, V. Gupta, G. G. Wildgoose and R. G. Compton, *Energy Environ. Sci.*, 2009, **3**, 228-236.
5. V. Khomenko, E. Frackowiak and F. Beguin, *Electrochimica Acta*, 2005, **50**, 2499-2506.
6. S. G. Kandalkar, J. L. Gunjakar and C. D. Lokhande, *Applied surface science*, 2008, **254**, 5540-5544.
7. J. R. Miller and A. F. Burke, *Interface-Electrochemical Society*, 2008, **17**, 53-57.
8. J. E. B. Randles, *Trans. Faraday Soc.*, 1948, **44**, 327-338.

CHAPTER FOUR

Supercapacitive Behaviour of NiO-MWCNT Prepared Using the SILAR Method

4.1 Spectroscopic and Microscopic Characterization of NiO and NiO-MWCNT nanocomposites

The deposition method adopted here is the so called Successive Ionic Layer Adsorption and Reaction (SILAR), please see experimental for detailed process [1-4].

4.1.1 Scanning Electron Microscopy Images

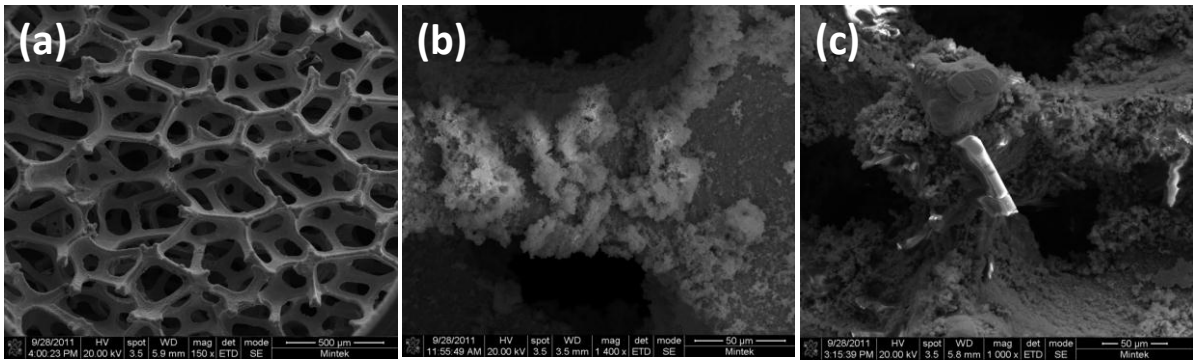

Figure 4.1: Typical SEM images of (a) bare NF (b) NF/NiO, and (c) NF/MWCNT-NiO

4.1.2 Energy-Dispersive X-ray Spectroscopy Analysis

Figure 4.2 represents profiles of the EDX analysis for bare NF, NF/NiO, NF/MWCNT-NiO and NF/MWCNT. As expected, both NF (a) and NF/NiO (b) gave nickel peaks, with the more oxygen peaks detected for the NF/NiO (b) and NF/MWCNT-NiO (c). The oxygen peaks in MWCNTs arise from the acid-functionalisation process. The Fe peaks observed in MWCNT-NiO (c) are due to the impurities from the commercial MWCNT, suggesting that Fe-based complexes were used in the synthesis of these MWCNTs. The K impurities may be due to the phosphate buffer solution used in the treatment of the MWCNTs.

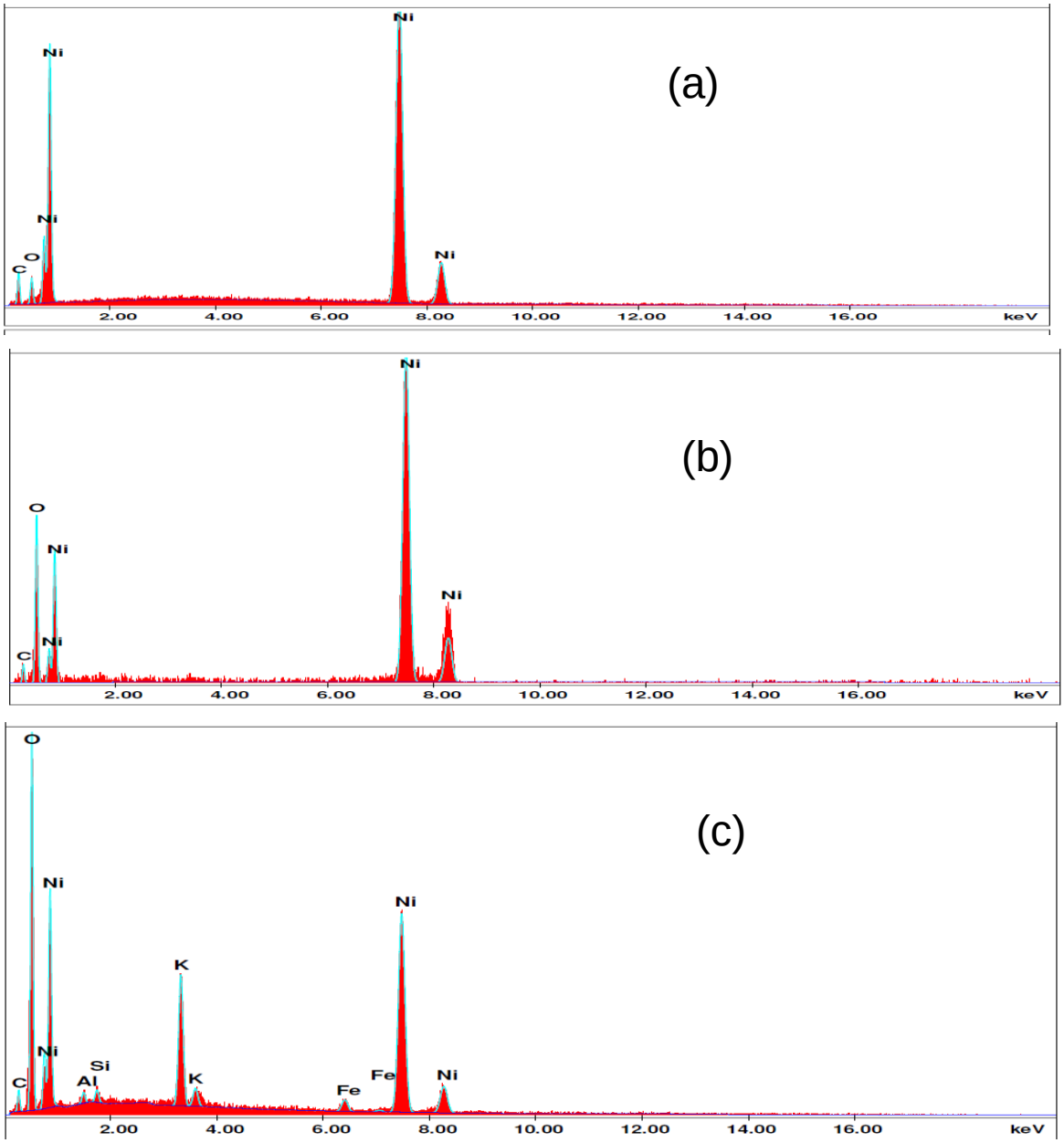

Figure 4.2: Typical EDX images of (a) bare NF (b) NF/NiO, and (c) NF/MWCNT-NiO

4.2 Supercapacitive behavior of NiO-MWCNT nanocomposites using SILAR method

4.2.1 Cyclic Voltammetry

Figure 4.3 presents the cyclic voltammograms of bare NF, NF/NiO, NF/MWCNT, and NF/MWCNT-NiO electrodes in 2M KOH at 25 mVs^{-1}. The current response follows this trend: NF/MWCNT-NiO > NF/NiO >> NF/MWCNT > bare NF. According to literature [5-7], voltammogram is due to the reversible reaction involving the NiO/NiOOH couple, i.e:

$$NiO + yOH^- \rightleftharpoons yNiOOH + e^- \quad (4.1)$$

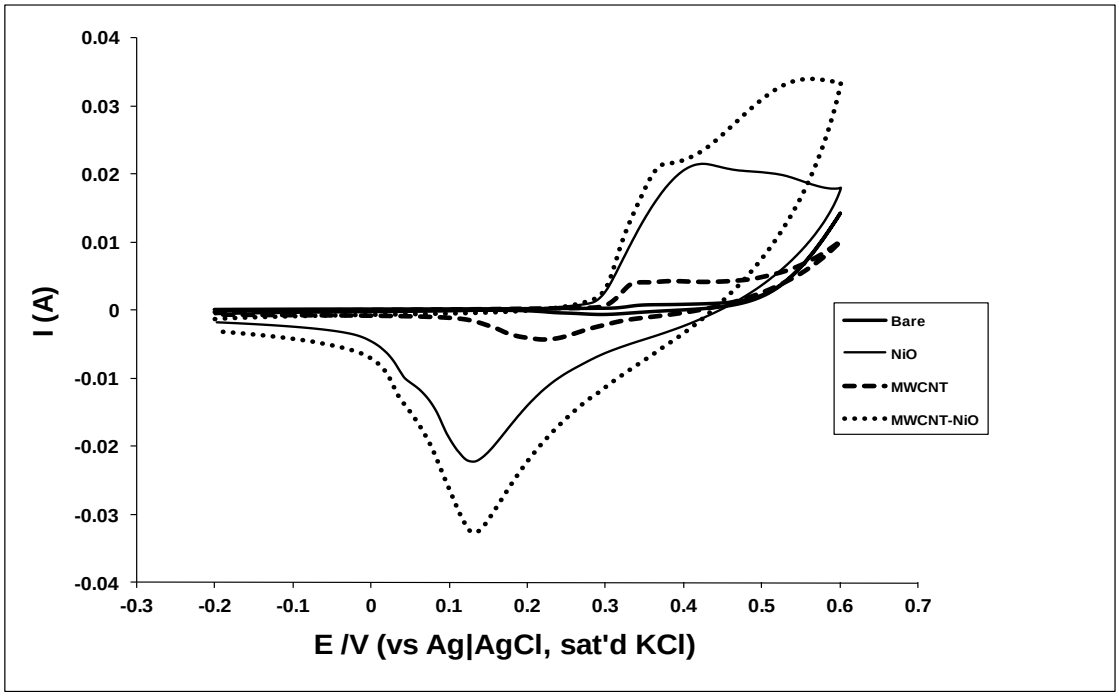

Figure 4.3: Comparative cyclic voltammograms of bare NF, NF/NiO, NF/MWCNT, and NF/MWCNT-NiO electrodes in 2M KOH at 25 mVs^{-1}.

Figure 4.4 shows the voltammograms of the NF/MWCNT-NiO at various scan rates (10 to 100 mVs^{-1}). Plot of peak current versus scan rate (inset) is linear, indicating diffusion-controlled process.

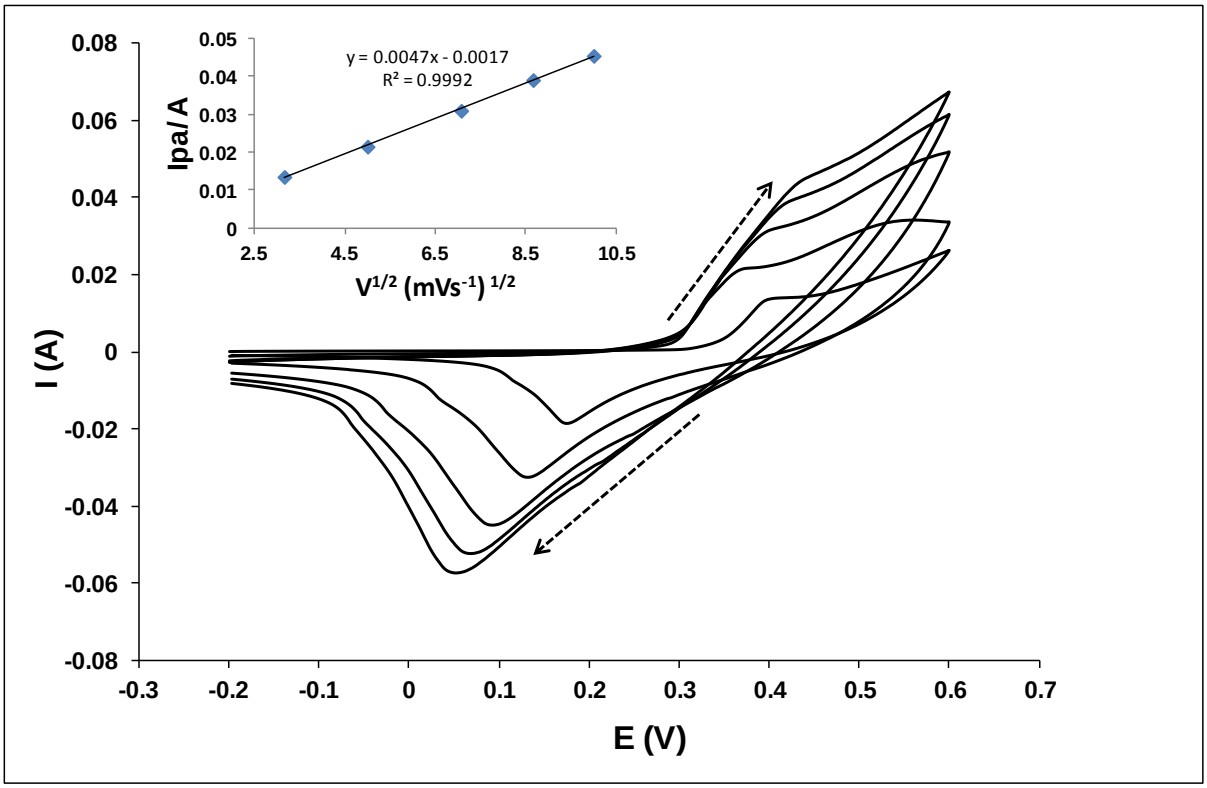

Figure 4.4: Scan rate studies of NF/MWCNT-NiO in 2M KOH. Scan rate increases from inner to outer as indicated by the arrows.

4.2.2 Charge-Discharge

Figure 4.5 shows the comparative galvanostatic charge-discharge curves obtained for the bare NF, NF/NiO, NF/MWCNT, and NF/MWCNT-NiO electrodes in 2M KOH.

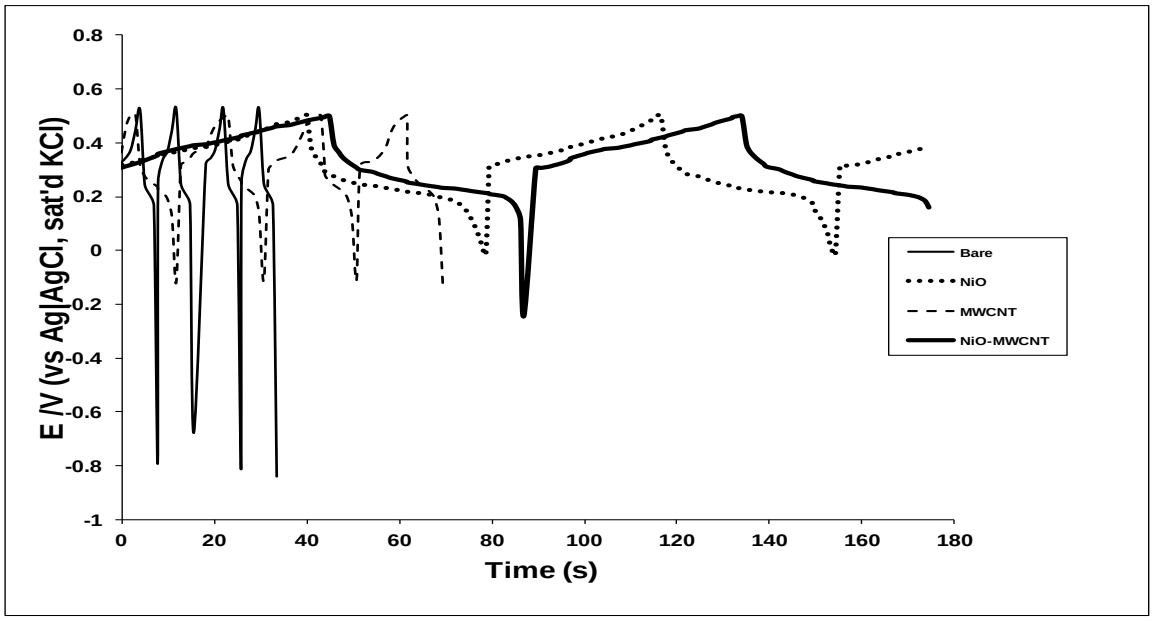

Figure 4.5: Typical comparative charge-discharge voltammograms of bare NF, NF/NiO, NF/MWCNT-NiO and NF/MWCNT in 2M KOH.

The supercapacitive parameters (specific capacitance, energy, power and efficiency) were obtained using the relevant equations described in chapter 1, and summarised in Table 4.1. The SC values follows this trend; NF/MWCNT-NiO > NF/NiO >> NF/MWCNT > bare NF, corroborating the CV data.

Table 4.1: Supercapacitive parameters of Nickel foam electrode modified with MWCNT, NiO and NiO-MWCNT

Electrode (On Nickel Foam)	**Supercapacitive parameters**					
	SC (Fg^{-1})	**SP (WKg^{-1})**	**SE ($WhKg^{-1}$)**	**n(%)**	**Applied current density (Ag^{-1})**	**f_o (Hz)**
NF/MWCNT	161.16	6081.00	16.55	140.45	10.00	8.69
NF/NiO	791.38	5491.49	58.58	119.33	10.64	13.90
NF/NiO-MWCNT	1034.43	10410.77	131.58	162.51	15.40	17.68

Figure 4.6 presents the long-term cyclability response of the NF/MWCNT-NiO, with no significant loss in capacitance after over 1000 cycles. This observation also suggests that MWCNT-NiO nanocomposite does not show significant structural changes during the course of charge-discharge processes.

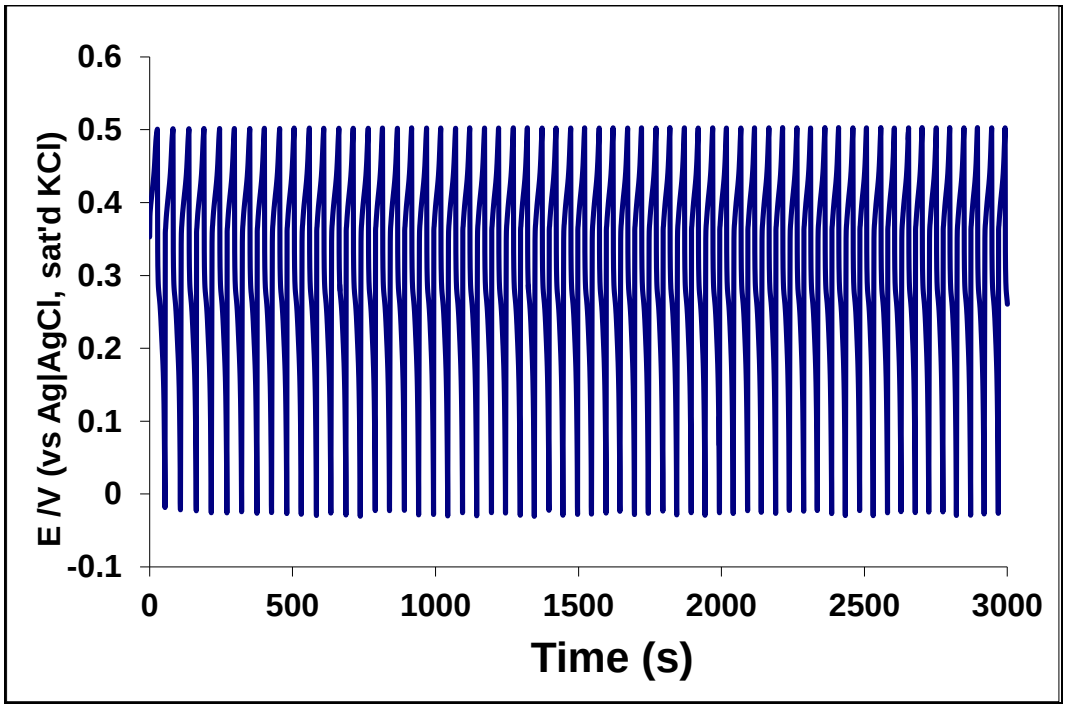

Figure 4.6: Long-term charge-discharge cycling of the NF/MWCNT-NiO in 2M KOH. Current density = 15 Ag^{-1}.

4.2.3 Electrochemical Impedance Spectroscopy

Figure 4.7 shows typical Nyquist plots of the NF/NiO-MWCNT obtained in 2M KOH at a fixed potential of 0.2 V. The "knee" frequency (f_o) values of NF/NiO-MWCNT with its precursors are presented in Table 4.1, with the MWCNT-NiO giving the highest value. Again, this is very interesting considering that most commercially available supercapacitors, including those specifically designed for higher power applications, operate at frequencies less than 1 Hz [8].

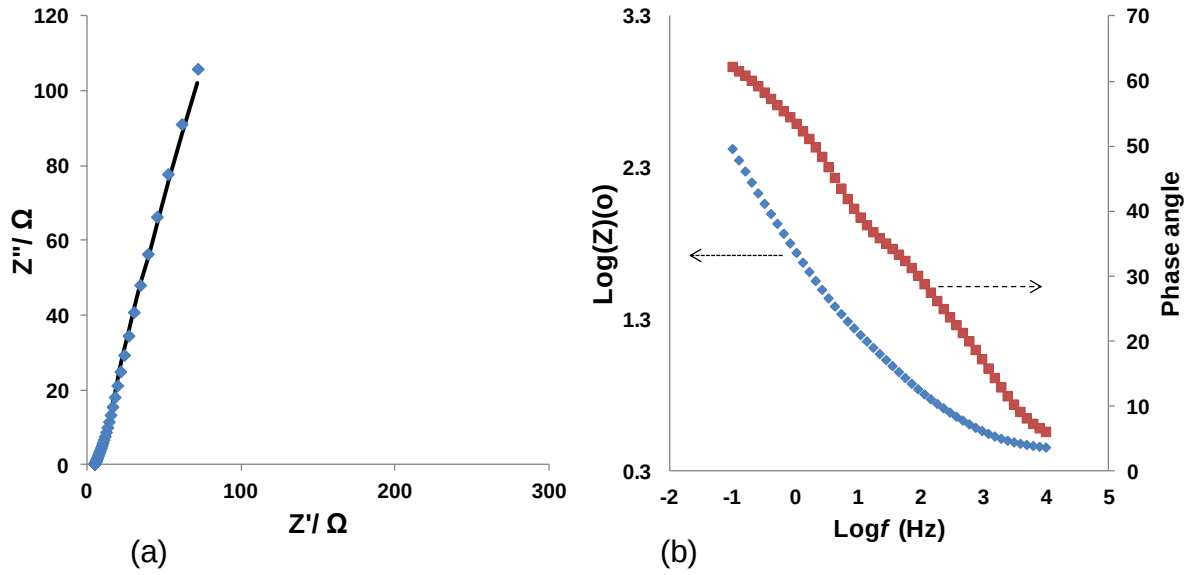

Figure 4.7: Typical Nyquist plot (a) and Bode plot (b) of the NF/NiO-MWCNT in 2 M KOH. Fixed potential = 0.2V

Table 4.2: Summary of EIS parameters of NF/NiO-MWCNT electrodes obtained from fitted impedance spectral using the modified Randles equivalent circuit model.

Electrode	**Circuit**	**R_s/Ω**	**Q**	**R_{ct}/Ω**	**C/mF**
NF/NiO-MWCNT	R_s (Q [R_{ct} + C])	4.70 ±0.030	(0.40 ±0.015)x10^{-3}	43.30 ±2.90	1.48 ±0.082

Conclusions

In this chapter, the behaviour of NiO-MWCNT has been interrogated using cyclic voltammetry, galvanostatic charge-discharge cycling and impedimetric techniques. A porous NiO-MWCNT composite was successfully synthesised and immobilised on nickel foam with the aid of SILAR electrode modification technique. The capacitive behaviour of NiO-MWCNT based electrode exhibit excellent supercapacitance as compared to that of its precursors (NiO and MWCNT). The excellent capacitance of NiO-MWCNT may be due to the positive synergism between the MWCNT and NiO. Galvanostatic method shows that NiO-MWCNT is capable of undergoing continuous charge-discharge process for more than a 1000 cycles without any significant deterioration in the stability. From table 3.1 the NiO-MWCNT based electrode exhibit high value of specific energy that may suggest that this type of electrode may be good for battery.

REFERENCES:

1. Y. Gao, S. Chen, D. Cao, G. Wang and J. Yin, *Journal of power sources*, 2010, **195**, 1757-1760.
2. O. Lupan, S. Shishiyanu, L. Chow and T. Shishiyanu, *Thin solid films*, 2008, **516**, 3338-3345.
3. V. N. Popov, *Materials Science and Engineering: R: Reports*, 2004, **43**, 61-102.
4. J. Yang, Z. Jin, Y. Chai, H. Du, T. Liu and T. Wang, *Thin solid films*, 2009, **517**, 6617-6622.
5. A. I. Inamdar, Y. S. Kim, S. M. Pawar, J. H. Kim, H. Im and H. Kim, *Journal of power sources*, 2011, **196**, 2393-2397.
6. X. Xia, J. Tu, X. Wang, C. Gu and X. Zhao, *J. Mater. Chem.*, 2010, **21**, 671-679.
7. Y. Zheng, M. Zhang and P. Gao, *Materials research bulletin*, 2007, **42**, 1740-1747.
8. J. R. Miller and A. F. Burke, *Interface-Electrochemical Society*, 2008, **17**, 53-57.

CHAPTER FIVE

Supercapacitive Behaviour of NiTAPc-NiO Nanocomposite

5.1 Spectroscopic and Microscopic Characterization

Based on the findings of chapters 3 and 4 where NF/NiTAPc and NF/NiO obtained by SILAR showed good performance, this present chapter is therefore aimed at finding the effect of electrodeposition processes and / or combined electrodeposition and SILAR on the supercapacitive properties of the NiTAPc-NiO composites.

5.1.1 Scanning Electron Microscopy Images

Figure 5.1 compares the SEM images of the bare NF and modified NF with NiO, NiTAPc and NiTAPc-NiO nanocomposites. In all cases, the modified NF electrodes are rough but porous, indicating non-homogenous deposition.

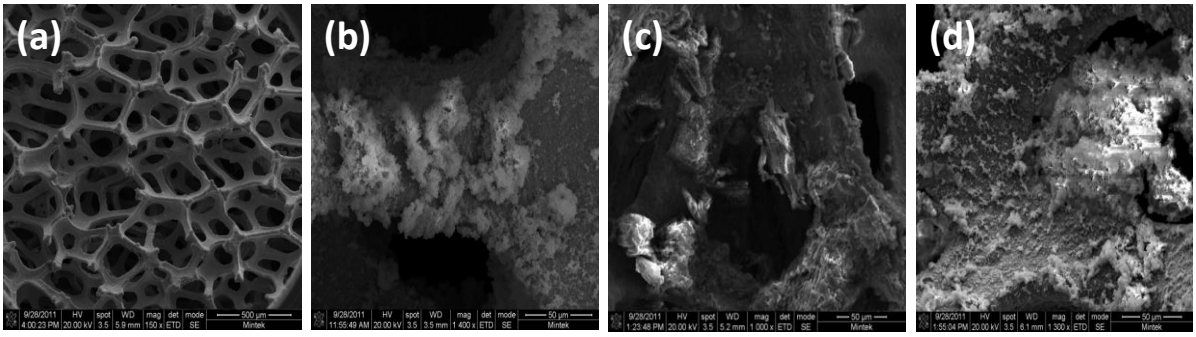

Figure 5.1: Typical SEM images of (a) bare NF (b) NF/NiO, (c) NF/NiTAPc, and (d) NF/NiTAPc-$NiO_{(S)}$

5.1.2 Energy-Dispersive X-ray Spectroscopy Analysis

Figure 5.2 represents profiles of the EDX analysis for bare NF, NF/NiO, NF/NiTAPc and NF/NiTAPc-NiO. Both NF (a) and NF/NiO (b) have already been described in chapter 4. As expected, both NF/NiTAPc (c) and NF/NiTAPc-NiO (d) gave nickel peaks. The prominent K peaks are associated with impurities from the phosphate buffer solution.

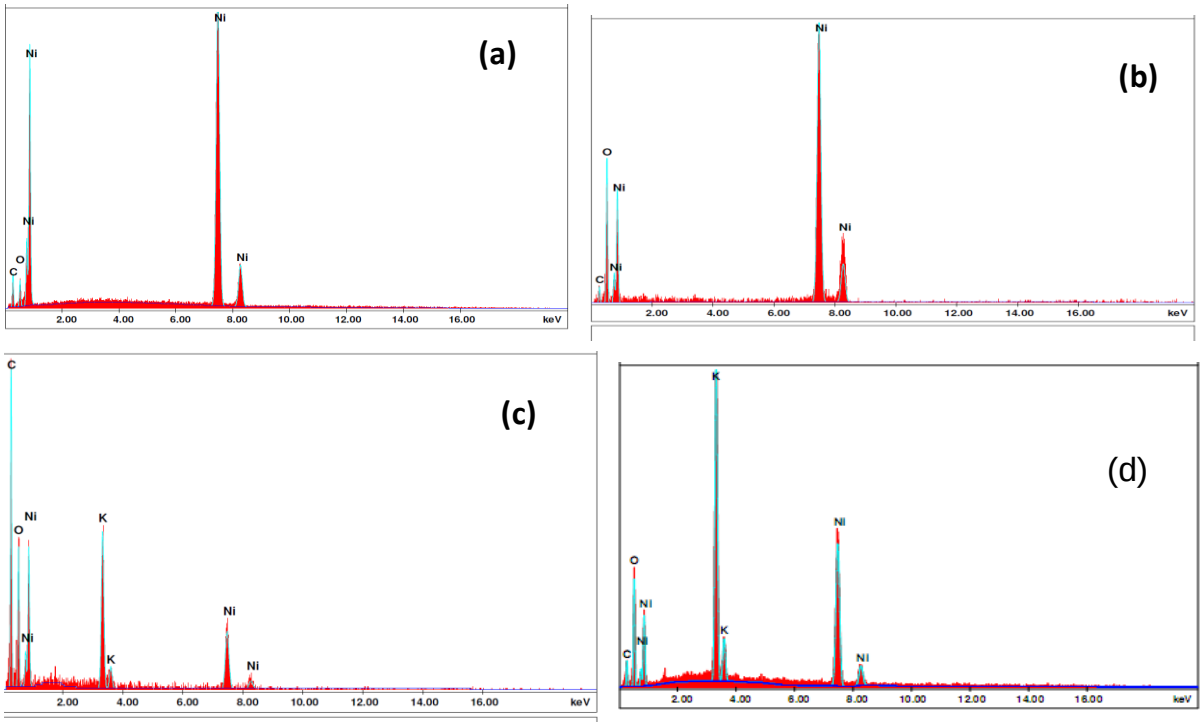

Figure 5.2: Typical EDX spectra of (a) bare NF (b) NF/NiO, (c) NF/NiTAPc**,** and (d) NF/NiTAPc-NiO.

5.2 Supercapacitive properties of NiTAPc-NiO nanocomposites

5.2.1 Cyclic Voltammetry

First, I wanted to find out if depositing NiTAPc first before depositing the NiO (NF/NiTAPc-NiO), or vice versa (NF/NiO-NiTAPc), will have any effect on the voltammetric response of the modified NF electrode. As seen in Figure 5.3, it is evident that NF/NiTAPc-NiO gave slightly higher current response compared to the NF/NiO-NiTAPc counterpart.

From this preliminary SILAR result (Figure 5.3), both NiTAPc and NiO were deposited on the NF using the electrodeposition technique (NF/NiTAPc-$NiO_{(E)}$), NiO first SILAR-deposited while the NiTAPc electrodeposited (i.e., NF/NiO-$NiTAPc_{(S-E)}$), and NiTAPc first electrodeposited while the NiO SILAR-deposited (i.e., NF/NiTAPc-$NiO_{(E-S)}$). As evident from Figure 5.4, the current response follows this trend: NF/NiTAPc-$NiO_{(E)}$ ≈ NF/NiTAPc-$NiO_{(E-S)}$ > NF/NiO-$NiTAPc_{(S-E)}$.

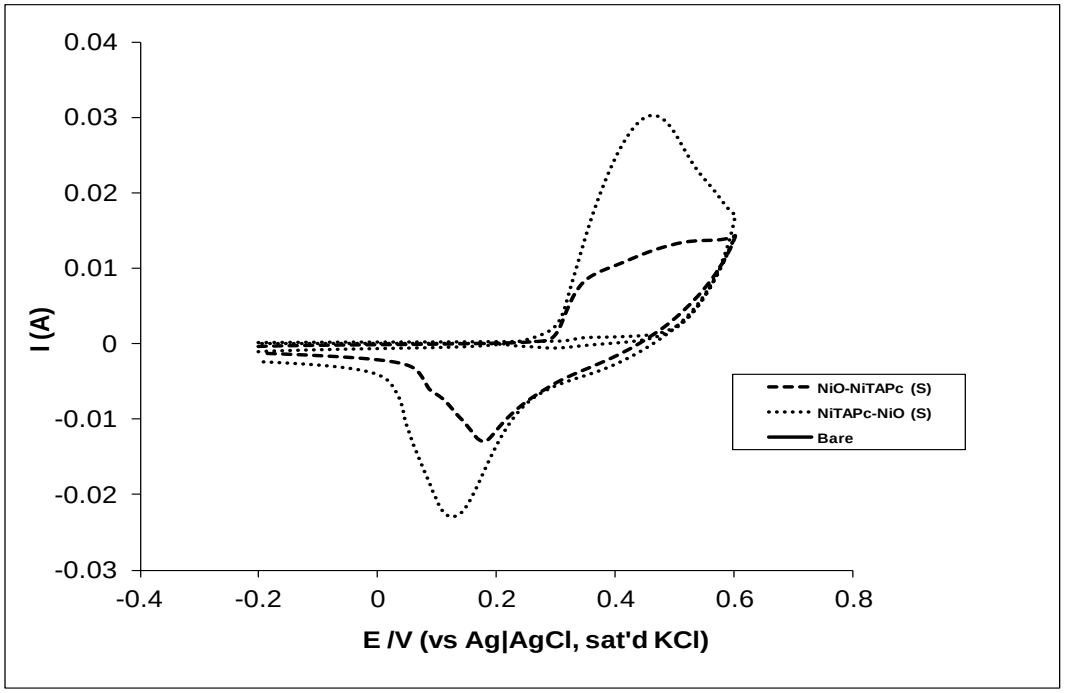

Figure 5.3: Comparative cyclic voltammograms of bare NF, NF/NiTAPc-$NiO_{(S)}$ and NF/NiO-$NiTAPc_{(S)}$ electrodes in 2M KOH at 25 mVs^{-1}.

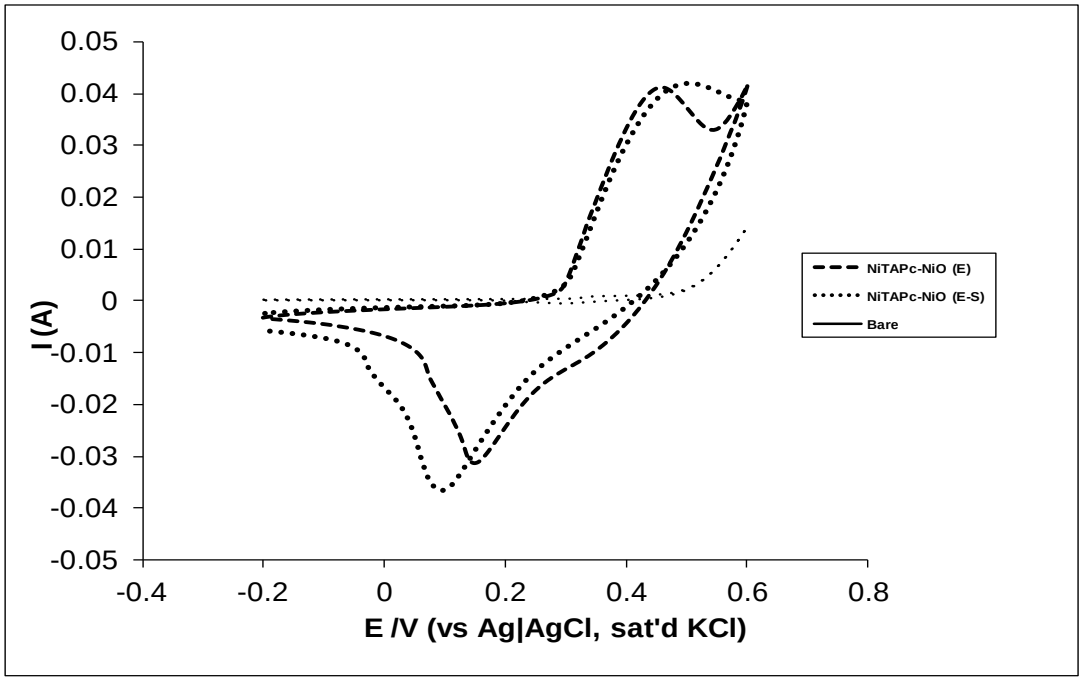

Figure 5.4: Comparative cyclic voltammograms of bare NF, NiTAPc-$NiO_{(E)}$, and NF/NiTAPc-$NiO_{(E-S)}$ electrodes in 2M KOH at 25 mVs^{-1}.

5.2.2 Charge-Discharge

Figure 5.5 shows the comparative galvanostatic charge-discharge curves obtained for the bare NF, NF/NiTAPc-$NiO_{(E)}$, NF/NiTAPc-$NiO_{(E-S)}$ and NF/NiO-$NiTAPc_{(S-E)}$ electrodes in 2M KOH at a fixed current of 20 mA. The supercapacitive parameters are summarised in Table 5.1, with the supercapacitive properties decreasing as follows: NF/NiTAPc-$NiO_{(E-S)}$ > NF/NiTAPc-$NiO_{(E)}$ > NF/NiO > NF/NiTAPc. In theory, the higher the applied current density, the lower the supercapacitive values. Thus, results in Table 5.1 are quite exciting considering that despite that high current density used for the NF/NiTAPc-$NiO_{(S-E)}$ (48 A/g), it showed highest supercapacitive values compared to those obtained at lower current densities, NF/NiTAPc-$NiO_{(E)}$ (40 A/g), NF/NiTAPc (21 A/g) and NF/NiO (11 A/g).

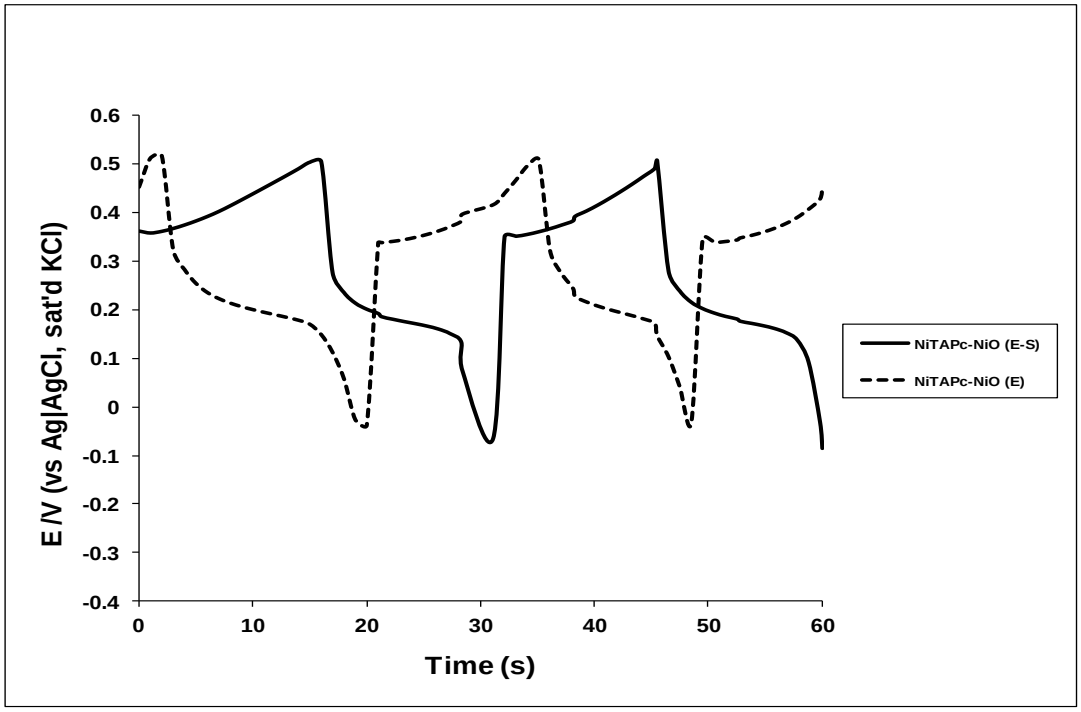

Figure 5.5: Typical charge-discharge voltammograms of NiTAPc-$NiO_{(E)}$, and NF/NiTAPc-$NiO_{(E-S)}$ electrodes in 2M KOH at a fixed current of 20 mA.

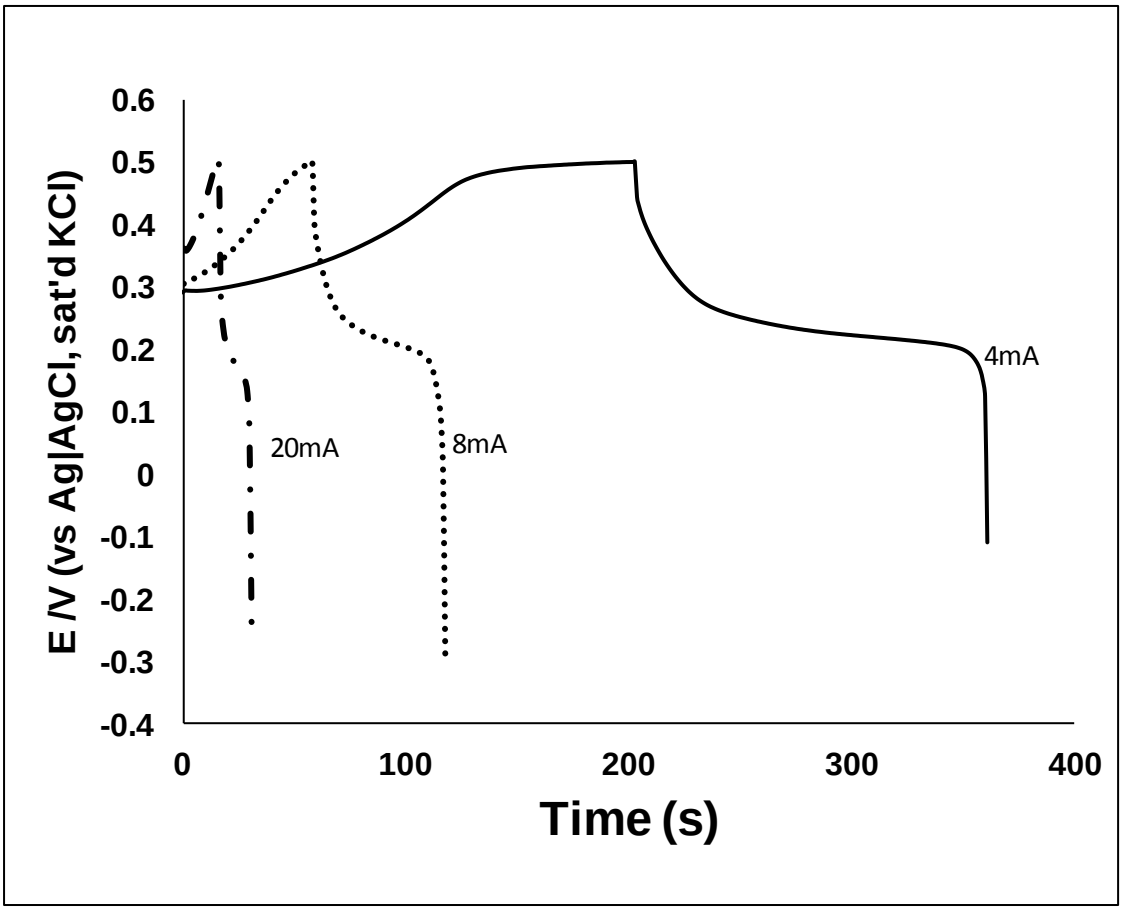

Figure 5.6: Overlaid charge-discharge voltammograms of NF/NiTAPc-$NiO_{(E-S)}$ electrode in 2M KOH at various currents.

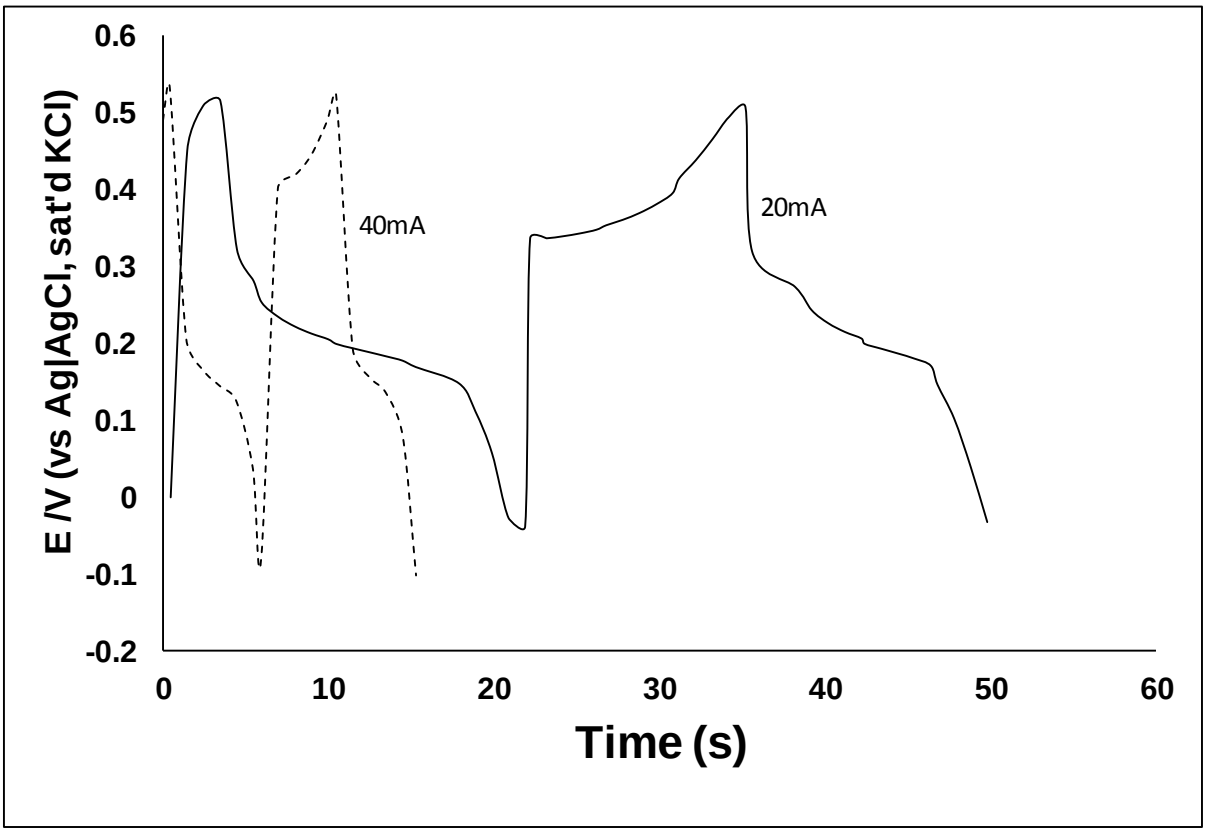

Figure 5.7: Overlaid charge-discharge voltammograms of NF/NiTAPc-$NiO_{(E)}$ electrode in 2M KOH at various currents.

Table 5.1: Supercapacitive parameters of Nickel foam electrode modified with NTAPc, NiO and NiTAPc-NiO $_{(E-S)}$

Electrode (On Nickel Foam)	**Supercapacitive parameters**					
	SC (Fg^{-1})	**SP (WKg^{-1})**	**SE ($WhKg^{-1}$)**	**n(%)**	**Applied current density (Ag^{-1})**	**f_o (Hz)**
NF/NiTAPc	415.65	15469.45	65.75	112.89	20.50	28.12
NF/NiO	791.38	5491.49	58.58	119.33	10.64	13.90
NF/NiTAPc- NiO$_{(E-S)}$	1278.59	26957.14	113.82	120.08	47.62	1256.00
NiTAPc-NiO$_{(E)}$	1116.93	20484.80	81.37	122.24	40.00	954.00

Considering the higher performance of the NF/NiTAPc-$NiO_{(E-S)}$, further studies were performed on the electrode. Figure 5.8 presents the long-term cyclability response of the of the NiTAPc-$NiO_{(E-S)}$, with no significant loss in capacitance after over 1000 cycles. This observation also suggests that NiTAPc-$NiO_{(E-S)}$ nanocomposite does not show significant structural changes during the course of charge-discharge processes.

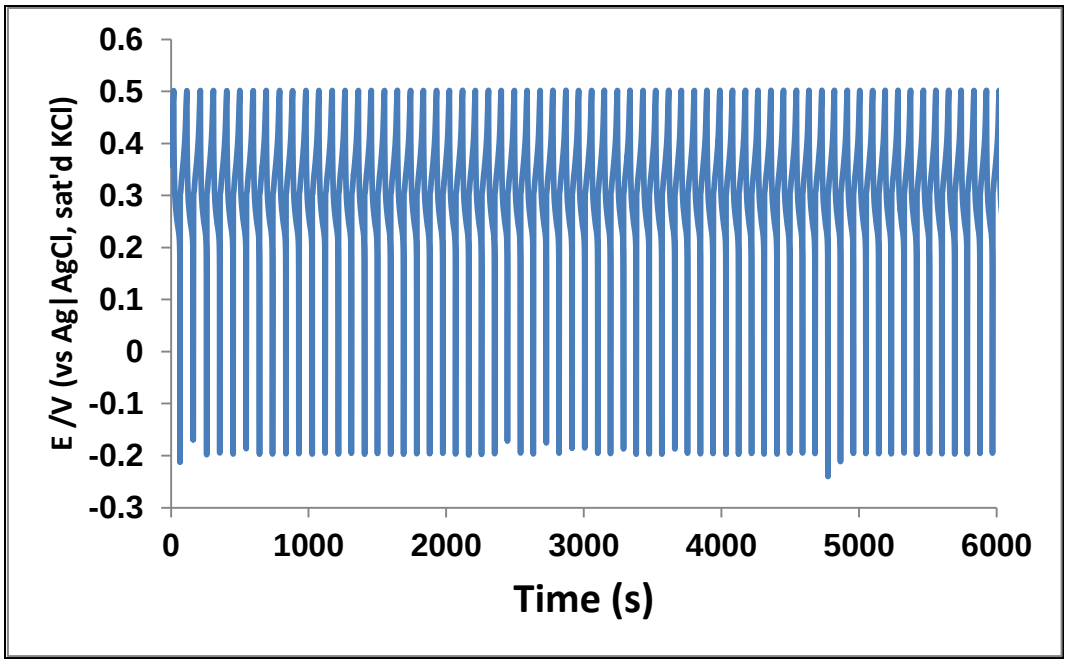

Figure 5.8: Long-term charge-discharge cycling of the NF/NiTAPc-$NiO_{(E-S)}$ in 2M KOH. Current density = 48 Ag^{-1}.

5.2.3 Electrochemical Impedance Spectroscopy

The "knee" frequency (f_o) of the NF/NiTAPc-$NiO_{(E-S)}$ is , which is quite high compare to most commercially available supercapacitors, designed for higher power applications that operate at frequencies less than 1 Hz [1].

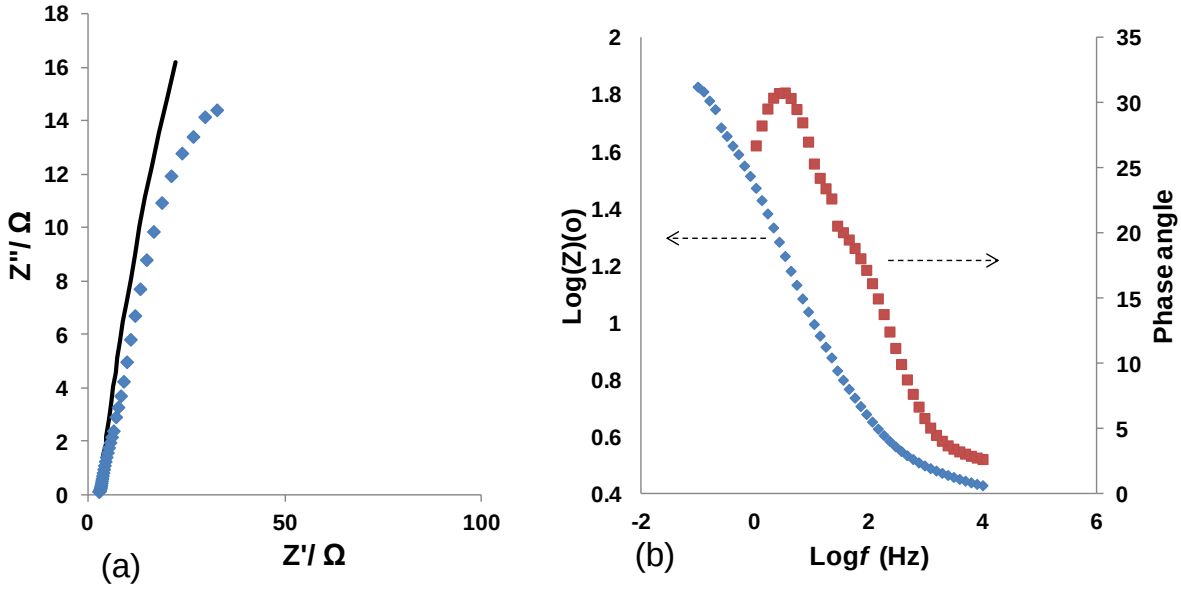

Figure 5.9: Typical fitted Nyquist plot (a) and Bode plot (b) of the NF/NiTAPc-$NiO_{(E-S)}$ in 2M KOH. Fixed potential = 0.2V

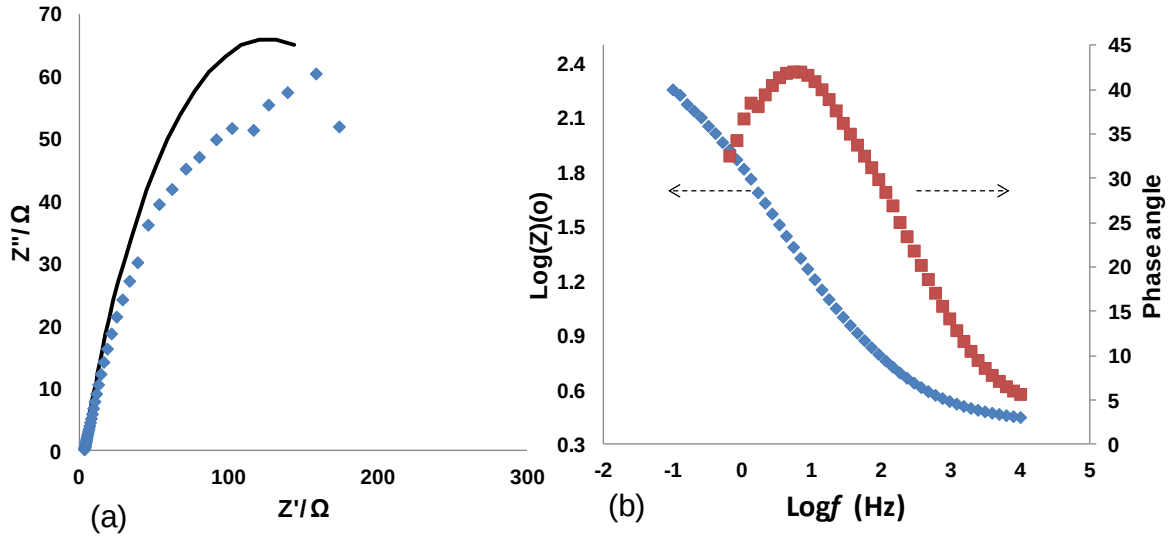

Figure 5.10: Typical fitted Nyquist plot (a) and Bode plot (b) of the NF/NiTAPc-$NiO_{(E)}$ in 2M KOH. Fixed potential = 0.2V

Table 5.2: Summary of EIS parameters of NF/NiTAPc-$NiO_{(E-S)}$ and NF/NiTAPc-$NiO_{(E)}$ electrodes obtained from fitted impedance spectral using the modified Randles equivalent circuit model.

Electrode	**Circuit**	**R_s/Ω**	**Q**	**R_{ct}/Ω**
NiTAPc-$NiO_{(E)}$	R_s (Q [R_{ct} + W])	2.81±0.103	(0.17 ±0.020)x10^{-3}	245.30 ±50.12
NiTAPc-$NiO_{(E-S)}$	R_s (Q [R_{ct} + W])	2.75±0.140	(0.31 ±0.070)x10^{-3}	109.80 ±43.00

Conclusions

In this chapter, the behaviour of NiTAPc-NiO has been interrogated for the first time, using both electrochemical deposition and SILAR techniques as electrode modification methods. A porous NiTAPc-NiO composite was successfully synthesised and immobilised on nickel foam. The effect of NiTAPc was obtained by interchanging the layers of NiTAPc and NiO on NiTAPc-NiO composite. Cyclic voltammetry, galvanostatic charge-discharge cycling and impedimetric techniques comfirmed the capacitive behaviour of NiTAPc-NiO based electrode exhibit excellent supercapacitance as compared to that of its precursors (NITAPc-NiO). The capacitance of NiTAPc-NiO electrodeposited and NiTAPc-NiO synthesised by both electrodeposition and SILAR were found to be comparative to each other though NiTAPc-NiO synthesised by both electrodeposition and SILAR has a specific capacitance slightly higher than that of electrodeposited as seen from overlaid cyclic voltammograms, overlaid galvanostatic charge-discharge cycling and impedimetric techniques. Galvanostatic method shows that NiTAPc-NiO synthesised by both electrodeposition and SILAR is capable of undergoing continuous charge-discharge process for more than a 1000 cycles without any significant deterioration in the stability. From table 5.1 the all of the electrode materials exhibit high value of specific energy that may suggest that this type of electrode may be good for battery though their capacitance values

are very high and power densities are high. Both a cost-saving techniques of electrodeposition and SILAR were able to be coupled to synthesise a very promising substrate for industrial applications of nickel oxide in electrochemical supercapacitors

REFERENCE

1. J. R. Miller and A. F. Burke, *Interface-Electrochemical Society*, 2008, **17**, 53-57.

CHAPTER SIX

Supercapacitive Behaviour of Oxidant-assisted SILAR-prepared Nickel Oxide Electrode

6.1 Comparative Cyclic Voltammetry

This chapter is a product of curiosity. During the final stages of this MSc studies, I came across a recent study that showed that the use of an oxidizing agent can improve the supercapacitive properties of NiO-based electrode [1]. Based on this literature, I decided to study NiO formed by SILAR as a model electrode using an oxidant, potassium persulphate ($K_2S_2O_8$). This electrode is represented here as NF/$NiO_{(S\text{-}ox)}$.

Figure 6.1 presents comparative CVs of the bare NF, NF/NiO(s) and NF/NiO(S-ox), proving that the NF/NiO(S-ox) gave better electrochemical response compared to the NF and NF/NiO(s).

Figure 6.2 shows the voltammograms of the NF/$NiO_{(S\text{-}ox)}$ at various scan rates (10 to 100 mVs^{-1}). Plot of peak current versus scan rate (inset) is linear, indicating diffusion-controlled process.

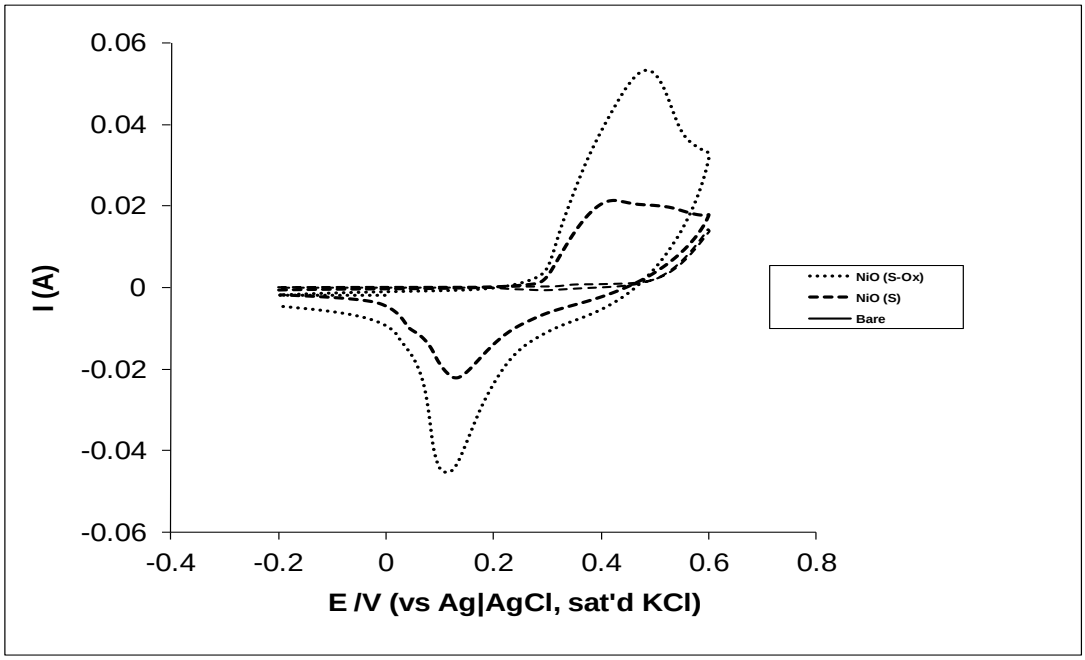

Figure 6.1: Comparative cyclic voltammograms of bare NF, NF/$NiO_{(S\text{-}ox)}$, NF/$NiO_{(S)}$ electrodes in 2M KOH at 25 mVs^{-1}.

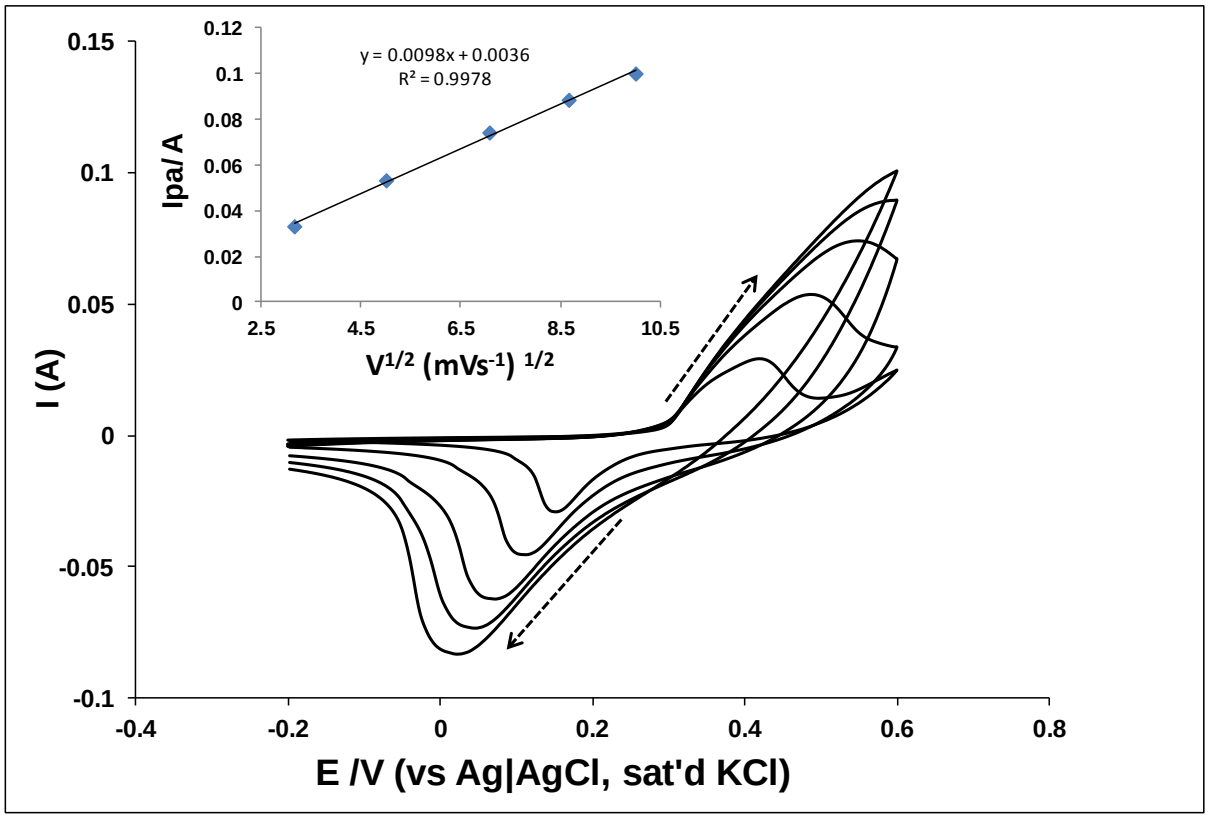

Figure 6.2: Scan rate studies of NF/$NiO_{(S\text{-}ox)}$ electrode in 2M KOH. Scan rate increases from inner to outer as indicated by the arrows

Table 6.1: Supercapacitive parameters of Nickel foam electrode modified with $NF/NiO_{(S\text{-}ox)}$ and $NF/NiO_{(S)}$

Electrode (On Nickel Foam)	**Supercapacitive parameters**					
	SC (Fg^{-1})	**SP (WKg^{-1})**	**SE ($WhKg^{-1}$)**	**n(%)**	**Applied current density (Ag^{-1})**	**f_o (Hz)**
$NF/NiO_{(S\text{-}ox)}$	1402.80	14444.71	146.85	133.18	23.53	754.00
$NF/NiO_{(S)}$	791.38	5491.49	58.58	119.33	10.64	13.90

6.2 Charge-Discharge

Figure 6.3 compares the galvanostatic charge-discharge curves obtained for the bare NF, NF/$NiO_{(S)}$, and NF/$NiO_{(S\text{-}ox)}$ electrodes in 2M KOH. The supercapacitive parameters are summarised in Table 6.1, with the supercapacitive properties decreasing as follows: NF/$NiO_{(S\text{-}ox}$ > NF/$NiO_{(S)}$ > bare NF. Interestingly, NF/$NiO_{(S\text{-}ox)}$ electrode gave the highest performance despite that it was obtained at a higher current density (23.5 mA/g) than the NF/$NiO_{(S)}$ electrode (10.6 mA/g).

Considering the higher performance of the NF/$NiO_{(S\text{-}ox)}$, it was subjected to long-term cyclability (Figure 6.4). It is found that the NF/$NiO_{(S\text{-}ox)}$ was stable with no significant loss in capacitance after over 1000 cycles, meaning that this electrode does not show significant structural changes during the course of charge-discharge processes.

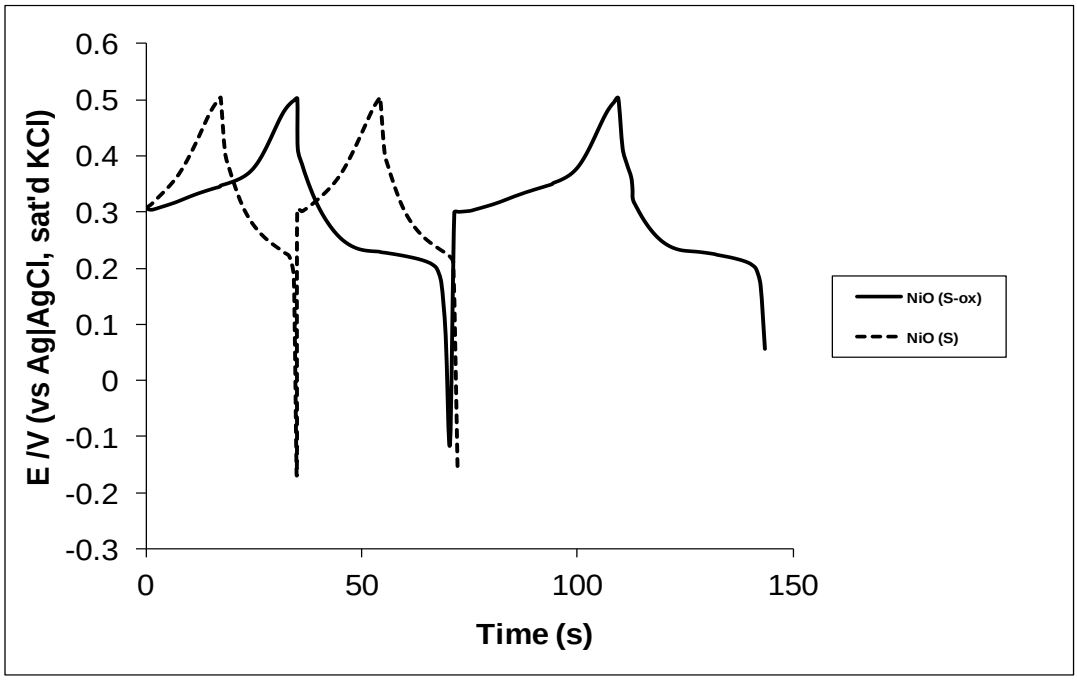

Figure 6.3: Typical charge-discharge voltammograms of bare NF, NF/$NiO_{(S\text{-}ox)}$ and NF/$NiO_{(S)}$ electrodes in 2M KOH.

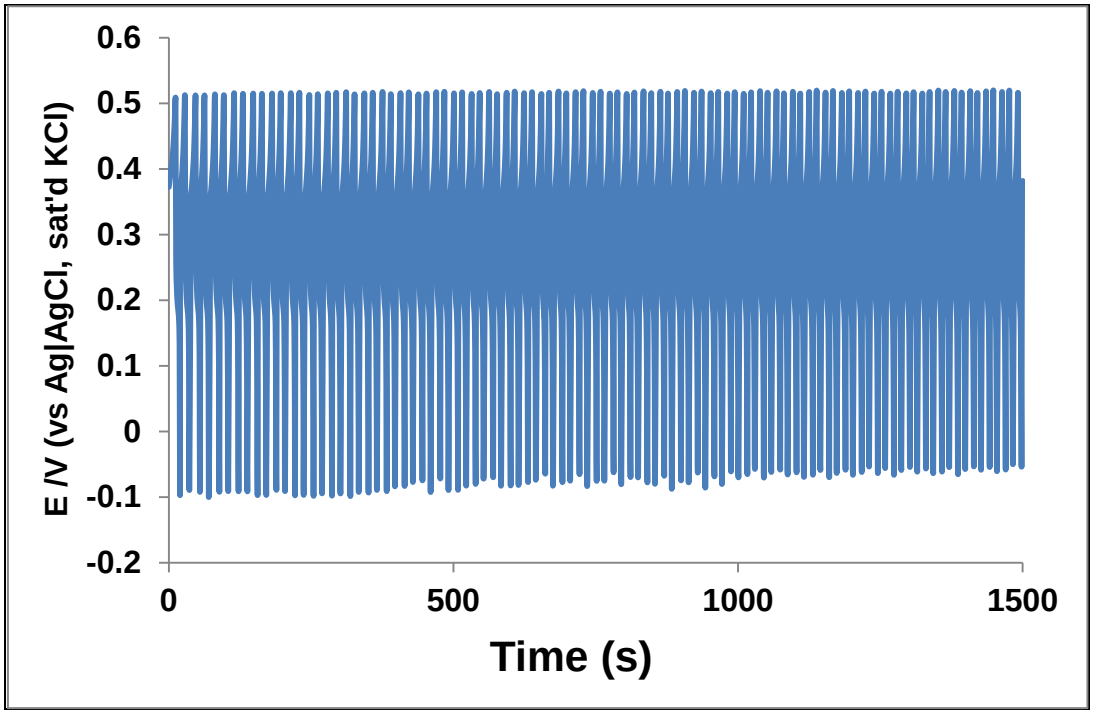

Figure 6.4: Long-term charge-discharge cycling of the NF/$NiO_{(S\text{-}ox)}$ in 2M KOH. Current density = 24 Ag^{-1}.

6.3 EIS Experiment

From the EIS experiment (Figure 6.5), the "knee" frequency (f_o) of the NF/$NiO_{(S\text{-}ox)}$ is 754 Hz, which is quite high compare to most commercially available supercapacitors designed for higher power applications that operate at frequencies less than 1 Hz [2].

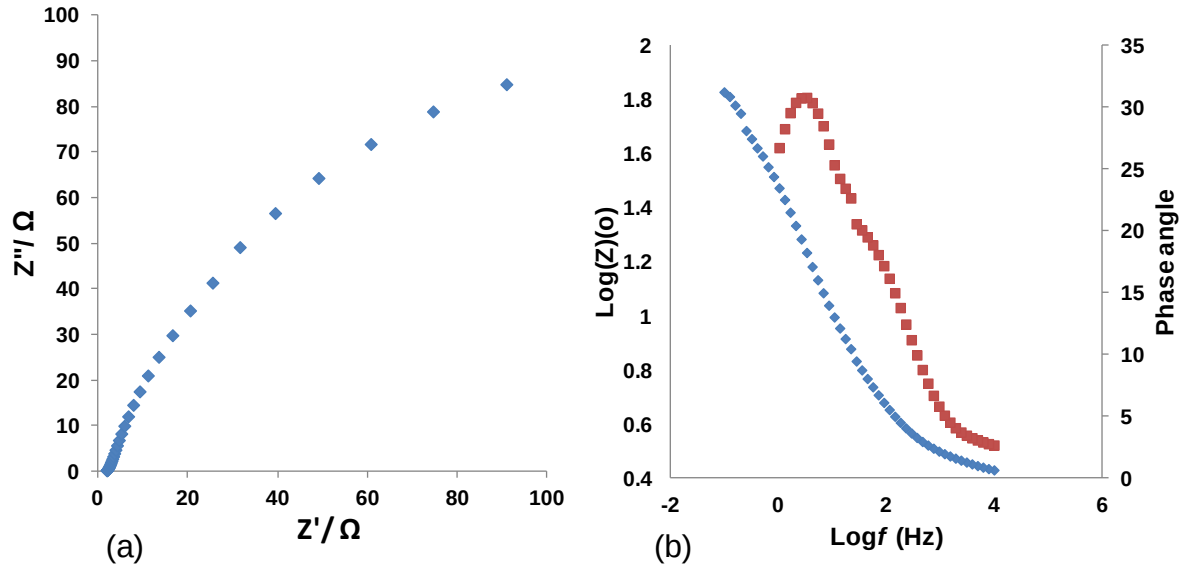

Figure 6.5: Typical Nyquist plot (a) and Bode plot (b) of NF/$NiO_{(S\text{-}ox)}$ in 2M KOH. Fixed potential = 0.2V

Conclusions

Nickel oxide films were synthesised and been immobilised by SILAR method on nickel foil. The specific capacitance, resistance, and cyclic stability of the nickel oxide, with and without the oxidant, electrodes were successfully analysed in 2 M KOH solution using cyclic voltammetry, galvanostatic charge-discharge cycling and impedimetric techniques. NiO based electrode with oxidant displayed excellent supercapacitive behaviour than that without any oxidant as seen from overlaid cyclic voltammograms, and overlaid galvanostatic charge-discharge cycling curves. The capacitive behaviour of NiO based electrode is affected by the introduction of an oxidant. Galvanostatic method shows that NiO integrated with an oxidant is capable of undergoing continuous charge-discharge process for more than a 1000 cycles without any significant deterioration in the stability. High value of specific energy may suggest that, both NiO and NiO-oxidant based electrodes may be used as a potential material for battery.

REFERENCES

1. Y. F. Yuan, L. Q. Yu, H. M. Wu, J. L. Yang, Y. B. Chen, S. Y. Guo and J. P. Tu, *Electrochimica Acta*, 2011, **56**, 4378–4383.

2. J. R. Miller and A. F. Burke, *Interface-Electrochemical Society*, 2008, **17**, 53-57.

CONCLUSIONS AND RECOMMENDATIONS

This thesis studied the electrochemical capacitive properties of nickel tetraaminophthalocyanine (NiTAPc), nickel tetraaminophthalocyanine incorporated with Nickel oxide (NiTAPc-NiO) and nickel oxide incorporated with multi-walled carbon nanotubes (NiO-MWCNT), using three different techniques known as successive ionic layer adsorption reaction (SILAR), electrodeposition and dip-dry. This study also reports on the effect of undoped polymer of poly-pyrrole (PPY) on NiTAPc. The physical properties of the synthesised materials were investigated using SEM and EDX, while the electrochemical properties were investigated using cyclic voltammetry (CV), charge-discharge (CD) and electrochemical impedance spectroscopy (EIS). The supercapacitive properties of NiTAPc film on nickel foam showed a maximum specific capacitance of 416.0 Fg^{-1}, a maximum power density of $15.50x10^{3}$ WKg^{-1} and a maximum specific energy of 66.0 $WhKg^{-1}$. However, the electrochemical capacitance of the NiTAPc integrated with PPY decreased significantly. This was surprising considering that PPY is known in the literature as an efficient supercapacitive polymer. This negative result is attributed to the undoped nature of the PPY used in this work. Further work is recommended to be carried out in the future to explore the use of doped PPY.

The NiO-MWCNT film on nickel foam gave a maximum specific capacitance of 1034.0 Fg^{-1}, power density of $10.41x10^{3}$ WKg^{-1} and a specific energy of 132.0 $WhKg^{-1}$. The NiTAPc-NiO film formed by

electrodeposition technique (NiTAPc-NiO_E) on nickel foam was found to possess a specific capacitance of 1117.0 Fg^{-1}, power density of 20.48 x 10^3 WKg^{-1} and a specific energy of 119.0 $WhKg^{-1}$. Interestingly, the electrode obtained by electrodeposition followed by SILAR (NiTAPc-NiO_{E-S}) gave slightly higher capacitive parameters (specific capacitance of 1279.0 Fg^{-1}, power density of 26.96 x 10^3 WKg^{-1}, and a specific energy of 114.0 $WhKg^{-1}$.

The NiO mixed with an oxidant (NiO_{S-ox}) film on nickel foam gave a specific capacitance of 1403.0 Fg^{-1}, power density of 14.44 x 10^3 WKg^{-1} and a specific energy of 147.0 $WhKg^{-1}$. In addition, the electrodes were found to be very stable even after repetitive cycling. Indeed, these electrodes have clearly proved that they may be suitable for use as potential supercapacitors.

In summary, further research is necessary in the future to fully explore the supercapacitive behaviour of these investigated electrodes with a view of improving their properties. Such futures studies should include the following:

(i) Studies using single cell (2-electrode) systems for real practical applications.

(ii) Exploring the applicability of the electrodes in lithium ion batteries. This is important considering that the findings in this work showed slow charge-discharge properties (resulting in high specific energy densities) which are typical

characteristics of lithium ion batteries (see Ragone plots, chapter 1).

(iii) The use of different media other than alkaline (i.e., acidic, neutral and organic media).

(iv) The use of different conducting substrates other than nickel foam.

(v) The use of doped conducting polymers.

APPENDIX

MANUSCRIPT

- Katlego Makgopa, and Kenneth I. Ozoemena, "Synergistic enhancement of the supercapacitive properties of nickel oxide integrated with nickel (II) tetra-aminophthalocyanine" [prepared].

POSTER PRESENTATION

- Katlego Makgopa, and Kenneth I. Ozoemena, Design and synthesis of nickel phthalocyanine-carbon nanotubes-conducting polymer ternary composite and application as supercapacitor. 11th International Conference on Frontiers of polymers and advanced materials, SOUTH AFRICA, May 22-27, **2011**